

ALMA MATER STUDIORUM-UNIVERSITY OF BOLOGNA

CAMPUS OF CESENA

DEPARTMENT OF ELECTRICAL, ELECTRONIC AND
INFORMATION ENGINEERING “GUGLIELMO MARCONI”

MASTER'S DEGREE IN BIOMEDICAL ENGINEERING

Finite Element modelling to predict wear in joint replacements

Subject of the thesis

Computational Biomechanics

Candidate:

Advisors:

Francesco Antonio Giannetti

Prof. Marco Viceconti

Ing. Cristina Curreli

A.Y. 2019/2020

Index

Index	3
List of Figures	5
Introduction	9
1. Basic concepts and state of art	11
1.1 Contact mechanics	11
1.1.1 Type of Contact	11
1.1.2 Hertz's theory	12
1.1.3 Geometrical characteristics of surfaces	13
1.2 Tribology	15
1.2.1 Wear	15
1.2.2 Friction	16
1.2.3 Lubrication	17
1.3 Joint prostheses	19
1.3.1 Anatomy, kinematics and biomechanics of hip joint	19
1.3.2 Hip replacement	22
1.3.3 Tribology in joint prostheses	28
1.4 Finite Element wear models of the hip replacements	31
2. Modelling wear in Ansys	38
2.1 Modelling workflow	38
2.2 Contact models in Ansys	39
2.2 Wear routine in Ansys	46
3. Simulating pin-on-disc and pin-on-plate wear tests with Ansys	51
3.1 Sensitivity analysis on the main input model parameters of hard-on-hard bearings	51
3.1.1 Test case description	51
3.1.2 Model inputs and scheme used for the analyses	52
3.1.3 Results	57
3.2 Soft-on-hard bearings	65
3.2.1 Wear test description	65
3.2.2 Model and simulation details	66
3.2.3 Results and experimental comparison	71
3.3 Bilateral wear	74
3.3.1 Wear test description	74
3.3.2 Model and simulation details	74
3.3.3 Results and experimental comparison	81
4. Wear simulation on hip replacement	85
4.1 Materials and methods	85
4.1.1 Geometry and materials definition	85
4.1.2 Mesh	86
4.1.3 Contact and wear implementation	87

4.1.4 Boundary conditions	89
4.2 Results	92
5. Conclusions	99
6. Bibliography	101
Ringraziamenti	106

Keywords: tribology, wear, joint protheses, Finite Element Models.

List of Figures

<i>Fig 1. 1 Compliant vs non-compliant contact</i>	11
<i>Fig 1. 2 Non-compliant surfaces in contact</i>	12
<i>Fig 1. 3 Contact between two spheres. Figure reproduced from [4]</i>	13
<i>Fig 1. 4 Structure of a real surface</i>	13
<i>Fig 1. 5 Average roughness vs average square roughness. Figure reproduced from [4]</i>	14
<i>Fig 1. 6 Behaviour of a fluid between two parallel plates. Figure reproduced from [16]</i>	18
<i>Fig 1. 7 Anatomy of pelvis. Figure reproduced from wikimedia.org</i>	19
<i>Fig 1. 8 a) Anterior and b) posterior view of the femur. Figure reproduced from wikimedia.org</i>	20
<i>Fig 1. 9 Flexion and extension. Figure reproduced from [1]</i>	20
<i>Fig 1. 10 Abduction and adduction. Figure reproduced from [1]</i>	21
<i>Fig 1. 11 a) Internal and b) external rotations. Figure reproduced from [1]</i>	21
<i>Fig 1. 12 Biomechanics of hip joint</i>	22
<i>Fig 1. 13 THR vs RHR. Figure reproduced from [4]</i>	24
<i>Fig 1. 14 Type of bearings: soft-on-hard vs hard-on-hard. Figure reproduced from [3]</i>	25
<i>Fig 1. 15 Some of the designs of the acetabular cup. Figure reproduced from [1]</i>	25
<i>Fig 1. 16 Some of the designs of the femoral head. Figure reproduced from [1]</i>	26
<i>Fig 1. 17 a) Zirconia, b) Biolox forte(alumina) and Biolox delta (ZTA). Figure reproduced from [1]</i>	27
<i>Fig 1. 18 Types of wear in joints prostheses. Figure reproduced from [12]</i>	29
<i>Fig 1. 19 a) Three-body model vs b) two-body model</i>	33
<i>Fig 1. 20 Acetabulum made with a) hexahedral or b) tetrahedral elements</i>	34
<i>Fig 1. 21 Femoral head made with a) hexahedral or b) tetrahedral elements</i>	34
<i>Fig 1. 22 Example of contact region; contact surface (red) target surface (blue)</i>	35
<i>Fig 2. 1 Classic workflow of FEM analysis in ANSYS</i>	38
<i>Fig 2. 2 CONTA174 elements</i>	40
<i>Fig 2. 3 Tangential and normal force</i>	41
<i>Fig 2. 4 Two bodies in contact with Asymmetric behaviour</i>	41
<i>Fig 2. 5 Two bodies in contact with Pure Penalty formulation</i>	42
<i>Fig 2. 6 Integration Point Detection vs Nodal Detection when two bodies is in contact</i>	44
<i>Fig 2. 7 Pinball Region when two bodies is in contact</i>	45
<i>Fig 2. 8 Window of Contact Tool</i>	46

<i>Fig 2. 9 Command Snippets for wear routine</i>	47
<i>Fig 2. 10 Example of error due to wear process</i>	48
<i>Fig 2. 11 Command Snippets for mesh nonlinear adaptivity</i>	49
<i>Fig 2. 12 SOLID285 vs SOLID 185 vs SOLID187</i>	49
<i>Fig 2. 13 User Defined Result to calculate wear depth for CONTA174 elements</i>	50
<i>Fig 3. 1 Window of Engineering Data</i>	52
<i>Fig 3. 2 Definition of the geometry of unilateral hard-on-hard pin on disc</i>	52
<i>Fig 3. 3 a) Mesh of pin on disc; b) mesh of pin; c) mesh of disc</i>	53
<i>Fig 3. 4 Settings for contact options of unilateral hard-on-hard pin on disc</i>	54
<i>Fig 3. 5 Command Snippets for wear routine of unilateral hard-on-hard pin on disc</i>	54
<i>Fig 3. 6 Boundary conditions of unilateral hard-on-hard pin on disc</i>	55
<i>Fig 3. 7 Command Snippets for remeshing of unilateral hard-on-hard pin on disc</i>	55
<i>Fig 3. 8 Analysis Settings options of unilateral hard-on-hard pin on disc</i>	56
<i>Fig 3. 9 Trends of maximum contact pressure of unilateral hard-on-hard pin on disc</i>	57
<i>Fig 3. 10 Trends of wear volume of unilateral hard-on-hard pin on disc</i>	58
<i>Fig 3. 11 Trends of wear depth of unilateral hard-on-hard pin on disc</i>	59
<i>Fig 3. 12 Trends of maximum contact pressure of unilateral hard-on-hard pin on disc with linear and quadric elements</i>	60
<i>Fig 3. 13 Trends of maximum contact pressure of unilateral hard-on-hard pin on disc with tetrahedrons and hexahedrons elements</i>	60
<i>Fig 3. 14 Trends of wear volume of unilateral hard-on-hard pin on disc with tetrahedrons and hexahedrons elements</i>	61
<i>Fig 3. 15 Trends of wear depth of unilateral hard-on-hard pin on disc with tetrahedrons and hexahedrons elements</i>	61
<i>Fig 3. 16 Trends of maximum contact pressure of unilateral hard-on-hard pin on disc before wear with different formulations</i>	63
<i>Fig 3. 17 Trends of maximum contact pressure of unilateral hard-on-hard pin on disc after wear with different formulations</i>	63
<i>Fig 3. 18 Trends of maximum contact pressure of unilateral hard-on-hard pin on disc before wear with different detection methods</i>	64
<i>Fig 3. 19 Trends of maximum contact pressure of unilateral hard-on-hard pin on disc after wear with different detection methods</i>	64
<i>Fig 3. 20 Trends of maximum contact pressure of unilateral hard-on-hard pin on disc as a function of Normal Stiffness</i>	65

<i>Fig 3. 21 Definition of the geometry of unilateral hard-on-soft pin on plate</i>	67
<i>Fig 3. 22 a) Mesh of pin on plate; b) mesh of pin; c) mesh of plate</i>	68
<i>Fig 3. 23 Settings for contact options of unilateral hard-on-soft pin on plate</i>	69
<i>Fig 3. 24 Command Snippets for wear routine of unilateral hard-on-soft pin on plate</i>	69
<i>Fig 3. 25 Boundary conditions of unilateral hard-on-soft pin on plate</i>	70
<i>Fig 3. 26 Command Snippets for remeshing of unilateral hard-on-soft pin on plate</i>	70
<i>Fig 3. 27 Analysis Settings options of unilateral hard-on-soft pin on plate</i>	71
<i>Fig 3. 28 Trends of maximum contact pressure of unilateral hard-on-soft pin on plate</i>	72
<i>Fig 3. 29 Trends of wear volume of unilateral hard-on-soft pin on plate</i>	73
<i>Fig 3. 30 Trends of wear depth of unilateral hard-on-soft pin on plate</i>	73
<i>Fig 3. 31 Definition of the geometry of bilateral hard-on-hard pin on plate</i>	75
<i>Fig 3. 32 Definition of the geometry of bilateral hard-on-hard pin on plate reduced</i>	75
<i>Fig 3. 33 a) Mesh of pin on plate; b) mesh of pin; c) mesh of plate</i>	76
<i>Fig 3. 34 Settings for contact options of bilateral hard-on-hard pin on plate, on the left are shown the settings in which the pin is defined as contact surface and on the right those in which the plate is defined as contact surface</i>	78
<i>Fig 3. 35 Command Snippets for wear routine of bilateral hard-on-hard pin on plate where the pin is the contact and the plate is the target</i>	78
<i>Fig 3. 36 Command Snippets for wear routine of bilateral hard-on-hard pin on plate where the plate is the contact and the pin is the target</i>	79
<i>Fig 3. 37 Boundary conditions of bilateral hard-on-hard pin on plate</i>	79
<i>Fig 3. 38 Command Snippets for remeshing of bilateral hard-on-hard pin on plate where the pin is the contact and the plate is the target</i>	80
<i>Fig 3. 39 Command Snippets for remeshing of bilateral hard-on-hard pin on plate where the plate is the contact and the pin is the target</i>	80
<i>Fig 3. 40 Analysis Settings options of bilateral hard-on-hard pin on plate</i>	81
<i>Fig 3. 41 Trends of wear volume of bilateral hard-on-hard pin on plate</i>	82
<i>Fig 3. 42 Trends of wear volume of unilateral pin and bilateral pin</i>	83
<i>Fig 3. 43 Trends of wear volume of unilateral pin, bilateral pin and bilateral pin with fine mesh</i> ..	83
<i>Fig 3. 44 Trends of wear depth of bilateral hard-on-hard pin on plate</i>	84
<i>Fig 4. 1 Definition of the geometry of hip replacement</i>	86
<i>Fig 4. 2 Mesh of acetabular insert</i>	87
<i>Fig 4. 3 Settings for contact options of hip replacement</i>	88
<i>Fig 4. 4 Command Snippets for wear routine of hip replacement</i>	88

<i>Fig 4. 5 Trends of the forces according with ISO 14242-1 [60]</i>	89
<i>Fig 4. 6 Trends of the angular rotation, specifically flex-extension around y axis, adduction-abduction around x axis and intra extra rotation around z axis according with ISO 14242-1 [60]</i>	89
<i>Fig 4. 7 Boundary conditions of hip replacement</i>	90
<i>Fig 4. 8 Reference system of hip replacement</i>	90
<i>Fig 4. 9 Command Snippets for remeshing of hip replacement</i>	91
<i>Fig 4. 10 Analysis Settings options of hip replacement</i>	91
<i>Fig 4. 11 Trends of maximum contact pressure of hip replacement</i>	92
<i>Fig 4. 12 Maps of the maximum contact pressure of hip replacement</i>	93
<i>Fig 4. 13 Map of the depth wear of hip replacement</i>	94

Introduction

Total hip replacement (THR) is one of the greatest achievements in orthopaedic surgery of the last century and today one of the most performed surgical procedure in the world. Specifically, over the past two decades, the number of THR performed every year in Italy has steadily increased to reach 100,000 implants in 2018. To date, available data show that total hip arthroplasty (THA) has an annual failure rate of between 0.5 % and 1.0 %. In other words, there is a 90-95% chance that the new joint lasts 10 years and an 80-85% chance that it lasts 20 years. Moreover, the younger population by virtue of increased life expectancy and activity level requires implants with increasing lifetime [1], [2].

For this reason, it is important to invest in this research field and study possible causes of implant failure in order to prevent negative outcomes after joint arthroplasty and increase the lifespan of the artificial joint. One of the main causes of implant failure is related to tribological aspects, specifically wear which is associated to material loss, modification of geometric surfaces, inflammatory reactions and osteolysis.

As a result, joint simulator wear tests are now mandatory to evaluate the design of prosthesis of an implant. Based on these tests, also called *in vitro*, the implants must be tested under standardised loading and kinematic conditions. Then, wear is usually quantified by the gravimetric methods, which allow to determine the loss of weight of the implant components. However, wear tests performed with joint simulators are very expensive and time consuming. Moreover, it is difficult to consider the real loading subject variability and replicate the wide range of boundary conditions related to different tasks such as walking, running, climbing stairs, and so on [3].

A valid alternative to experimental tests in the laboratory is the use of computational methods, also called *in silico*, based on finite element models (FEM). These methods are faster and cheaper in providing wear predictions. In addition, on the contrary of hip simulators, they can simulate different loading and kinematic conditions of the system. Although these methods are considered promising today for providing evidence of medical device safety and/or efficacy, several more steps need to be taken before they can be used in clinical practice [4], [5]. One of them is related credibility assessment: FE wear models need to be first validated against experimental measurements.

This thesis project aims to deeply investigate FEM for modelling the wear phenomenon in THR in order to develop a computational method that can be used to support and accelerate wear tests performed with hip joint simulators at the Rizzoli Orthopaedic Institute in Bologna.

In the first part of the work, a first FEM model was created, using the Ansys® Workbench software, to simulate a *hard-on-hard* pin on disc test. The results obtained, in terms of maximum contact pressure, wear volume and wear depth, were found in good agreement with experimental results available in the literature. In addition, in this part of the work, a mesh convergence and a sensitivity analysis were conducted to respectively evaluate the effect of the mesh density and of the different contact and wear parameter settings on the model results. Also, in this part of the thesis, a FEM model was realised to simulate a *soft-on-hard* pin on disc test and the possibility to model bilateral wear using the software Ansys was investigated.

In the second part of the work, a finite element model of a *hard-on-soft* hip protheses was developed. A wear test performed with a 32 mm ceramic-polyethylene hip replacement described in the literature was simulated by implementing all the loading and kinematic conditions. The results in terms of predicted wear volume and wear map were compared with the experimentally measured ones. Also, the possibility to reduce the computational cost of FE wear analyses of hip replacements was investigated considering an implicit kinematic strategy and exploring different possible static loading conditions.

1. Basic concepts and state of art

In the initial part of this chapter, the general basic concepts of contact and tribology are described. A biomechanical description of the hip joint is then presented, followed by a description of the hip prosthesis and of the phenomenon of wear in hip prosthesis. In the final part of this chapter, a state of the art of the main finite element models used to simulate hip prosthesis wear, is reported.

1.1 Contact mechanics

1.1.1 Type of Contact

The contact theory determines the stresses and the deformations that arise when the surfaces of two solid bodies are in contact. The main types of contact between two bodies, on a geometric level, are compliant and non-compliant (*Fig 1.1*).

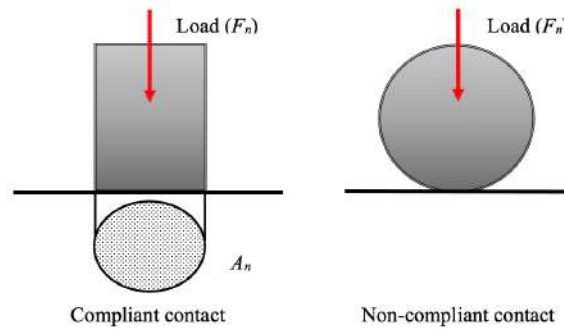


Fig 1. 1 Compliant vs non-compliant contact

The compliant contact, e.g., hinges or spherical pairs, takes place on a defined region, which is called nominal contact area (A_n). Moreover, it is possible to define a nominal contact pressure (p_0), as described in following equation, defined as the ratio between the normal load (F) and the nominal contact area.

$$p_0 = \frac{F}{A_n} \quad Eq. 1.1$$

Non-compliant contact, unlike the previous one, occurs on one point or on a line. This point represents the origin of a reference system (x, y, z), where, for example, x and y are the coordinates of the points in the plane tangent to the two surfaces in O and z is the normal axis. The equations that describe the shape of the two surfaces are defined below:

$$z_1 = f_1(x, y) \quad Eq. 1.2$$

$$z_2 = f_2(x, y) \quad Eq. 1.3$$

Moreover, the equation which represents the separation (h) between the two undeformed surfaces is defined as follows (Fig 1.2):

$$h = z_1 + z_2 = f(x, y) \quad Eq. 1.4$$

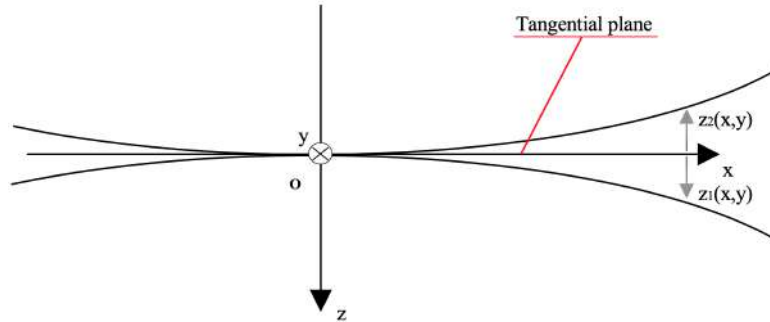


Fig 1. 2 Non-compliant surfaces in contact

For example, hip prostheses are considered to be compliant or conformal couples when the head and the acetabular cup have the same nominal radius, while when they do not have the same nominal radius, they can be defined as not compliant or non-conformal [4].

1.2.2 Hertz's theory

The evaluation of the nominal pressure in non-compliant contact is obtained thanks to the Hertz's theory (1881). The latter, which solves the problem analytically, assumes that, when two spheres are in contact, the interacting surface can be approximated by a plane circle of radius a (Fig. 1.3), which depends on the load (F), on the equivalent radius (R) and on material properties of two bodies (Young modulus E_1, E_2 and Poisson's ration ν_1, ν_2) according to the following equation:

$$a = \sqrt[3]{\frac{3FR}{4E}} \quad Eq. 1.5$$

where R and E are calculated as follows:

$$\frac{1}{R} = \frac{1}{R_1} \pm \frac{1}{R_2} \quad Eq. 1.6 \quad \frac{1}{E} = \frac{1 - \nu_1^2}{E_1} + \frac{1 - \nu_2^2}{E_2} \quad Eq. 1.7$$

In the case of the equivalent radius, the positive sign, is used when the coupling takes place between two external spheres while the negative sign is used when one sphere is inserted into another, as in the case of hip prothesis.

Furthermore, using this contact radius value (a), it is also possible to calculate the maximum normal pressure (p_{max}) in the contact area according to the following equation:

$$p_{max} = \frac{3F}{2\pi a^2} \quad Eq. 1.8$$

Hertz's theory is based on the following hypotheses: solids are homogeneous, isotropic and elastic therefore Hooke's law is valid, the contact must be no-compliant so the dimensions of the contact area are small compared to the radius of curvature of the contact bodies, between the two bodies there are no sliding friction forces and therefore during contact only the normal force acts, the contact surfaces are continuous and can be represented by second order polynomials before the deformation and the force F_N is normal to the tangential plane, which defines two contact surfaces [4], [6]–[10].

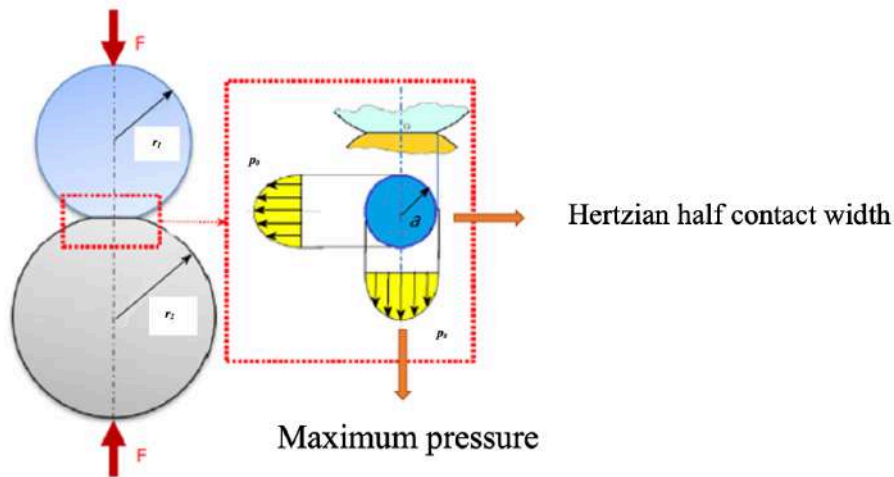


Fig 1. 3 Contact between two spheres. Figure reproduced from [4]

1.1.3 Geometrical characteristics of surfaces

Hertz's theory, as mentioned above, refers to the ideal condition in which the surfaces are smooth and uncontaminated. However, the real surface of a solid body is characterised by a certain degree of roughness. Therefore, in every real surface it is possible to highlight the presence of three layers: the contamination layer (e.g., gas, grease, adsorbed lubricants), the reaction layer (e.g., oxides) and the plastic deformation layer resulting from manufacturing processes, as described in the following figure.

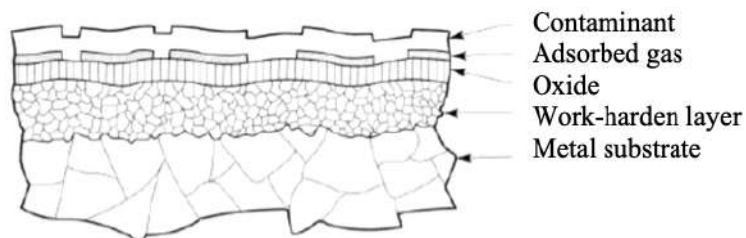


Fig 1. 4 Structure of a real surface

The plastic deformation layer or hardened layer is the result of plastic deformation processes, machining and heat treatment. Its depth and properties depend on the process used and the frictional

characteristics of the surface. In some cases, an amorphous or nanocrystalline layer, called Beilby, affects the top of the hardened layer. This layer is formed as a result of the processing with drastic superficial melting or heating, followed by rapid cooling. Furthermore, if the metal is not kept in an inert environment (oxygen-free) and it is not a noble metal, an oxide is formed above the hardened layer or the Beilby's layer.

The oxide layer, under normal conditions, is characterised by a layer of adsorbed gas. The outer layer, instead, is made up of contaminants such as dust, grease, dirt, residues of lubricants or compounds used in cleaning, or pollutants coming from the environment. Therefore, it is possible to affirm that the external surface presents characteristics and properties very different from the internal body. Therefore, the integrity of the surface, which influences the final properties of the object, is of fundamental importance [7], [11].

The roughness of a surface can be described by the average roughness (R_a) and the average square roughness (R_q). These quantities, represented in *Fig 1.5*, are defined by the following two equations:

$$R_a = \sqrt{\frac{1}{n} \sum_{i=1}^n |y_i|} \quad \text{Eq. 1.9} \quad R_q = \sqrt{\frac{1}{n} \sum_{i=1}^n y_i^2} \quad \text{Eq. 1.10}$$

where y is the value of the ordinate of the points representing the roughnesses (profile height) with respect to the average reference line and n the total number of roughnesses.

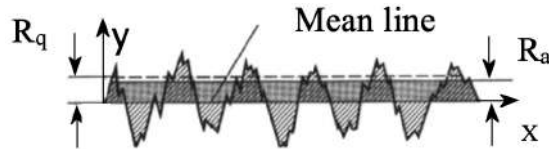


Fig 1.5 Average roughness vs average square roughness. Figure reproduced from [4]

Another very important parameter that characterises surfaces is the actual contact area. Specifically, due to the roughness, two surfaces pressed against each other come in contact only in correspondence to the surface roughness, which therefore defines the real contact area (A_r). The latter is always smaller than the nominal one (A_n) and according to a ratio that depends on the distribution and entity of the surface irregularities, on the entity of the applied force and on the mechanical characteristics of the materials. Therefore, the real area is the sum of the single areoles (A_i) in correspondence to each contact roughness, as described in following equation:

$$A_r = \sum_{i=1}^N A_i \quad \text{Eq. 1.11}$$

where N is the number of contacts roughnesses [4].

1.2 Tribology

Tribology is the science that studies friction, lubrication and wear, i.e., phenomenon and processes that can occur when contact surfaces are in the relative motion. The name tribology is coined in the 60's, using as a base a Greek root where the verb *tribo* means rubbing and the noun *tribos* means friction. However, the most correct definition is given by Halling in the *Introduction to tribology* and where he defines it as “*the science and technology of interacting surfaces in relative motion and relative substances and practices*”. A tribosystem is defined as a “*system consisting of two bodies in contact, in relative motion, with a possible third body in between*”. A tribosystem dissipates energy by friction and the loss of mass in the form of fragments, with consequent superficial damage or breakage, causing the phenomenon of wear. Friction and wear are not intrinsic properties of the material, but they are characteristics of the tribological system. There are several parameters that influence the behaviour of a tribological system. For this reason, it is necessary to consider the type of relative motion among the components, the possible presence of oil film under pressure, the presence of polluting particles, the type of materials in contact in terms of mechanical, chemical-physical and microstructural properties, the shape and surface conditions of the tribo-elements. Moreover, temperature, relative velocity and specific load are also important parameters [1].

1.2.1 Wear

Wear is the surface damage, followed by loss of material or its transfer between articulated surfaces. Wear can be classified into adhesive, abrasive, fatigue, corrosive, erosion, impact, and fretting wear. Adhesive wear is caused by the presence of local welding between roughnesses, which hinders the relative movement of surfaces, and by the presence of high pressures caused by contact points. When the microjunctions break at the interface between the two bodies, no wear occurs. The surfaces are modified due to plastic deformation, but the amount of material remains the same as before the contact. On the other hand, when the microjunction drags part of the weaker material, the mechanism of wear occurs. It is possible to reduce this type of wear by increasing the surface roughness and hardness of the surfaces involved, or by inserting layers of contaminants such as oxygen, oxides, water, or oils. In adhesive wear behaviour the lost mass is proportional to the distance, to the load applied and to the hardness of the material.

Abrasive wear occurs when a very hard surface slides on softer surfaces. It can be classified as two-body abrasive wear or three-body abrasive wear and, in this last case, the particles are harder than both surfaces. Two-body abrasive wear, also called erosive wear, is caused by the presence of

roughness which, like spikes, cut the material they rub against. Three-body abrasive wear is caused by the presence of material particles interposed between the two surfaces in a relative manner. From a practical point of view, the first one can be eliminated with a suitable surface finish, while the second one requires suitable filters and a well-thought-out design of the machinery.

Fatigue wear occurs when the surface is affected by cyclic loads or thermal expansions that transmit cracks along the material. To reduce this type of wear, it is necessary to reduce contact forces and thermal cycling, i.e., the frequency of reheating and cooling. For optimum results, it is recommended to eliminate impurities between surfaces, local defects and inclusions of foreign materials in the bodies involved.

Corrosive wear happens in the presence of oxidising or corroding metals. When pure metal surfaces come in contact with the surrounding environment, oxide films are generated on their surfaces due to contaminants in the environment such as water, oxygen or acids. The last ones are continuously removed by abrasive and adhesive wear mechanisms and they are always recreated by pure metal-contaminant interactions. This type of wear can be reduced by trying to create a pollutants-free environment and subjected to minimal temperature changes. Moreover, the oxides contribute to reducing the coefficient of friction between surfaces or they can be used as excellent abrasives, since in many cases they are harder than the metal to which they belong.

Erosion wear occurs when free particles, solid or liquid, hit a surface, causing abrasion. The mechanisms involved are of various kinds and depend on certain parameters, such as impact angle, particle size, impact velocity and the material of which the particles are made.

Fretting wear occurs in systems subjected to more or less intense vibrations, which cause relative movements between contact surfaces in the nanometre range. This type of wear can be accelerated by the presence of corrosive substances, the increase of temperature, normal load and sliding amplitude [7], [12]–[14].

1.2.2 Friction

Friction is the resistance/dissipative force that opposes the relative movement between two bodies, and it can be divided into static and dynamic. The first is the force that prevents two bodies, placed on a rough surface and initially at rest, from moving if the force, acting in a parallel direction, does not exceed a certain value. The second is the force that opposes the motion of a body sliding on a surface.

Friction is quantified through a coefficient, called coefficient of friction (μ or COF), defined as the ratio between the tangential force (T) and the normal force (F) at the interface, as described by the following equation [4]:

$$\mu = \frac{|T|}{|F|} \quad Eq. 1.12$$

The value of COF depends on the contact materials, surface roughness, presence of a lubricant, etc. COF describes the first law of friction, enunciated by engineer Amontons in 1699 but discovered by Leonardo Da Vinci and Newton, i.e., the friction is independent of the nominal contact area. The second and third laws, enunciated by Coulomb in 1875, establish respectively that the friction force is proportional to the normal load; in other words the ratio between F_T and F_N is μ and the dynamic friction is independent of relative sliding velocity [15].

Friction between metal surfaces mainly occurs through a thin oxide film, the thickness of which can be reduced by normal load and by the plastic deformation of the roughness. As for ceramic materials, friction is mostly influenced by the elastic deformation of the asperities. Finally, polymers, which have a viscoelastic behaviour, follow the first law of friction only for low normal loads. In contrast, for high loads or very smooth surfaces the COF decreases as the normal load increases because the roughness is nearly flattened due to the high material compliance [4].

1.2.3 Lubrication

Lubrication is introduced to limit energy dissipation caused by friction. A lubricant, liquid or solid, is positioned between the contact surfaces in order to limit contact between the asperities, in other words to reduce the friction force. An estimate of the distance between the asperities of the mating surfaces is expressed through the parameter λ , given by the ratio between the minimum film thickness (h_{min}) and the composite roughness of the two surfaces, as described in the following equation:

$$\lambda = \frac{h_{min}}{\sqrt{R_{q1}^2 + R_{q2}^2}} \quad Eq. 1.13$$

where R_q is the mean square roughness and subscripts 1 and 2 distinguish the two bodies in contact. The general relationship between μ and λ is represented by the Stribeck curve [4], [16]–[19].

Lubrication regime can be classified as a function of λ in three lubrication regimes. Boundary lubrications, where $0.1 < \lambda < 1$, is characterised by an extended contact area. Mixed lubrication, where $1 < \lambda < 3$, is characterised by a small contact area and it can also be called elastohydrodynamic

lubrication. Fluid-film lubrication, where $\lambda > 3$, is characterised by completely separate surfaces and the fact that the load is fully supported by the fluid film of the lubricant [4], [5], [17]–[19].

The lubrication can be described by equations of Reynold, derived from Navier-Stokes' equations. This phenomenon can be explained, in a simplified way, by the following figure, where there are two flat plates separated by a fluid moving in a relative way with a relative velocity (u).

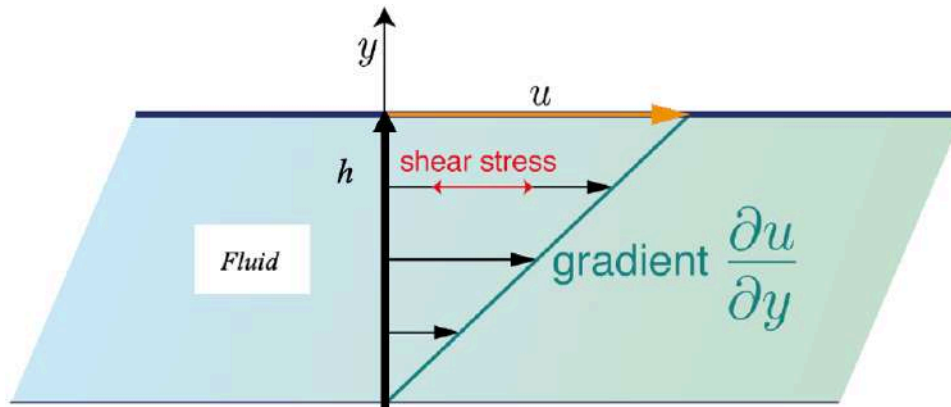


Fig 1. 6 Behaviour of a fluid between two parallel plates. Figure reproduced from [16]

The particles, which adhere to the surface in motion, acquire their velocity u while those adhering to the fixed surface have zero velocity. Therefore, a velocity gradient is obtained through each cross-section of the distance, approximately given by u / h and correlated to the shear stress of the fluid through its viscosity, as described by the following equation [16]:

$$\tau = \mu \frac{\partial u}{\partial y} \approx \mu \frac{u}{h} \quad Eq. 1.14$$

Therefore, a tangential force (T) develops at the interface between the plates and the fluid, which is proportional to the area of the surfaces (A) and to the shear force (τ), as described in following equation [16]:

$$T = A\tau \quad Eq. 1.15$$

The mathematical discussion becomes much more complex when, for example, the fluid is non-Newtonian and therefore numerical approaches are needed to solve the equations that describe the system [16], [18], [19].

1.3 Joint prostheses

1.3.1 Anatomy, kinematics and biomechanics of hip joint

The hip joint is a type of ball-in-socket joint where the acetabular cup is the socket, and the femoral head is the ball. The pelvis is made up of four bones, the sacrum, the two iliac bones and the coccyx, which represent the connection between the axial skeleton, consisting of the head, the spine and the rib cage, and the skeleton of the lower limbs. The pelvis (*Fig 1.7*) has the function of supporting the weight of the upper body and connecting the upper body to the lower limbs. The iliac bone, flat in shape, is composed by the ilium, the ischium and the pubis, which are initially separated by a cartilaginous layer but tend to join together once they reach skeletal maturity, forming the acetabular cup or cotyle.

The acetabulum is located at the centre of the outer surface of the coxal bone. The inner surface of the cup is covered by a layer of cartilage, except for the central region, called acetabular fossa, which hosts the ligamentum teres, adipose tissue and blood vases. The outer edge of the acetabulum is attached to the glenoid labrum, a fibro-cartilaginous structure that helps proper femoral head seating and hip joint stability by increasing joint congruence and deepening the acetabulum to accommodate a larger portion of the femur. Finally, the acetabulum is closed by the transverse acetabular ligament of the glenoid labrum.

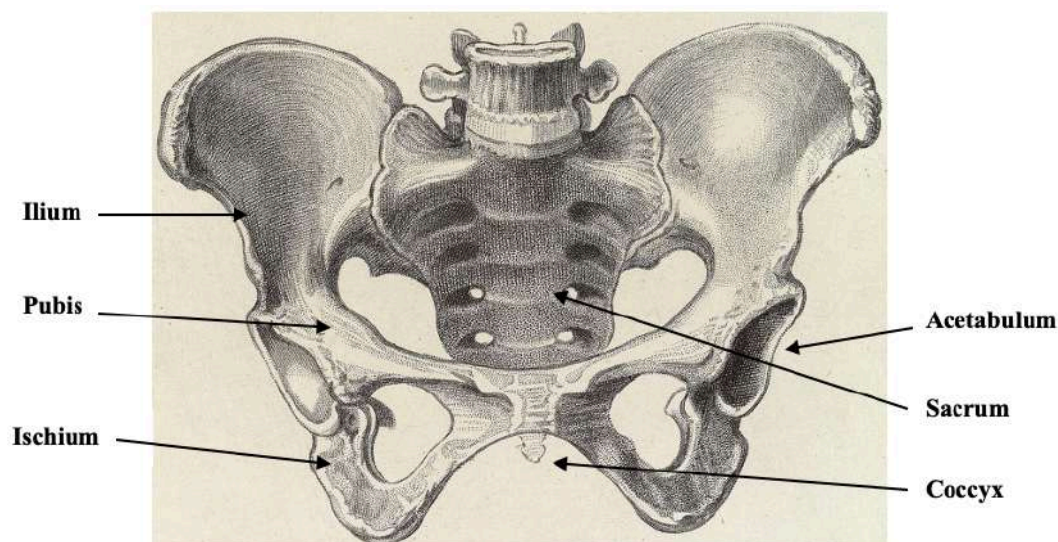


Fig 1. 7 Anatomy of pelvis. Figure reproduced from wikimedia.org

The femur (*Fig 1.8*) is the longest bone in the human body and plays a key role in walking. It consists of a central body, the diaphysis, and two ends, the proximal and distal epiphyses. The proximal epiphysis is composed of the femoral head, the femoral neck and two bony prominences where numerous muscles insert, called greater and lesser trochanter. The distal epiphysis is characterised by

the medial and lateral condyles that act as insertion sites for muscles and ligaments. The femoral head is covered by cartilage, with the exception of its central part, called the fovea capitis, where the ligamentum teres inserts.

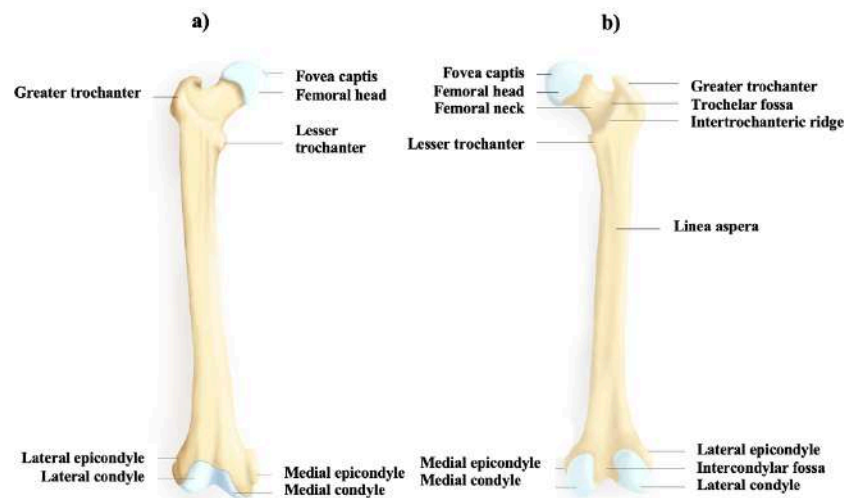


Fig 1. 8 a) Anterior and b) posterior view of the femur. Figure reproduced from wikimedia.org

The hip joint is made stable by the joint capsule that runs from the beginning of the glenoid labrum to the base of the femoral neck, by the ligaments, specifically the iliofemoral, ischiofemoral, pubofemoral, and teres ligaments, and by the muscles.

The hip joint is lubricated by synovial fluid, which allows for low-friction motion, even when the joint surfaces are subjected to high pressures. Synovial fluid is produced by the synovial membrane, which covers the inner surface of the joint [1], [20].

The hip joint allows the flexion/extension (Fig 1.9), the abduction/adduction (Fig 1.10) and the intra-extra rotation (Fig 1.11). The flexion, whose range varies from 0 to 130 degrees, is the motion of bringing the thigh up towards the abdomen. The main flexor muscles are the quadriceps femoris, which in turn is divided into rectus femoris, vastus lateralis, vastus medialis and vastus intermedius, the iliopsoas, the sartorius, and the pectineus.

The extension, whose range varies from 0 to 30 degrees, is the opposite of flexion. The main flexor muscle are the gluteus maximus, the semimembranosus, the semitendinosus, and the biceps femoris.

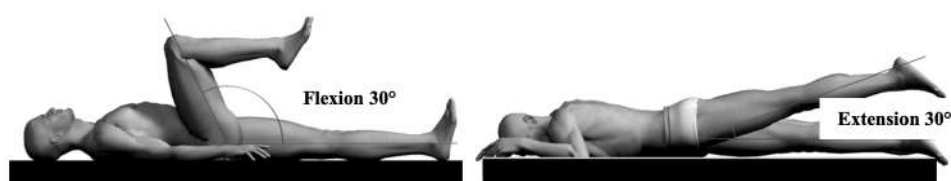


Fig 1. 9 Flexion and extension. Figure reproduced from [1]

Abduction, whose range varies from 0 to 45 degrees, is the movement that brings the leg away from the plane of body symmetry. The main abductor muscles are the gluteus minimum, gluteus medius, gluteus maximus, and the piriformis muscles and tensor of lateral muscle.

Adduction, whose range varies from 0 to 30 degrees, is the movement that brings the leg closer the plane of body symmetry. The main adductor muscles are the long, short and great adductor muscles, the pectineus and gracilis muscles.

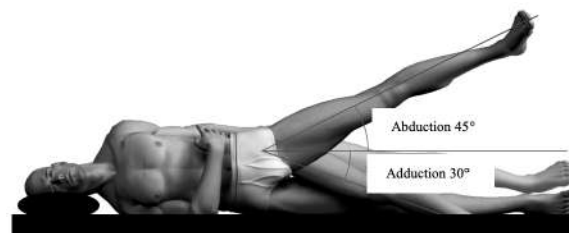


Fig 1. 10 Abduction and adduction. Figure reproduced from [1]

The movements that allow the hip to turn inward and outward are called internal and external rotations whose range varies from 0 to 30 degrees and 0 to 40 degrees, respectively. The main muscles for intra-rotation are the gluteus medius, minimum and lateral fascia tensor while for extra-rotation they are the biceps femoris, gluteus maximus and piriformis.

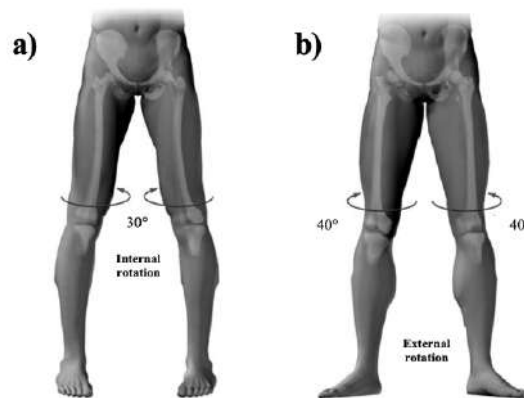


Fig 1. 11 a) Internal and b) external rotations. Figure reproduced from [1]

The hip joint, during locomotion, is subjected to external forces such as gravity or inertia, and internal forces of muscular origin, which tend to continuously balance each other. The body weight, with bi-podal stance, is distributed equally on the hips and the centre of gravity is positioned approximately in the fifth lumbar spine. On the other hand, in the case of mono-podal support, the weight distribution is not equal between the two hips, but it only weights on the support joint and the centre of gravity tends to move towards the free limb. It is possible to identify the forces acting, as defined in the following equation, on the joint through the vectors P , M and R , which represent, respectively, the partial body weight, defined as partial because it is the weight of the subject minus the weight of the

supporting limb, the muscular force exerted by the abductor muscles and the resulting resultant force. The parameter b , which is the distance between the centre of rotation of the hip and the greater trochanter, represents the lever arm of the abductor muscles, while the parameter a is the lever arms of the partial body weight force.

$$M \cdot b = P \cdot a \quad \text{Eq. 1.16}$$

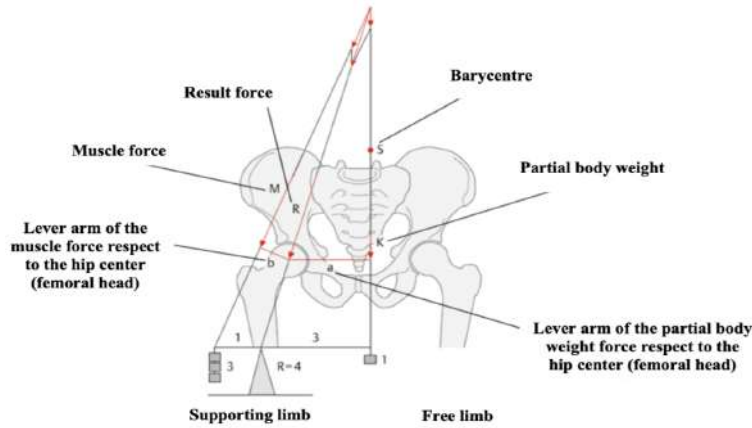


Fig 1. 12 Biomechanics of hip joint

From the above image it can be deduced that the arm of the partial weight force is about three times the arm of the muscle force, therefore the muscle force required to oppose the rotational moment is about three times the partial weight force. Moreover, the resulting force, acting on the hip joint, will be about 4 times the body weight [1].

1.3.2 Hip replacement

The most common pathological condition leading to THA is primary osteoarthritis, which is a degenerative process caused by degeneration of cartilage. Secondary osteoarthritis is caused by bone deformation that may be due to congenital conditions such as developmental dysplasia of the hip, Legg-Calvè-Perthes disease, congenital femoral epiphysis, achondroplasia, haemophilia, or post-traumatic disorders such as femoral neck fractures or acetabular fractures. Another possible pathology is osteonecrosis of the femoral head, which can develop after femoral neck fracture or traumatic hip dislocation, etc. Finally, possible pathologies are rheumatologic diseases such as rheumatoid arthritis, which causes an inflammatory response that thickens and destroys the cartilage layer, ankylosing spondylitis, sequelae of septic arthritis of the hip such as pyogenic arthritis, tuberculosis, and bone tumours involving the proximal femur. A hip implant includes contraindications, such as the presence of acute infection in any region of the body and any medical condition such as heart disease, lung disease, liver disease, etc., which increases operative risks [1], [2], [6], [21]–[23].

Hip replacements, whose pioneer and developer was Sir John Charnley (1960), along with knee and shoulder replacements, are artificial joint replacements that attempt to restore the mobility lost by the native hip joint (*Fig 1.13*). Hip prostheses can be classified, according to geometry and material, in THR and resurfacing (RHR). THR consists of the acetabular cup, the femoral head, the femoral stem and the femoral neck. The acetabular cup is composed of an outer shell, called cotyle or backing, and of an internal liner, called insert. The shell is fixed to the pelvis using surgical cement or mechanical insertion. The liner, which acts as cartilage, is the counterpart of the femoral head with half-spherical shape and it ensures mechanical stability of the acetabular cup. The acetabular cup, in general, is the critical element of the system specifically if the acetabulum is made of materials less resistant than the head. This choice is justified by the desire to ensure correct kinematics despite the phenomenon of wear. The femoral head is a spherical joint, which is placed inside the artificial acetabulum. The most significant head parameter is the diameter, which plays a significant role in determining the achievable range of motion of the artificial hip joint and its stability against dislocation. Specifically, several studies show that the use of a larger ball can reduce dislocation accidents. Another relevant parameter is roughness, which influences the tribological characteristics of the implant. The femoral stem is inserted into the medullary canal of the femur with mechanical coupling or surgical cements after resection of the femoral head and neck and drilling of the medullar canal. The length of stem varies between 130-140 mm to ensure stability of the device and to make the surgery minimally invasive. Its most important functions are to fix the femoral side of the prosthesis and to provide uniform load distribution in the surrounding bone tissue. In some cases, the neck and stem are part of the same component, and the prostheses are called monoblock, while in modular prostheses the stem and the neck are separate parts. Modular models allow greater modification of the prosthesis geometry, allowing the implants to be set in ways which most appropriately fit the patient's anatomical or pathological requirements. However, the increased number of components and junctions does additionally increase the risk of fretting corrosion. In some standard prostheses, the use of a collar between the stem and neck helps to minimize the migration of wear debris and it also ensures primary fixation of cementless stems.

RHR is an alternative form of hip arthroplasty, in which the femoral head is not removed, but trimmed and capped with a smooth metal covering. On the contrary, the damaged bone and cartilage within the socket are removed and replaced with the shell. In general, RHR is characterised by larger heads in order to increase implant stability and range of motion of the hip joint after surgery, to reduce a rate of dislocation and prosthesis bearing wear, and to facilitate revision surgery. For these reasons RHR is the recommended option for young and active patients [1], [4], [20]–[22], [24].

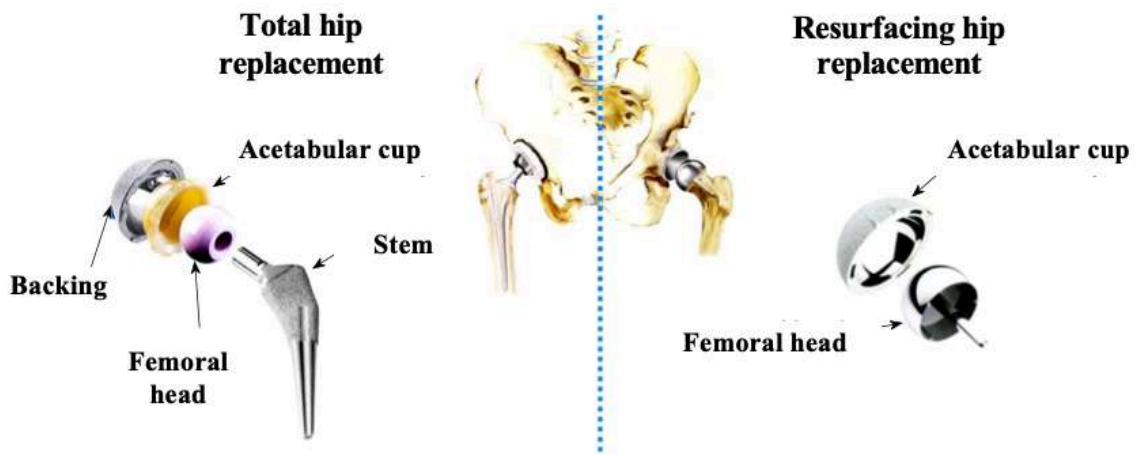


Fig 1. 13 THR vs RHR. Figure reproduced from [4]

As mentioned earlier, hip replacements can be cemented and uncemented. The first ones are characterised by the presence of a thermoplastic, linear and amorphous polymer called polymethylmethacrylate (PMMA) which assures fixation of the implant to the bone, filling the free space between them and allowing uniformed distribution of loads. Specifically, thanks to its low elastic modulus it accepts the stresses caused by the difference in stiffness between the metal and the bone. PMMA cements may exhibit various biocompatibility-related problems, such as local tissue damages, due to the exothermic nature of the cement setting reaction. Uncemented prostheses are placed within the prepared cavity by pressing the implant. They require close contact with the bone to facilitate integration and a porous coating with hydroxyapatite, which is a ceramic material with chemical and structural properties very similar to the bone surface. The choice between either of these implants depends on the surgeon's preference, the individual patient's age and the patient's activity. For example, in younger and more active patients, due to the high osteogenic activity of the bone, cementless implants are recommended. On the other hand, cemented implants are recommended for elderly patients or patients suffering from diseases that affect bone metabolism [21], [22].

The most used biomaterials are polymers (P), metals (M) and ceramics (C). The shell is always made with metals, usually pure titanium or stainless steel, the liner is made with polymers, usually ultra-high molecular weight polyethylene (UHMWPE) or highly cross-linked polyethylene (HXLPE), the femoral head is made with metals, like Co-Cr-Mo or stainless steel and ceramic like alumina (pure or BIOLOX delta) or zirconia, the femoral stem and the femoral neck are made with metals, specifically titanium alloy or stainless steel. The most common material combinations for bearing surfaces are metal on plastic (MoP), ceramic on plastic (CoP), ceramic on ceramic (CoC), and metal

on metal (MoM), as shown in the following figure. In these acronyms, the first letter refers to the cup material and the third to the head [1], [4]–[6], [20], [25]–[27].



Fig 1. 14 Type of bearings: soft-on-hard vs hard-on-hard. Figure reproduced from [3]

The most commonly used polymer in hip replacement is UHMWPE (Fig 1.15). It is a semi-crystalline polymer composed of a crystalline phase, in which the macromolecules fold into ordered lamellae, and an amorphous, disordered phase. The process of making UHMWPE is called polymerization, which is characterised by the possible formation of debris that causes adverse biological reactions to the surrounding tissues causing osteolysis. For this reason, highly cross-linked polyethylene (XLPE) is introduced, which is developed using high-dose (50-100 kGy) radiation, gamma rays or electrons. The irradiation generates a quantity of free radicals whose oxidation causes degradation of mechanical properties. Complete elimination of free radicals is difficult due to the limited mobility of these radicals within the polymer's crystal structure. One strategy to reduce free radicals is post-irradiation remelting, which leads to improved oxidation and wear resistance. However, it leads to a decrease in the crystallinity of the polyethylene and thus a loss of strength. A second strategy is to add appropriate stabilizing additives, whose role is to decrease the reactivity of radical species, slow down oxidation processes, and preserve the chemical, physical, and mechanical bonds inherent in polyethylene. The ideal stabilizing additive is vitamin E, as it is used as a natural antioxidant in the physiological processes of the human body. However, the actual contribution of vitamin E in the wear mechanism of acetabular cups is unclear as of today [1], [4], [8], [20], [26], [28]–[32].

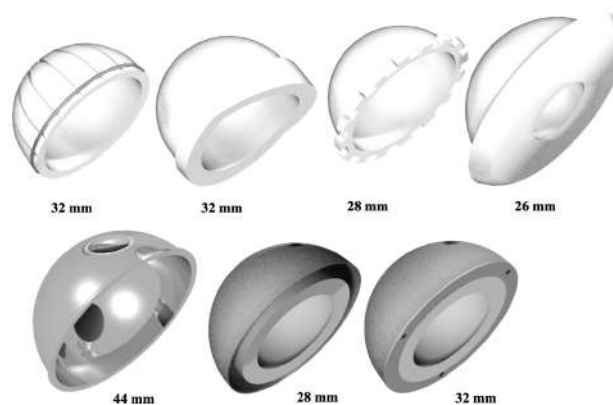


Fig 1. 15 Some of the designs of the acetabular cup. Figure reproduced from [1]

The metal materials used in hip replacement are cobalt-chromium-molybdenum (CoCrMo) alloys, chrome-cobalt (CoCr), titanium alloys (Ti₆Al₄V) and stainless steel, characterised by high hardness, toughness, wear resistance and surface finish (*Fig 1.16*). CoCrMo is the most commonly used because it is characterised by a good corrosion resistance, a high wear resistance and a higher hardness. However, its main limitation is related to its poor fatigue resistance and its high cost. It can be divided in high-carbon alloys (carbon content >0.20%) and low-carbon alloys (carbon content <0.08%). The first one has face-centered cubic structure that may have a wear resistance better than the second one that has a hexagonal close-packed structure. A limit observed for these types of implant is the release of metal ions (Co and Cr) with effects on the immune system, mutagenesis and carcinogenesis [1], [4], [20], [23], [26], [29]–[32].

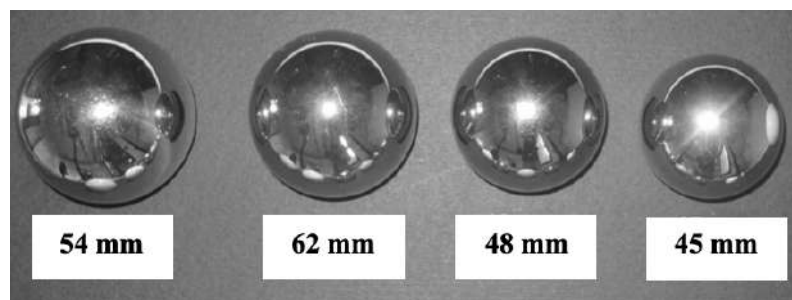


Fig 1. 16 Some of the designs of the femoral head. Figure reproduced from [1]

The most used ceramics in the orthopaedic field are alumina, zirconia, zirconia-toughened alumina composites (*Fig 1.17*). Alumina ceramic (Al₂O₃) is widely used for their thermo mechanical and tribologic properties, specifically it shows a very high hardness. The main limitation of alumina is its low wear resistance, caused by its intrinsic brittleness due to a combination of material impurities, poor implant design, and sterilization procedures, such as autoclaving and rapid cooling. Zirconia ceramic (ZrO₂) is introduced in the manufacture of femoral heads because of its high specific strength and toughness, which reduce the risk of fracture. However, hardness and thermal conductivity are lower than alumina, not allowing its clinical use in articulating ceramic couples. A further disadvantage is the technology used for zirconia manufacturing, particularly critical and therefore relatively expensive. However, the introduction of ceramic composite materials based on alumina and zirconia, called Zirconia Toughened Alumina (ZTA), has led to a real revolution in the orthopaedic field. In the 2000s the first ZTA material introduced in clinic is a composite known under the trade name of BIOLOX[®] delta. It is obtained by microscopic crack-tip shielding mechanism characterised by chemical-physical reactions in which at the first time the hardness and the stiffness of the alumina matrix increase. The second reaction leads to increased hardness, strength, fracture toughness, and reliability of the ceramic, due to the formation of platelets. Finally, the third reaction

leads to high fracture toughness, strength and reliability, by the formation of submicron-size yttria tetragonal zirconia polycrystals (Y-TZP) grains finely and evenly dispersed within the alumina matrix. To conclude, the idea is to combine the tribological properties of alumina with the mechanical properties of Y-TZP. The presence of Zirconia aggregates is identified as the main issue leading to ageing sensitivity. Operating an optimal dispersion at acid pH can avoid the Zirconia aggregates formation, but when the percolation threshold level (16 vol.%) is exceeded ageing cannot be avoided. In conclusion, despite ceramic's excellent material and wear properties, concerns remain about the risk of ceramic fractures, noise, and squeaking [1], [4], [5], [18], [20], [25], [27], [32].

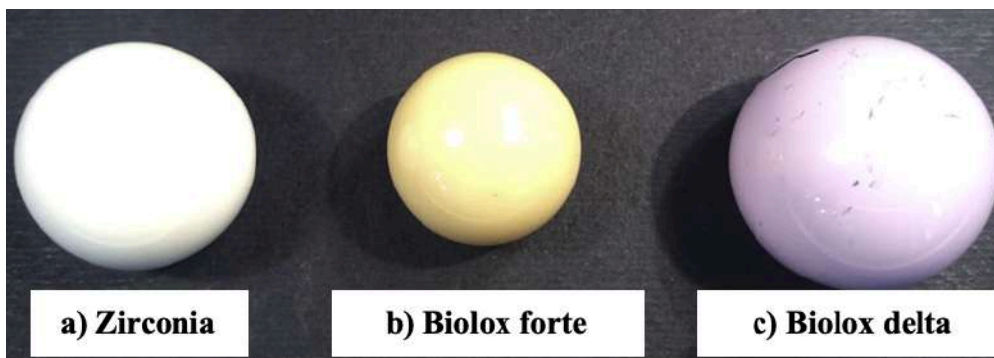


Fig 1. 17 a) Zirconia, b) Biolox forte(alumina) and Biolox delta (ZTA). Figure reproduced from [1]

The table below shows the values of elastic modulus, coefficient of Poisson and average roughness of the three main materials used for hip replacements [4], [5].

Table 1.1 from [4]

Material	Elastic modulus (GPa)	Coefficient of Poisson	Average roughness (μm)
UHMWPE	0.5-2	0.4	0.1-2
CoCrMo	230	0.3	0.01-0.05
Biolox delta	350	0.26	0.001-0.005

The supporting surfaces of the femoral head and cup are shaped with a spherical geometry, characterised by the radii of the head and cup, that give a clearance C_l . The radial clearance is the difference between the radius of the acetabular cup and that of the femoral head. The following table shows the diameter of the head (D_h) and the clearance (C_l) [4], [5].

Table 1.2 from [4]

Head/Cup	D_h (mm)	C_l (μm)
MoP	22.2-44	160-400
CoP	22.2-36	160-400
MoM	22.3-54	50-150
MoM _{RHR}	42.54	50-300
CoC	22.2-44	20-100

From the following tables it is possible to state that ceramic femoral ball heads allow a surface smoothness higher than metal femoral heads, resulting in lower friction rates. However, ceramic femoral ball heads can only be produced with smaller diameters than metallic materials due to the limitations of the production technology. In addition, the need for larger inner and outer diameters of the acetabular inserts will result in a smaller shell thickness, as the physical space for insertion is determined by the anatomy of the pelvis, leading to a lower quality of fixation and thus to lower mechanical stability. For these reasons, brittle and soft materials cannot be used as liners when using large diameter heads. Therefore, MOM is currently the only successful material combination available for large diameter hip joints [1].

1.3.3 Tribology in joint prostheses

Wear in hip prosthesis, associated with material loss between the head and the acetabular, is characterised by the release of particles that inflame the surrounding tissues and tend to migrate to other tissues and organs. Debris is eliminated from the human body through macrophages, which seek to phagocytize the foreign particles and release pro-inflammatory cytokines, i.e., protein molecules that induce osteolysis of the bone, a process characterised by bone resorption. As a result, wear, in addition to causing chronic inflammation, leads to loosening problems and consequently, worn prostheses must be removed and replaced. Therefore, wear provides a measure of device life and is generally evaluated, from a clinical perspective, on an annual scale. Several studies show that wear reduces the life of the implant by many years and represents one of the most relevant tribological phenomenon to be studied [20], [23], [33]–[36].

Wear of artificial prostheses can be distinguished in four distinct methods (*Fig 1.18*) that differ according to the area that is affected by the wear process. The first one (*a*) takes place between the surfaces that make up the joint coupling, in the case of the hip prosthesis between the metal or ceramic femoral head and the polyethylene insert. The second one (*b*) occurs when an unintended contact characterises the two surfaces. For example, when the polyethylene is completely worn, and the femoral head comes into contact with the metal acetabular back. The third one (*c*) happens in the presence of a "*third body*" between the mating surfaces such as cement particles, hydroxyapatite or others. Finally, the fourth one (*d*) occurs when two surfaces move with respect to each other in an unpredicted manner [12].

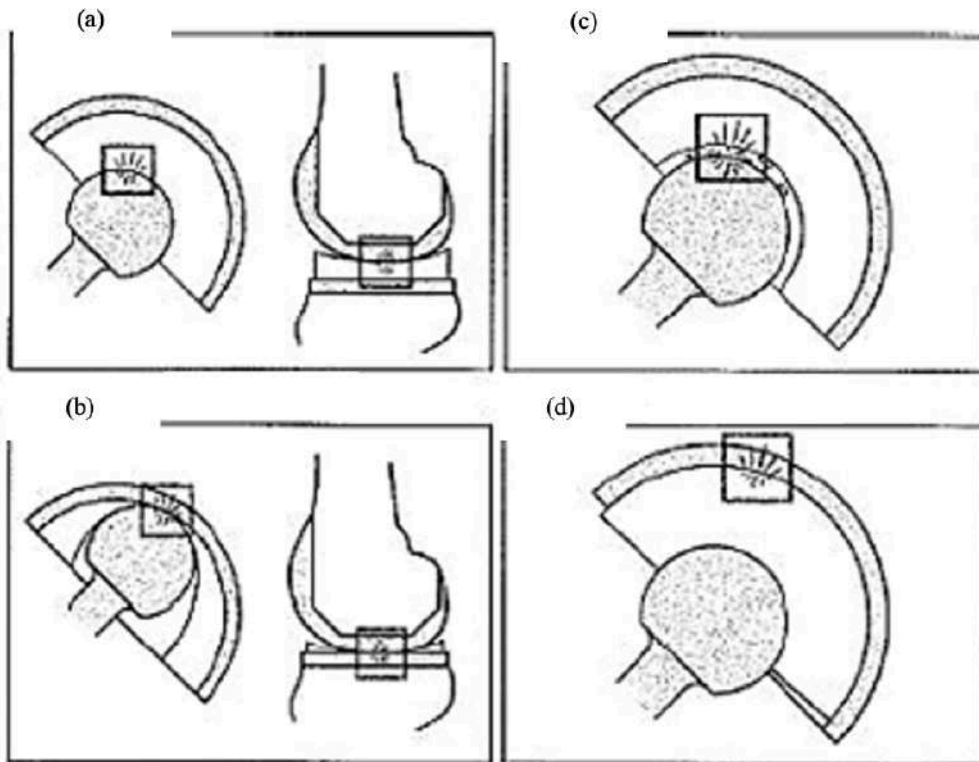


Fig 1. 18 Types of wear in joints prostheses. Figure reproduced from [12]

The main parameters affecting wear are roughness, head diameter, clearance and liner thickness. As for roughness, several studies show that volumetric wear and wear depth increase with very rough surfaces. Regarding head diameter, as mentioned earlier, large diameter heads are used in clinical practice to improve implant stability. However, it has been shown that a larger femoral head, when not lubricated, induces a larger wear volume due to increased contact area and sliding distance and a shallower wear depth caused by lower pressures on the bearing surfaces. On the contrary, when the coupling is lubricated, larger heads are characterised by lower wear volume and greater wear depth. As for clearance, it is shown that large clearance is associated with decreased volumetric wear and increased linear wear [1], [23], [30], [37].

The quantities used to evaluate the wear of hip prostheses are wear volume expressed in mm^3 (V_{cli}) and wear depth expressed in mm (h_{clin}). The typical values of these two quantities, observed clinically, are summarised in the table below where M_c stands for 10^6 cycles. These values are characterised by a high variability, caused both by the characteristics of the patient (age, sex, body weight index, daily activities) and by his physiological/pathological conditions. In addition, it is important to note that wear volume is a global indicator of wear on a body, whereas wear depth is a local indicator that provides insight into where and how joint surfaces become damaged.

Head/Cup	V_{cli} (mm³/Mc)	h_{cli} (mm/Mc)
MoP	10-500 (80)	30-500 (50)
CoP	15-50	30-150
MoM (RI)	0.1-25	1-50
MoM (SS)	0.05-4	0.1-1
MoM_{RHR} (RI + RS)	0.2-2.9	0.2-10
MoM_{RHR} (ADT)	0.2-95	1.5-46
CoC	0.005-2	0.01-1

As for THR implants, MoP bearing is characterised, respectively, by $50 \mu\text{m}/10^6$ and $80 \text{ mm}^3/10^6$, while MoM bearing by lower values, up to 2 orders of magnitude. CoP implant, but also CoC, is introduced as alternative to MoM bearing, to improve the long-term performance of hip prostheses and overcome the problem of the release of metal ions, which causes cytotoxicity, hypersensitivity and neoplasia. CoP bearing is characterised by $30\text{-}150 \mu\text{m}/10^6$ and $15\text{-}50 \text{ mm}^3/10^6$, while CoC by $0.01\text{-}1 \mu\text{m}/10^6$ $0.005\text{-}2 \text{ mm}^3/10^6$ due to its hardness, good chemical resistance, high tensile strength, and good fracture toughness. However, the main limitation of CoC bearing, but also of those CoP, in addition to their fragility, is squeaking, i.e., the audible sound generated by these implants during movement. However, CoC bearing has a lower wear rate and lower friction than MoM, MoP and CoP despite highly cross-linked polyethylene (XLPE) reduces wear rates of 40% compared to conventional polyethylene. Moreover, CoC bearing has very low surface roughness, good lubrication conditions and high wettability and consequently its lubrication properties are improved. Friction can be reduced by lubrication, while the low friction coefficient of ceramic biomaterial leads to an improvement in the tribological behaviour of the coupling. However, CoC and CoP bearings require an accurate surgical procedure based on correct positioning of all components.

Regarding RHR implants, the wear rate of coating systems is still an open question. Indeed, some successful MoM_{RHR} devices show lower wear rates with $0.2\text{-}10 \mu\text{m}/10^6$ and $0.2\text{-}2.9 \text{ mm}^3/10^6$ respectively. On the other hand, an important proportion of these implants, which show an adverse tissue reaction (ADT) at the time of removal, are subjected to high wear rates in the range of $1.5\text{-}46 \mu\text{m}/10^6$ and $0.2\text{-}95 \text{ mm}^3/10^6$. One of the main causes of excessive wear of MoM_{RHR} is the excessive cup inclination which leads to collision between the femur head and the edge of the acetabular cup. This failure is called stripe wear and it is a result from misalignment between the centre of femoral head and the centre of the acetabular cup [1], [4], [18]–[20], [25], [26], [30], [35], [38]–[41].

Wear varies with the boundary conditions, the geometry, the material properties, the kinematics, the load history, and the lubricant type. The latter strongly influences COF; specifically, a higher concentration of proteins in the lubricant increases COF for all types of equipment except MoM equipment, which likely uses a protective protein layer deposited on the bearing surfaces. For this reason, it is crucial, in order to obtain reliable friction measurements, to perform tests using lubricants with a rheological behaviour as close as possible to synovial fluid. The most commonly used lubricant to replace synovial fluid is bovine serum with a certain protein content (g/L). Theoretical and experimental studies on lubrication involving the hip prosthesis, but this is also true for other types of prosthesis, attempting to estimate the minimum film thickness, comparing it to the roughness of the mating surfaces and evaluating the lubrication regime [3], [4], [26].

As defined above the lubrication regime can be classified in boundary lubrications, mixed lubrication and fluid-film lubrication. Boundary lubrications occur when one surface is hard and the other is soft like hard-soft bearings. Mixed lubrication occurs when the contact surfaces are characterised by asperities, as in the case of the MoM bearing, which allow the penetration of a lubricating fluid forming an almost complete layer. Fluid-film lubrication occurs in *hard-on-hard* couplings between non-deformable well-polished surfaces with optimal clearance. Fluid film lubrication can be achieved in CoC and CoP bearings due to the high ceramic hardness and very low surface roughness [4], [5], [18], [19], [34].

1.4 Finite Element wear models of the hip replacements

In finite element analysis, the structure under analysis is discretised into a finite number of elements connected by nodes. The nodes are identified by spatial coordinates, characterized by degrees of freedom, and subjected to loads/ displacements; interpolated functions, also called shape functions, are used to define the relationships between the element displacement at any point and element nodal displacement. The equations for each element are combined into a system of equations as shown below:

$$[K]\{u\} = \{f\} \quad Eq. 1.17$$

where $[K]$ is the stiffness matrix, as size $n \times n$, where n is the total degrees of freedom of the system, $\{u\}$ and $\{f\}$ are column matrices with n components, which represent nodal displacement fields and nodal force fields, respectively [10].

The pioneer of finite element analysis, to predict wear in joint replacements, like hip, knee, shoulder, ankle and spine, is *Maxian et al. (1996 a, b, c)*. His model describes a metallic femoral head

articulating on a polyethylene acetabular cup. Specifically, it determines the wear in acetabulum caused by 3D loading and bending and extension movement during the walking phase, by varying some parameters such as head diameter and cup thickness and showing that only the first one has a strong influence on wear rates. Specifically, it is observed that a larger head leads to greater volumetric wear, but less depth wear as later suggested also by *Raimondi et al. (2001)* and *Wu et al. (2003)*. However, *Raimondi et al.* and *Fialho et al. (2007)* show that the volumetric wear considering only the flexion extension is reduced by a factor of 1.7 compared to that obtained considering the flexion extension and abduction-adduction, highlighting the importance of joint kinematics on the validity of the results [1], [8], [23], [32], [39], [40], [42]–[44].

Raimondi et al and *Bevil et al (2001)* take in consideration femoral head roughness and abduction-adduction and intra-extra rotation, in addition to flexion-extension. Their model shows that wear is linearly dependent on patient weight, femoral head diameter, surface roughness, clearance, and cup elastic modulus [23], [39], [40]. *Teoh et al. (2002)*, *Wang et al (2003)* and *Wu et al. (2003)* introduce in their model the elasto-plastic behaviour of UHMWPE, assuming that the material starts to behave plastically when a critical stress value (8 MPa) is reached [23], [39], [42], [44]. *Brown et al (2002)*, taking up the model of *Teoh et al.*, introduce the head roughness, underlining the high inter-patient variability of the wear rate, as clinically observed [23], [39], [44].

Fialho et al. (2008) also propose a model in which they correlate wear and heat, by simultaneously solving Archard's law and the heat equation. The simulations consider different materials, daily activities (e.g., walking and jogging), and individuals, considering the same implant geometry. As expected, wear rates are doubled for the jogging cycle compared to the walking cycles, due to a significant increase in load. Thermal analysis shows greater heat generation in MoP and MoM systems rather than CoP and CoC due to the higher coefficient of friction of the metal surfaces. The model does not determine a direct correlation between heat generation and contact pressure, in fact in some cases the latter is very high, and heat generation is very low. This could be explained by the fact that heat generation also depends on sliding distance in addition to pressure and by the fact that the model neglects other heat transfer mechanisms such as blood convection [23], [39].

The most significant aspects of a finite element wear model are geometry, materials, mesh, boundary conditions, contact region, wear routine and creep. As for geometry, the model usually includes a sphere, which represents the head of the femur and a hollow half sphere with some thickness which represents the acetabular cup. The last one, in general, consists only of the liner because the volumetric wear rate, obtained by making an acetabulum consisting of both the liner and the shell, is

shown to increase by less than 1%. Regarding the modelling of the surrounding bone, it is shown to have a negligible effect on the wear results as well. For this reason, it is possible to distinguish between a two-body defined model and a three-body defined model, as shown in the figure below [23].

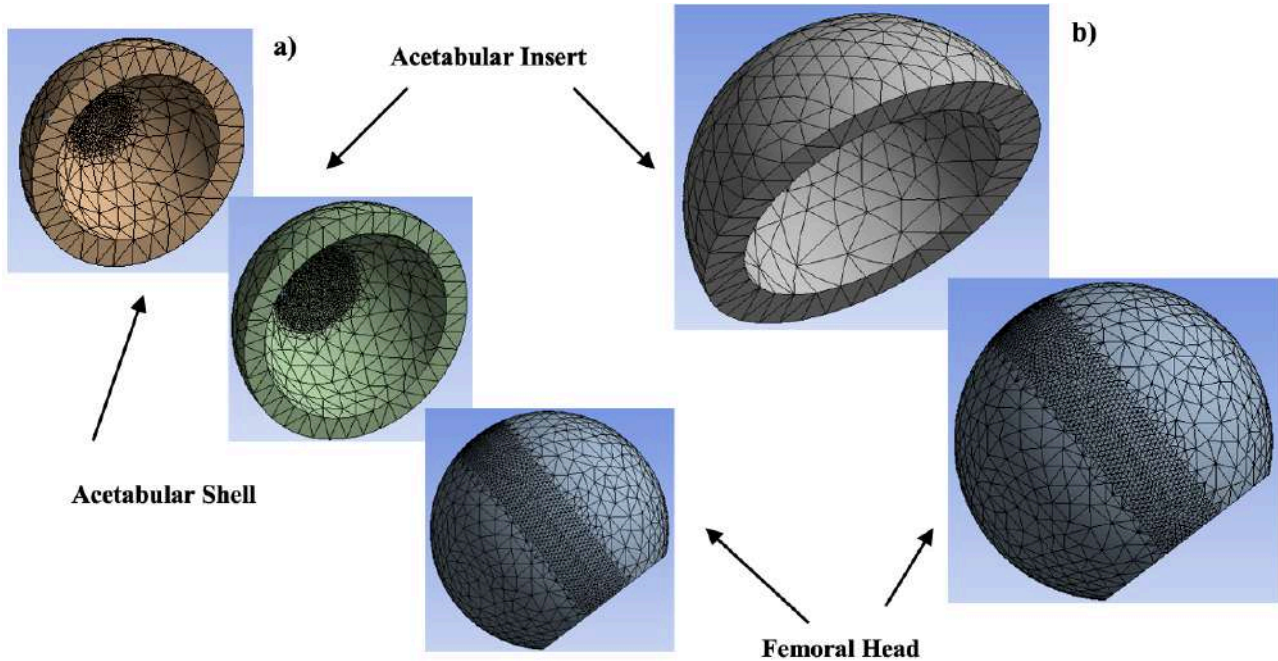


Fig 1. 19 a) Three-body model vs b) two-body model

As for the choice of material, the femur head usually is modelled with a hard material such as CoCrMo alloy with elastic modulus of 210 GPa and Poisson's ratio of 0.3 while the insert is modelled with a soft material such as UHMWPE. The last one is usually considered a linear elastic and isotropic, with a value of elastic model equal to 1.4 GPa and Poisson's coefficient equal to 0.3. However, these assumptions are correct as long as the plastic behaviour of the material is neglected. For example, the following stress-strain relationship is introduced to consider the plastic behaviour of the UHMWPE [23], [40]:

$$\sigma = A (1 - e^{-B\varepsilon}) \quad Eq. 1.18$$

where A and B are two constants and ε is the deformation.

Regarding mesh, it represents the discretization of the virtual domain necessary to transform the continuous body into a finite number of nodes and elements. The most used type of elements are generally hexahedral and tetrahedral elements (Fig 1.20 and Fig 1.21). Hexahedral elements are usually preferred because they give greater accuracy than tetrahedral elements. However, they involve a higher computational cost. Consequently, the choice of which element to use depends on

the level of accuracy needed. Indeed, a too coarse mesh results in an inaccurate solution but a low computational cost, while fine mesh becomes impracticable from the computational point of view but provides very accurate results. Moreover, tetrahedral elements also allow for easier re-meshing [20], [45].

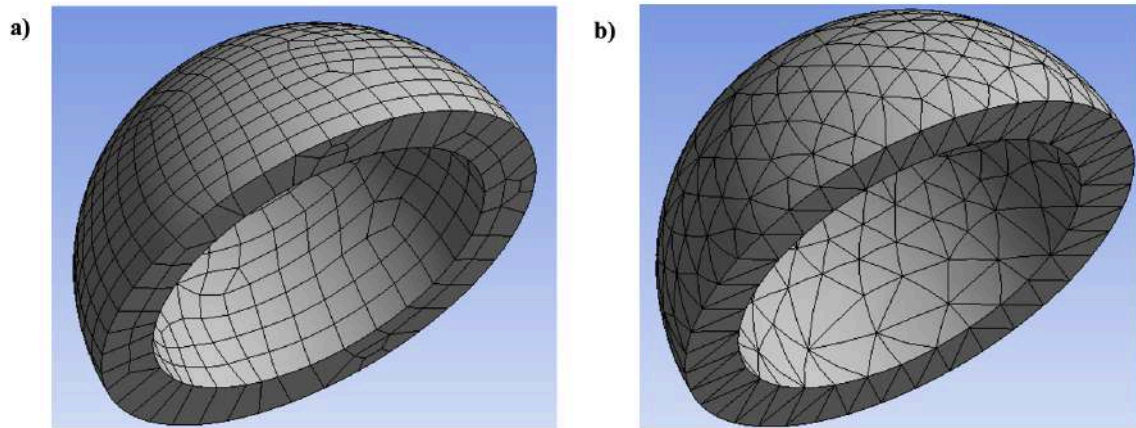


Fig 1. 20 Acetabulum made with a) hexahedral or b) tetrahedral elements

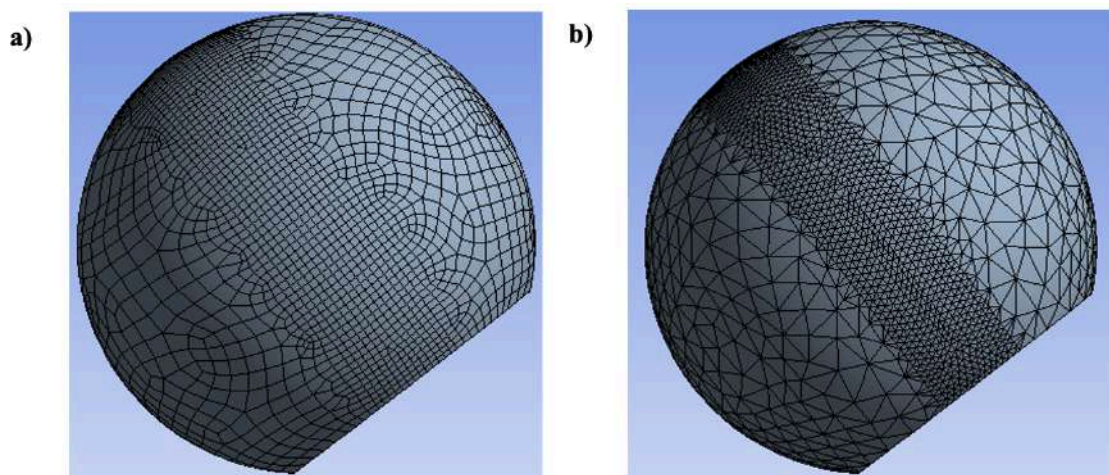


Fig 1. 21 Femoral head made with a) hexahedral or b) tetrahedral elements

Regarding the load and kinematic inputs reported in the study by Paul in 1966, they are obtained from gait studies of patients using stereophotogrammetry or using the ISO 14242 standard, where walking is considered as a task. Specifically, the only movement considered in the ISO 14242 standard is flexion-extension, because it is the movement that most affects the hip joint during walking. However, as previously described, neglecting abduction-adduction and intra-extra rotation movements leads to underestimation of wear. For this reason, the efforts are being made to apply increasingly realistic conditions to the models, which can also consider other types of tasks such as running, stair climbing, etc. However, these new protocols are not yet universally accepted or

standardised. To date, most models provide simplified boundary conditions in which only one vertical load component and the flexion-extension component are considered, despite underestimating the wear volume by a factor of up to 1.7 compared to that predicted by the simulator [1], [8], [23], [32], [40], [44]–[47].

As for the contact region, the contact pair is the head/liner articulation interface in case of two-body model plus the liner/shell interface in case of three-body model. Between the two contact pairs, the headline/liner interface is the surface most exposed to wear. When defining a contact region in Ansys Workbench®, one surface is called *target* and the other *contact* (Fig 1.22). The *target* surface is the surface of the hard material, e.g., acetabular head and shell; while the *contact* surface is the surface of the soft material, which in general is the liner [23], [30], [48].

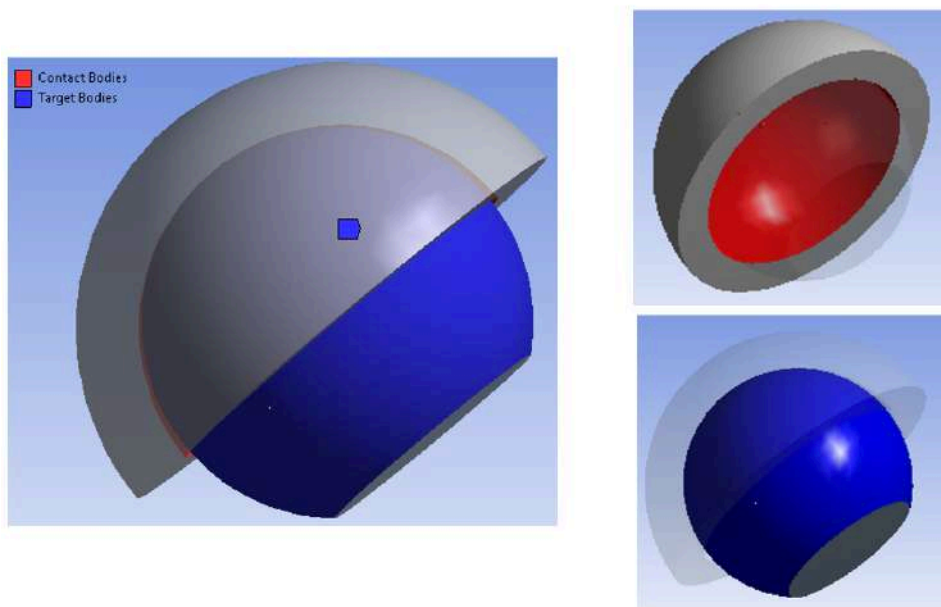


Fig 1. 22 Example of contact region; contact surface (red) target surface (blue)

Regarding wear laws, most numerical models describe the wear evolution over time by implementing Archard's wear law (1956). Models implementing Archard's law determine the surface wear volume (mm^3) with the following equation:

$$V_w = K_w FS \quad \text{Eq. 1.19}$$

where K_w is the coefficient of wear (usually expressed in mm^3/Nm ; examples shown in the table below ([23], [46]), that can be obtained from experimental studies (e.g., pin-on-disc or hip wear simulator). F is the load (N), and S is the sliding relative distance (m) between contacting surfaces. The wear coefficient varies according to the material of the counter-face, the roughness of the hardest surface, the temperature, the frequency of load and the lubricating fluid [23], [46].

The previous equation is rewritten as follows by discretizing the entire gait cycle into time intervals:

$$V_w = \sum_1^n K_w F_i S_i \quad \text{Eq. 1.20}$$

where, n are the time intervals and F_i and S_i are, respectively, the load and sliding distance at the i -th discrete instance [4], [30], [39], [46], [48].

Numerical study	Bearing material	Wear coefficient (mm³/Nm)	Type of test
<i>Maxian et al.</i>	UHMWPE/CoCr	1.0656e ⁻⁶	Hip simulators
<i>Hung and Wu et al.</i>	UHMWPE/CoCr	3.5e ⁻⁷	Hip simulators
	UHMWPE/SS	8.0e ⁻⁷	Hip simulators
	UHMWPE/Alumina	1.0e ⁻⁷	Hip simulators
<i>Sfantos and Aliabadi</i>	UHMWPE/CoCr	1.76e ⁻⁶	Hip simulators
	UHMWPE/Alumina	1.51e ⁻⁶	Hip simulators
<i>Lin et al.</i>	UHMWPE/CoCr	1.48e ⁻⁶	Hip simulators
<i>Saiko and Ahlross</i>	UHMWPE/CoCr	1.99e ⁻⁶	Pin on disc
<i>Saiko et al.</i>	UHMWPE/CoCr	1.65e ⁻⁶	Pin on disc
<i>Hill et al.</i>	UHMWPE/CoCr	0.58e ⁻⁶	Pin on disc
SS: Stainless steel; CoCr: Cobalt-chrome alloy; UHMWPE: ultra-high molecular weight polyethylene			

From the Archard's equation it is possible to obtain, by dividing both members by the contact area, a more general formula describing the wear depth at each contact node P :

$$h(P) = K_w \int_{\gamma_P} p(P, s) ds = K_w \int_T p(P, s(t))v(P, s(t))dt \quad \text{Eq. 1.21}$$

where s is the arc length along the point trajectory γ_P , p the contact pressure and v the sliding velocity.

The most important parameter of Archard's law is the wear coefficient, which is sometimes considered constant in space and time; while in other cases, dependent on contact pressure, on the cross-shear ratio and on surface roughness. However, it is unclear whether using wear coefficients that depend on pressure, roughness, and cross-sectional shear actually improves the results in terms of wear volume and wear depth [23].

The cross-shear phenomenon takes into account anisotropic wear due to the anisotropic material behaviour of plastic: in the principal molecular orientation of the polymeric chains, the wear resistance increases. The Cross-Shear Ratio (CSR) is defined as the ratio between the friction work (W_T) in the perpendicular direction to principal molecular orientation and the total friction work ($W_T + W_P$), where W_P is the friction work in the principal molecular direction, as described in the following equation [23], [30], [44]:

$$CSR = \frac{W_T}{W_T + W_p} \quad Eq. 1.22$$

To date, the effect of cross-shear on the computational wear modelling is only considered for the hip and knee joint. However, introducing cross-shear dependent effects, the predicted wear rate only increased less than 10% [23].

The effect of pressure is inversely proportional to the wear coefficient. However, several studies show that considering both effects, pressure and cross-shear, the estimated volumetric wear rate is 2.8 % lower. Alternatively, a wear model that depended on the contact area was constructed, where the wear rate has improved but still underestimated by a factor of less than 2% [23], [30], [44].

The effect of roughness on wear is investigated by modifying the wear coefficient, such as by specifying the value of the wear coefficient on specific regions of the femoral head.

As for creep, it is the process of accumulation of inelastic deformation in the presence of constant stress over time, especially in the first million loading cycles. This is important because it causes significant volume changes in the insert when it is made of UHMWPE. The creep change turns out to be in a linear relationship with time, on a logarithmic scale, and pressure. It is modelled with the followed relationship:

$$\varepsilon_{creep} = K\sigma \log(t) \quad Eq. 1.23$$

where K is a constant, σ sigma is the contact pressure and t is the time [8], [23], [30].

Finally, it is important to underline that the finite element solution methods are generally divided into the implicit and the explicit methods. The implicit FEA method iterates to find the approximate static equilibrium at the end of each load increment. For a nonlinear problem, the computation can be extremely expensive because the global stiffness matrix has to be assembled and inverted many times. Therefore, the implicit method is preferable to analyse static problems, where the load is time independent and inertial effects are negligible. The explicit method determines a solution by advancing the kinematics state from one time increment to the next, without iteration. It is more robust and efficient for complicated problems, such as dynamic events, nonlinear behaviours and complex contact conditions. However, in order to obtain accurate results from the explicit method, the time increment has to be extremely small. Therefore, an explicit analysis typically requires many thousands of increments. It is possible to summarize by stating that the implicit methods are more accurate but require a high computational cost and a careful convergence analysis, while the explicit methods offer less accurate results but are characterised by a low computational cost and do not present problems of non-convergence [23].

2. Modelling wear in Ansys

The following chapter describes the general workflow, the contact settings and wear routine implemented in the Ansys® commercial software. After a brief description of the classic simulation pipeline, the main contact settings, that can be changed for the realization of the chosen finite element model, are explained in the first part. In addition, the requirements and limitations of the wear routine are described in the second one.

2.1 Modelling workflow

The classic workflow (*Fig 2.1*) that characterizes a FEM analysis in the Ansys® software involves the following three phases: Pre-processing (PREP7), Solving (SOLU), Post processing (POST1 or POST26), and Validation. In the first phase the materials are chosen, and the geometry of the model is created. In the second phase the boundary conditions are applied, and the options for the solution are set. In the third step, consistent results are obtained, and the analysis is performed. In the last phase, the results obtained are compared with those coming from experimental tests or with analytical solutions (e.g., Hertz theory) to verify that the solution of the program is reasonable. The Ansys® software workflow is described because the results described below are obtained with it, but there are also others software such as ABAQUS and ALTAIR.

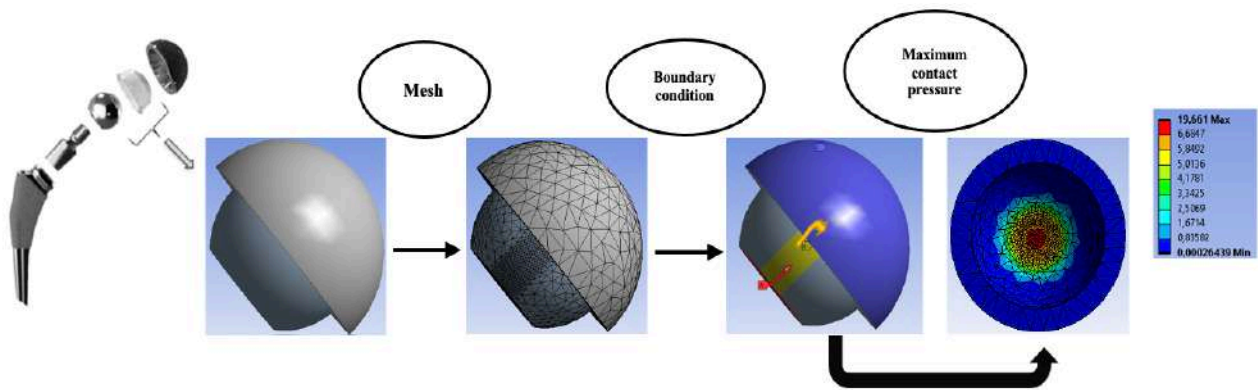
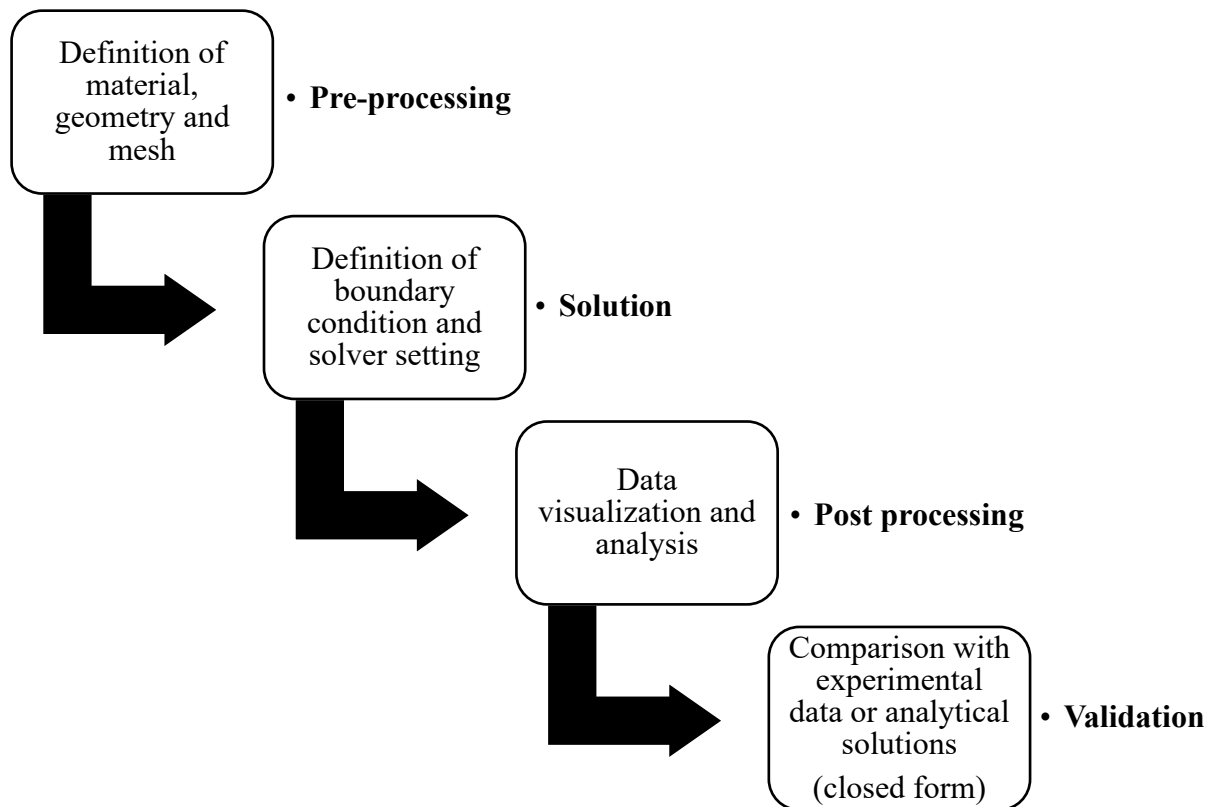


Fig 2. 1 Classic workflow of FEM analysis in ANSYS



2.2 Contact models in Ansys

The main causes of nonlinearity in a FE analysis are the presence of contact between two surfaces, large geometry deformation and material behaviour. As for the geometry, in order to consider its change over time due to the phenomenon of wear, it is necessary to update the mesh by shifting the current nodal coordinates of the contact surface by an amount obtained by the computed wear depth. For hip prostheses case, this is usually done on the radial directions defined with respect to the centre of the original insert and the nodal coordinates of the surface. This aspect will be discussed in more detail in the following chapter on wear.

Contact in the Ansys® Workbench software defines the interaction between two surfaces, called “*Contact*” and “*Target*”. Specifically, it is necessary to choose a contact surface characterised by one or more elements of the following type: *CONTA171*, *CONTA172*...*CONTA177*, and a target surface characterised by *TARGET169* and/or *TARGET170* elements. For three dimensional static structural analyses the most used elements are *CONTA174* (Fig 2.2) and *TARGET170*. The main contact settings are “*Type*”, “*Behaviour*”, “*Formulation*”, “*Small Sliding Contact*”, “*Trim Contact*”, “*Detection Methods*”, “*Penetration Tolerance*”, “*Normal Contact Stiffness*”, “*Pinball Region*” and “*Interface Treatment*” [49], [50].

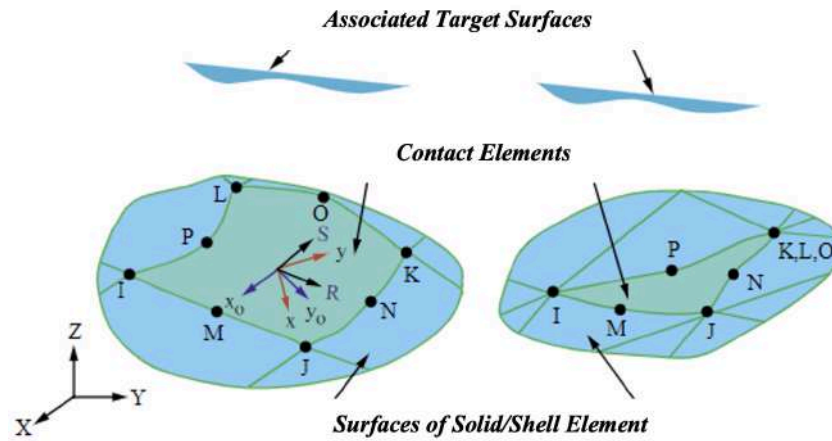


Fig 2. 2 CONTACT174 elements

The “Type” of contact in the Ansys® software can be distinguished in “Bonded”, “No separation”, “Frictionless”, “Rough” and “Frictional”. “Bonded” type, which is the default setting, applies to all contact regions i.e., surfaces, solids, lines, faces, edges. It does not permit penetration, sliding and separation between faces or edges. It also allows for a linear solution because the contact length or area does not change during load application and because two surfaces cannot separate in normal direction. “No Separation” type, compared with “Bonded”, applies only to faces of 3D solids or edges of 2D plates and it permits the sliding between surfaces. “Frictionless” type is standard unilateral contact, and it accepts a nonlinear solution because the contact area may change with the application of the load and because two surfaces can separate in normal direction. In addition, the coefficient of friction is assumed to be zero so as to allow free sliding. “Rough” type is similar to the “Frictionless”, but it models the perfectly rough friction contact not allowing for a sliding, indeed it assumes an infinite coefficient of friction between the bodies. Furthermore, it only applies to faces of 3D solids or edges of 2D plates and, by default, no automatic closing of gaps is performed. “Frictional” type defines an equivalent shear-stress as a function of the contact pressure and the friction coefficient which can take on any value as long as it is positive. Once the shear stress, known as *sticking*, has been overcome, the two geometries begin to slide with respect to each other. As for the friction coefficient, “Frictional” type of contact is based on Coulomb’s law, reported below:

$$F_{tangential} \leq \mu F_{normal} \quad Eq.2.1$$

where μ is the coefficient of static friction, $F_{tangential}$ is the tangential force, which is parallel to the surface, and F_{normal} is the normal force, which is perpendicular to the surface, as described by following figure. Below there is a table that summarises what has been said about the type of contact [49], [50].

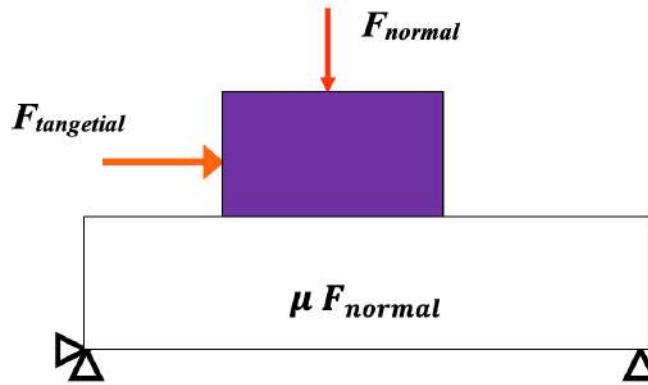


Fig 2. 3 Tangential and normal force

Type of contact	Penetration* ¹	Separation* ²	Sliding
<i>Bonded</i>	No	No	No
<i>No separation</i>	No	No	Yes
<i>Frictionless</i>	No	Yes	Yes ($\mu = 0$)
<i>Rough</i>	No	Yes (No Resistance)	No ($\mu = \infty$)
<i>Frictional</i>	No	Yes	Yes (Resistance $\sim \mu$)

*¹Target cannot penetrate in Contact; *² upwards

The “Behaviour” can be distinguished in “Asymmetric” and “Symmetric”. In the “Asymmetric” behaviour contact and target elements are defined on a single surface, while in the “Symmetric” behaviour contact and target elements are defined on both surfaces. In the “Asymmetric” behaviour the nodes of the contact surface cannot penetrate into the target surface while the opposite is possible (Fig 2.4). On the contrary, in the “Symmetric” behaviour the nodes of the contact and target surfaces cannot penetrate each other [50].

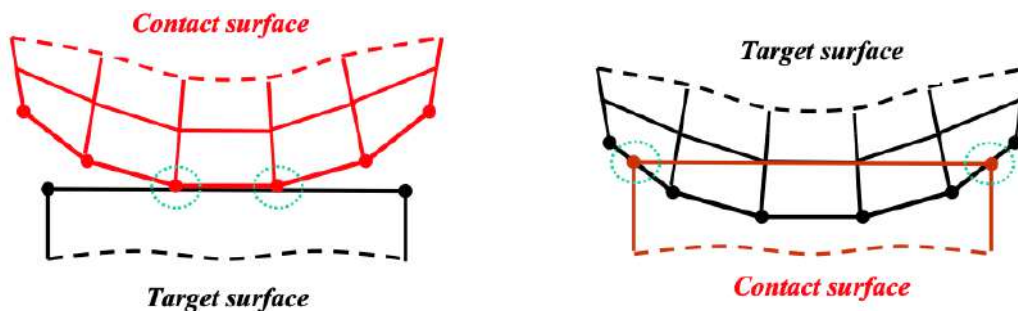


Fig 2. 4 Two bodies in contact with Asymmetric behaviour

The results given by the “Asymmetric” behaviour refer only to the contact surface while those given by the “Symmetric” one refer to both surfaces. For this reason, the interpretation of the data provided by the “Symmetric” behaviour is more complex. For example, in the last case the maximum contact

pressure must be evaluated as the average of both surfaces while in the “*Asymmetric*” case the maximum contact pressure is evaluated only on the contact surface. In addition, the “*Symmetric*” behaviour also results in a higher computational effort. Consequently, in general, the “*Asymmetric*” behaviour is preferred [49], [50].

The following guidelines must be followed when the contact and target surfaces in the “*Asymmetric*” behaviour are defined:

- the convex surface is defined as “*Contact*” whereas the flat or concave surfaces are defined as “*Target*”
- the surface with a fine mesh is defined as “*Contact*” and the surface with a coarse mesh is defined as “*Target*”
- the surface with lower order elements is defined as “*Contact*” while the surface with higher order elements is defined as “*Target*”. However, for 3-D contact with surface nodes the opposite holds
- the softer surface is defined as “*Contact*” and the stiffer surface is defined as “*Target*”
- the larger surface is defined as “*Target*” [50]

A very important aspect of contact is its physical compatibility, that is the impossibility for two surfaces in contact to penetrate each other. For this reason, the Ansys® software offers several different contact formulations to enforce compatibility at the contact interface. The “*Formulations*” can be divided in “*Pure Penalty*”, “*Augmented Lagrange*”, “*Normal Lagrange*” and “*Multi-Point Constraint*” (“*MPC*”). “*Pure Penalty*” formulation is based on the following equation where k_{normal} is the stiffness of material, $x_{penetration}$ is the penetration of the nodes of the contact surfaces into the target surface and F_{normal} is the load (Fig 2.5):

$$F_{normal} = k_{normal} x_{penetration} \quad Eq. 2.2$$

It assumes, for a finite contact force, a very high stiffness, ideally infinite, to neglect the penetration of the nodes. It is recommended for “*Bonded*” and “*No separation*” type of contact.

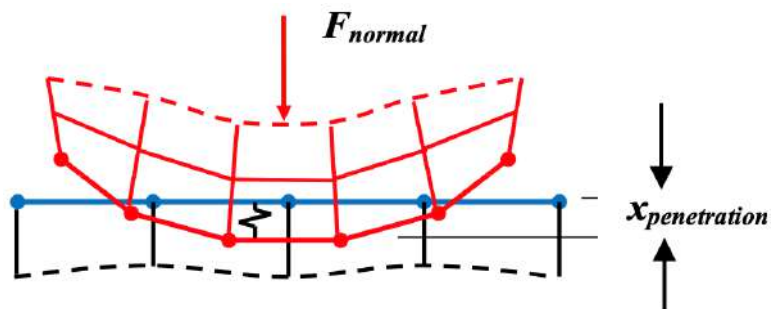


Fig 2. 5 Two bodies in contact with Pure Penalty formulation

“*Augmented Lagrange*” formulation, compared to “*Pure Penalty*” formulation, adds an additional control (λ) to the previous equation in order to reduce the amount of penetration, as shown in the following equation. In other words, it is less sensitive to the magnitude of the contact stiffness and, for this reason, it is preferred in nonlinear problems. It is recommended for general “*Frictionless*” or “*Frictional*” types of contact where large deformations and nonlinearities are present.

$$F_{normal} = k_{normal} x_{penetration} + \lambda \quad Eq. 2.3$$

“*Normal Lagrange*” formulation adds an extra degree of freedom i.e., contact pressure, compared to the previous two formulations to satisfy contact compatibility. As a result, the contact force is explicitly solved as an extra DOF rather than resolving it as contact stiffness and penetration. Therefore, it imposes almost zero penetration, it does not require “*Normal Contact Stiffness*” and it needs a direct solver, which may be more computationally expensive than the other formulations. Moreover, “*Normal Lagrange*” formulation has convergence problems and a high sensitivity to discretization.

Finally, “*Multi-Point Constraint*” formulation adds constraint equations to tie the displacements between touching surfaces. Indeed, it is a direct and efficient way to link surfaces of contact regions which are bonded. This approach is not penalty-based nor Lagrange multiplier-based. Moreover, large deformation effects are supported with “*MPC*”. Below there is a table that summarizes what has been said [49], [50].

	<i>Pure Penalty</i>	<i>Augmented Lagrange</i>	<i>Normal Lagrange</i>	<i>MPC</i>
Convergence	Good (few equilibrium iterations)	Good (many equilibrium iterations)	Good (many equilibrium iterations)	Good (many equilibrium iterations)
Stiffness	Sensitive	Less sensitive	No contact stiffness required	No contact stiffness required
Penetration	Uncontrolled	Controlled	Near-zero	No
Type of contact	All	All	All	Only Bonded
Behaviour	All	All	Asymmetric	Asymmetric
Detection	Gauss Point & Nodes	Gauss Point & Nodes	Nodes	Nodes

“*Small Sliding Contact*” (default option) assumes that the contact surface has a relatively small sliding movement, that is less than 20 % of the contact length, during the entire analysis. Moreover, it assumes that each contact detection point always interacts with the same target element, determined

in the initial configuration. This setting can solve complex contact models for which finite slider logic may encounter some difficulties and models that have low quality geometry or coarse mesh contact regions. However, the small slip assumption must be valid for the entire analysis, otherwise the finished sliding contact must be used [51].

“Trim Contact” option is generally set to “Off” in the presence of large deformations and wear phenomenon that can abruptly change the state of the contact and cause convergence problems. Basically, this setting removes contact and target elements that are outside of the user specified tolerance prior to solving, but it can increase the penetration between two bodies. Moreover, this option ensures that the target elements are meshed across the entire surface of the lower block [49].

The “Detection Methods” can be divided into “Integration Point Detection” and “Nodal Detection” (Fig 2.6). The first one is dubbed “Gauss Point” while the second one can be divided into “Nodal-Normal From Contact”, “Nodal-Normal To Target” and “Nodal-Projection Normal From Contact”. Contact detection at “Gauss Point” is the default option, but in order to use wear routine it is necessary to set the option to “Nodal Detection”. “Nodal Detection” is characterised by smoother pressure plots and longer convergence times. Moreover, it is unstable for some combinations of surfaces. “Pure penalty” and “Augmented Lagrange” formulations use “Gauss Point” detection by default. “Normal Lagrange” and “MPC” formulation use “Nodal Detection” by default [49], [50].

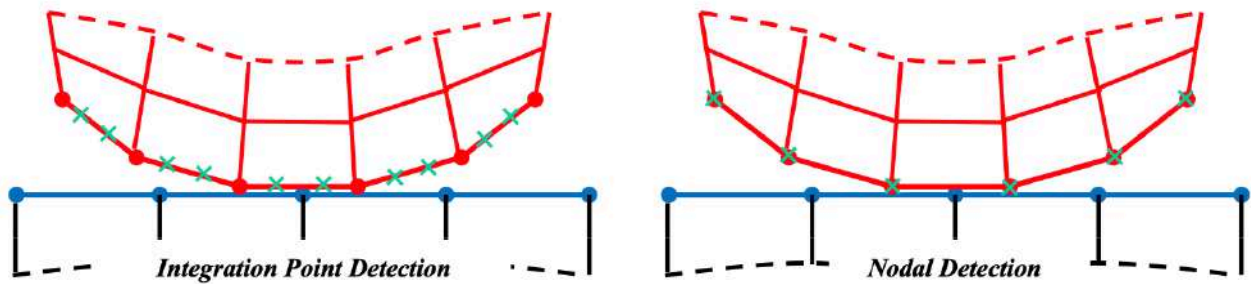


Fig 2. 6 Integration Point Detection vs Nodal Detection when two bodies is in contact

“Penetration Tolerance” is set to 10 % of the element depth, and it is not used to limit the final penetration, but it is a convergence tool [50].

The “Normal Contact Stiffness” (FKN) is the most important parameter that affects accuracy and convergence behaviour. A high stiffness value gives a small penetration, which means a better accuracy but with convergence problems. On the contrary, a small value of stiffness can cause high penetrations, making the contact unphysical. For these reasons, it is necessary to determine a value

of stiffness high enough to provide small penetration, but also low enough to provide adequate convergence tolerance. In general, it is possible to change the FKN by adding a value that is multiplied by the one obtained from the code. Moreover, it is possible to update at each iteration its value to reduce penetration, however the computational cost can increase [49].

The “*Pinball Region*” defines the boundary between near-field and far-field open status (Fig 2.7). The “*Pinball Region*” is the distance calculated by the code or it is user defined. Specifically, the contact elements interaction points (“*Gauss Points*” or “*Nodal Points*”) must be related to a target element in order to the contact to be considered near-field. “*Pinball Region*” is a circle (in 2-D) or a sphere (in 3-D) with its centre in the “*Gauss Points*” or “*Nodal Points*”. The computational cost of contact depends on its size, indeed for distant elements, and therefore open contacts, calculations are simple and require short time, on the contrary when the elements are closed, in other words there is a fine mesh, the calculations are slower. For “*Frictionless*” and “*Frictional*” type of contact, the software checks if the contact and target surfaces are truly touching. If they are touching, the software checks if they are sliding or separating. Afterward, if they are touching and penetrating, the software checks if the penetration exceeds the tolerable amount and it makes adjustments. In other words, for “*Frictionless*” and “*Frictional*” type of contact, if the contact and target elements are close enough to be inside the “*Pinball Region*”, the software makes all sorts of checks and adjustments to make sure that the contact behaviour is adequately captured. Therefore, the “*Pinball Region*” is used because it provides computational efficiency, differentiating between near and far open contact, and because it determines the amount of allowable gap and the depth at which the initial penetration is resolved [49].

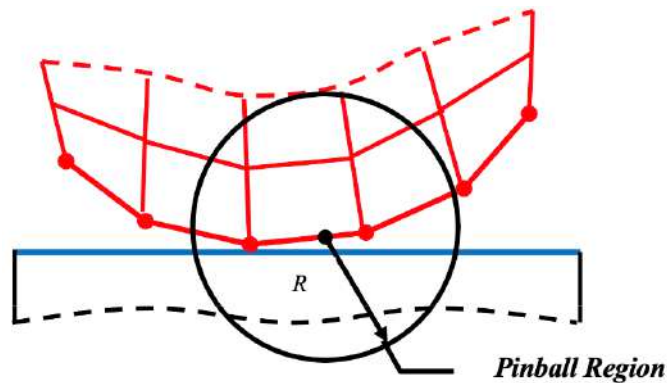


Fig 2. 7 *Pinball Region* when two bodies is in contact

The “*Interface Treatment*” can be divided into “*Adjust To Touch*” and “*Add Offset*” which in turn can be divided into “*Ramped Effects*” and “*No Ramping*”. The first setting allows to close any gap or penetration automatically obtaining a touching position. However, it is important to note that the automatic closure depends on the “*Pinball Region*”, so it is necessary that the radius is greater than

the smallest gap distance. The first setting is useful when the geometry is perfectly tangent, but a tiny gap is created due to the discretization in meshing. The second one allows to specify a positive or negative distance to offset the contact surface. Specifically, a positive value tends to close a gap while a negative value tends to open a gap. Moreover, “*Ramped Effects*” applies the interference gradually over several substeps within a load step, while “*No Ramping*” applies 100 % of the “*Interface Treatment*” in the first step and it is recommended when the convergence is difficult [49].

The Ansys® software allows to define, under the “*Connections*” branch, the so called “*Contact Tool*” (Fig 2.8) to verify the initial information (“*Status*”, “*Gap*”, “*Penetration*”, “*Pinball Region*”, etc.), but also, under the “*Solution*” branch, to verify the final information and the transfer of loads, forces and moments across the various contact regions. Information such as “*Status*”, “*Gap*”, “*Penetration*” and “*Pinball Region*” for each region can be very useful for the verification of the result and the troubleshooting. “*Geometric Gap*” and “*Geometric Penetration*”, for example, are the physical gap and penetration that exist in the contact region between solid bodies. While “*Gap*” and “*Penetration*” values are derived from “*Add Offset*” adjustments [49].

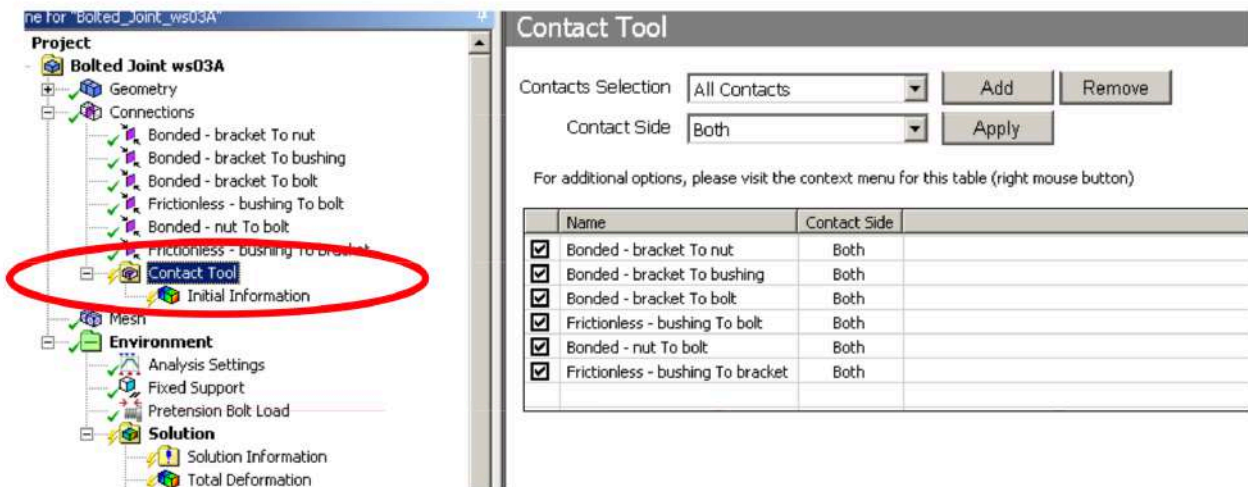


Fig 2. 8 Window of Contact Tool

2.2 Wear routine in Ansys

The wear, as affirmed previously, is the progressive loss of material from the surface of a solid body when it is in contact and in relative motion with respect to another body. Wear modelling in the Ansys® software takes place in two different phases. The first one involves defining the model with which the wear is calculated, for example Archard's law, the second one involves updating the geometry. In other words, the loss of material is simulated by moving the contact nodes based on the

computed wear depth. Archard's law in the Ansys® software is implemented with the following equation:

$$\dot{w} = \frac{dh}{dt} = \frac{K}{H} P^m V^n \quad Eq. 2.4$$

where w is the rate of wear depth (h), K is the dimensionless wear coefficient, H is the hardness of material under wear, P is the contact pressure, m is the exponential coefficient of contact pressure, V is the sliding velocity and n is the exponential coefficient of sliding velocity [50]. The Archard model is implemented inserting a Command Snippets, specifically with *TB*, *WEAR* command and *TBOPT* = *ARCD*. The material constants required by the model are specified as data from constants C1 to C4 on the *TBDATA* command. These constants represent the wear coefficient (K), the hardness of material (H), the contact pressure exponent (m) and the sliding velocity exponent (n). The fifth constant, C5, gives further control on how the Archard model is implemented. The constants C6, C7 and C8 can be used to define the direction cosines of the wear direction. The *TBFIELD* command is used in combination with *TBDATA* if it is necessary to define the wear as a function of temperature and/or time. An example of a Command Snippets, inserted in the contact branch, for the Archard wear model is given in the following figure, where *PINCID* is the name that identifies the contact pair [50].

```

Commands
1  ! Commands inserted into this file will be executed just after the contact region definition.
2  ! The type and mat number for the contact type is equal to the parameter "cid".
3  ! The type and mat number for the target type is equal to the parameter "tid".
4  ! The real number for an asymmetric contact pair is equal to the parameter "cid".
5  ! The real numbers for symmetric contact pairs are equal to the parameters "cid" and "tid".
6
7  ! Active UNIT system in Workbench when this object was created: Metric (mm, kg, N, s, mV, mA)
8  ! NOTE: Any data that requires units (such as mass) is assumed to be in the consistent solver unit system.
9  ! See Solving Units in the help system for more information.
10
11
12  PINCID=CID
13
14  !Wear Material Details
15
16  K1=(1.2E-07)*25  ! (C1) Wear coefficient that include the effect of velocity
17  H1=1             ! (C2) Hardness coefficient
18  m1=1            ! (C3) Pressure coefficient
19  n1=0            ! (C4) Velocity coefficient (=0, because it is included in K1)
20  C5=0            ! (C5) Use contact pressure in the wear calculations
21
22  TB,WEAR,PINCID,,ARCD  !ACTIVATE WEAR MODEL
23  TBFIELD,TIME,0        !WEAR PROPERTIES WILL BE DEFINED FOR TIME = 0
24  TBDATA,1,0,1,1,0,0   !NO WEAR FOR CONTACT ELEMENTS
25  TBFIELD,TIME,1        !WEAR PROPERTIES WILL BE DEFINED FOR TIME = 1
26  TBDATA,1,0,1,1,0,0   !NO WEAR FOR CONTACT ELEMENTS
27  TBFIELD,TIME,1.0001  !WEAR PROPERTIES WILL BE DEFINED FOR TIME = 1.0001
28  TBDATA,1,K1,H1,m1,n1,C5 !ASSIGN WEAR PROPERTIES TO CONTACT ELEMENTS
29  TBFIELD,TIME,200     !WEAR PROPERTIES WILL BE DEFINED FOR TIME = 200
30  TBDATA,1,K1,H1,m1,n1,C5 !ASSIGN WEAR PROPERTIES TO CONTACT ELEMENTS
31

```

Fig 2. 9 Command Snippets for wear routine

Wear calculations are based on contact pressure by default. However, when the fifth constant is set to 1 rather than zero, the calculations are based on the nodal stresses of the solid elements beneath the contact elements instead of contact pressure. This option is preferable for “Symmetric” contact behaviour, because the stress distribution of the underlying elements is often smoother than the

contact pressure distribution. Therefore, the nodal stresses allow for a more uniform pattern. However, the real advantage of this setting is still unclear and under discussion [50].

The wear increment, calculated as the product between the wear rate and the increase over time, is the same for each element by averaging the increase of wear on the contact area with both behaviours. The wear direction for each contact point is opposite to the normal contact at that point and it is specified through the wear increment. However, a direction can be specified through the constants C6, C7 and C8 on the *TBDATA* control, as mentioned above. It is very important to note that the repositioning nodes leads to a loss of equilibrium, consequently an additional iteration is required to achieve convergence, which is easier to achieve with small time increments [50].

Wear process worsens the quality of the underlying solid elements, blocking the simulation due to element distortion, as shown in the following figure.

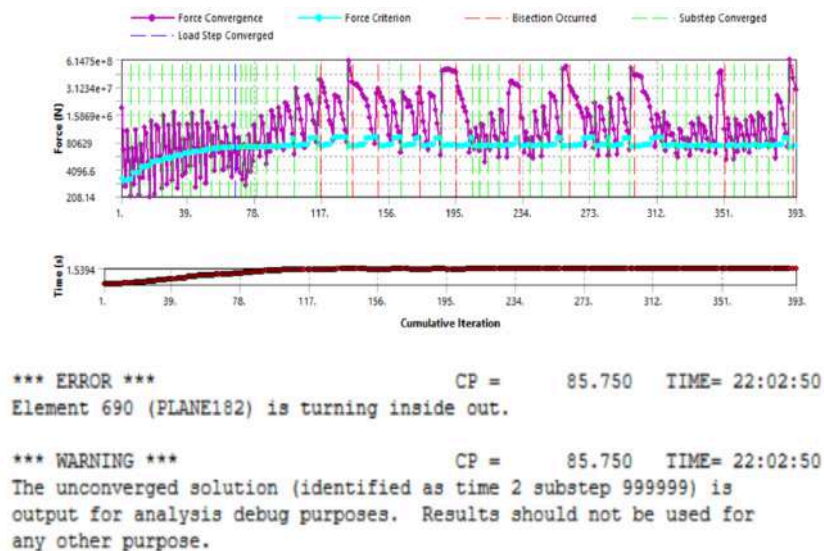


Fig 2. 10 Example of error due to wear process

To overcome possible errors due to wear and continue the analysis, mesh nonlinear adaptivity routine or manual rezoning can be used to improve the mesh. Mesh nonlinear adaptivity routine (Fig 2.12), inserted as a Command Snippets in the “*Static Structural*” branch, provides that accumulated wear and lost volume are initialised to zero when the analysis restarts because the geometry is updated. Mesh nonlinear adaptivity routine, used by both types of contacts behaviours, requires the definition of contact elements that are undergoing wear (*CONWEARELEM*) and the definition of the command *NLADAPTIVE* or *NLAD* with wear option in order to trigger adaptivity based on a “*Critical Ratio*” [49], [50].

```

Commands
1  ! Commands inserted into this file will be executed just prior to the ANSYS SOLVE command.
2  ! These commands may supersede command settings set by Workbench.
3
4  ! Active UNIT system in Workbench when this object was created: Metric (mm, kg, N, s, mV, mA)
5  ! NOTE: Any data that requires units (such as mass) is assumed to be in the consistent solver unit system.
6  ! See Solving Units in the help system for more information.
7
8
9  /SOLU
10
11 !Define component for NLAD
12 allsel,all,all
13 esel,s,type,,PINCID
14 cm,CONWEARELEM,elem
15 allsel,all,all
16
17 !Define non linear adaptivity criterion
18 NLAD,CONWEARELEM,ADD,CONTACT,WEAR,0.80 !MORPH AFTER 80% IS LOST IN WEAR
19 NLAD,CONWEARELEM,ON,ALL,ALL,1,,200
20 NLAD,CONWEARELEM,LIST,ALL,ALL
21

```

Fig 2. 11 Command Snippets for mesh nonlinear adaptivity

In the figure above, the adaptivity of the mesh runs whenever wear, at any contact point, exceeds 80 % of the average height of underlying solid contact elements. Moreover, it is also important to define the timing of activation of the criterion. In this case, the criterion is checked at each step and the total duration is 200 seconds.

The requirements to implement the wear routine in the Ansys ® software and the current limitations are listed below [49], [50].

1. Wear is only active for quasi-static and transient dynamic analysis.
2. It is recommended the use of solid structural elements or matched solid structural elements for the underlying elements (under the contact elements). Specifically, the solid elements recommended are *PLANE182*, *PLANE183*, *SOLID185*, *SOLID186*, *SOLID187*, and/or *SOLID285*. Moreover, wear routine is not available for laminated solids.

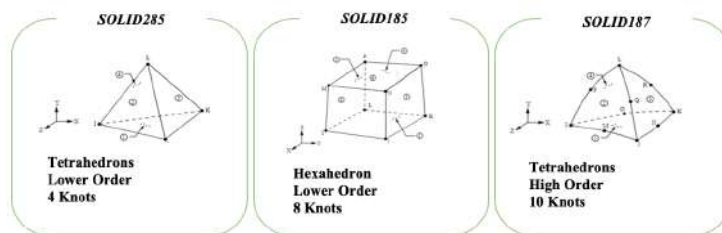


Fig 2. 12 SOLID285 vs SOLID 185 vs SOLID187

3. It is recommended to use “*Augmented Lagrangian*” ($KEYOPT(2) = 0$) or “*Pure Penalty*” formulation ($KEYOPT(2) = 1$). Other algorithms, such as “*MPC*” ($KEYOPT(2) = 3$) formulation may be characterised by convergence problems.

4. Wear is only available when the contact detection point is a "Nodal Point" ($KEYOPT(4) = 1, 2 \text{ or } 3$). Specifically it is recommended the detection method of "Nodal-Normal To Target" ($KEYOPT(4) = 2$).
5. Wear is available for "Frictionless" ($KEYOPT(12) = 2$), "Rough" ($KEYOPT(12) = 3$) and "Frictional" ($KEYOPT(12) = 4$) types of contact.
6. It is recommended to use the "Asymmetric" behaviour to shape the wear. However, the "Symmetric" contact behaviour can be used if wear affects both surfaces of bodies, but it can also be obtained by defining two "Asymmetric" behaviours.
7. The substeps must be very small in order to reduce the increase of wear. A large increase can abruptly modify the state of contact and it causes difficulties of convergence.
8. To capture accurately the contact pressure distribution a very fine mesh is required at the interface. However, the computational effort can drastically increase.
9. In case of high wear, it is recommended to use mesh nonlinear adaptivity routine to improve the quality of the mesh by morphing it. Specifically, the geometry is updated, and the wear is initialised to zero at each time. Moreover, it is necessary to define the "Critical Ratio" as the relationship between the amount of wear and the underlying solid element's height.
10. Mesh nonlinear adaptivity routine and manual rezoning are available for elements *CONTA171*, *CONTA172* and *CONTA174*.

In order to visualize the wear results, precisely, the wear volume and the wear depth, it is necessary to proceed as follows: for the wear volume it is required to insert in "Solution Information" a "Contact Tracker", specifying as type "Volume Loss Due to Wear". In the same way it is possible to display other quantities such as maximum contact pressure, contact air, etc. For the wear depth, instead, it is necessary to insert in "Solution" a "User Defined Result", using a specific command according to the type of contact element used. As an example, for the *CONTA174* elements it is possible to calculate the wear depth in a particular direction and at a particular node, as described in the following image [49].

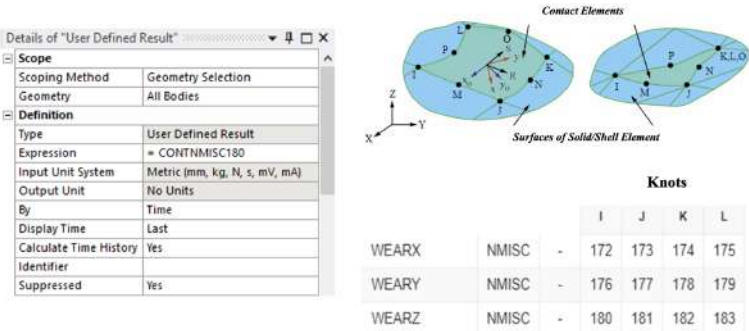


Fig 2. 13 User Defined Result to calculate wear depth for *CONTA174* elements

3. Simulating pin-on-disc and pin-on-plate wear tests with Ansys

3.1 Sensitivity analysis on the main input model parameters of *hard-on-hard* bearings

The following two sections explain the test case description and the finite element model of pin on disc. The third one compares the results of the experimental test with those obtained from the model.

3.1.1 Test case description

The finite element wear model of pin on disc is validated by comparing the results obtained in terms of wear depth with those determined by *Podra et al* in 1999 [52] in their experiment. The last one describes a pin on disc test, where both bodies are made of metallic material and where the final wear depth of the pin and wear coefficient are obtained experimentally.

In *Podra's* experiment, the pin has a spherical tip with a radius of 5 mm, and it is subjected to a load of 200 N. The pin axis is positioned at a distance equal to 19.7 mm from the disc axis and it is subjected to a sliding velocity of 25 mm/s for a total of 120 s, equal to a sliding distance of 3 m. Both the pin and the disc are made of steel with an elastic modulus of 210 GPa and a Poisson's coefficient equal to 0.3.

The dimensional wear coefficient (k), obtained from *Podra's* experiment, and used in the simulation is equal to:

$$k = 1.25 \times 10^{-7} \text{ MPa}^{-1} \quad \text{Eq. 3.1}$$

Therefore, according to Hertz's theory and Archard's law, the contact area radius (Semi Hertian impression area), the maximum contact pressure and the wear volume are equal to:

$$a_h = 8 \text{ } \mu\text{m} \quad \text{Eq. 3.2}$$

$$P_{max} = 1294.5 \text{ MPa} \quad \text{Eq. 3.3}$$

$$V_{wear} = 7.875 \times 10^{-3} \text{ mm}^3 \quad \text{Eq. 3.4}$$

3.1.2 Model inputs and scheme used for the analyses

The characteristics of the two materials, such as elastic modulus and Poisson's coefficient are modified in the “Engineering Data” block of the “Static Structural” of project (Fig 3.1). Specifically, the pin and the disc have an elastic modulus of 210 GPa and a Poisson’s coefficient of 0.3.

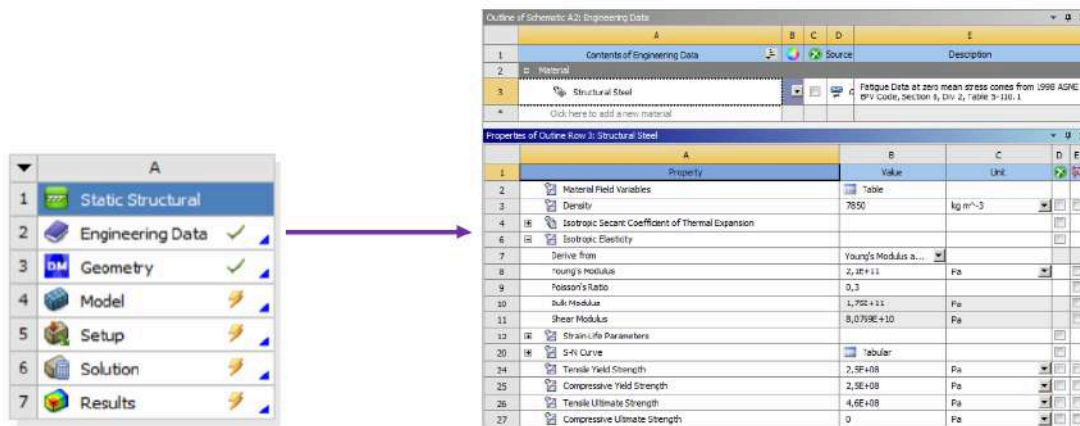


Fig 3. 1 Window of Engineering Data

The following geometric model (Fig 3.2) is created using Design Modeler. Firstly, the pin is made as a half sphere using the “Primitives” command in the section “Create” and the “Boolean” tool in the same section by setting the “Sphere”, with a radius of 5 mm, as the “Target Body” and the “Box”, with dimensions and positions so that the radius of the sphere is equal to 5 mm, as the “Tool Body”. Then the disk is made like the pin but using the “Cylinder” with a size of 5 mm. When performing Boolean operations on two or more bodies it is necessary to set the “Box Operation group details” to “Add Freeze” option. In addition, before making the geometry, it is important to change the measuring system so that the results obtained are consistent with the experimental ones.

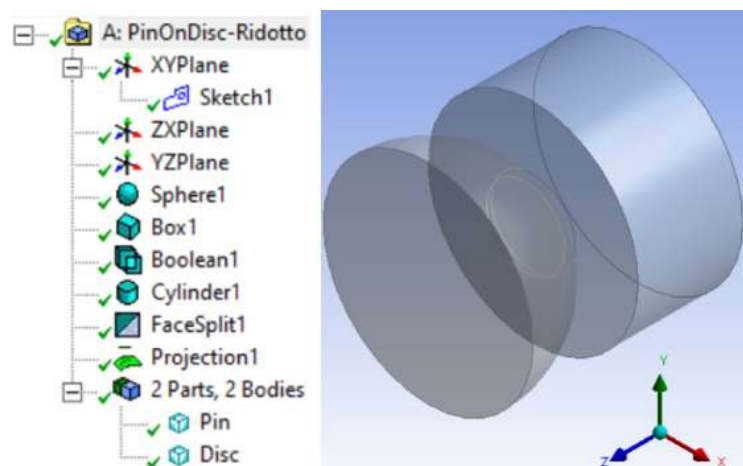


Fig 3. 2 Definition of the geometry of unilateral hard-on-hard pin on disc

As for the mesh, the “*Element Order*” in “*Defaults*” item is set to “*Linear*” (*SOLID185*). However, it could also be set to “*Quadratic*” (*SOLID187*) although this would increase the computational cost. The “*Error Limits*” in “*Quality*” item is set to “*Standard Mechanical*”, which uses quality error limits that are less strict than those used by Mechanical APDL. The last one uses the default setting, called ‘*Aggressive Mechanical*’. Afterward, a “*Method*” is inserted by selecting the two bodies as “*Geometry*” and by setting them as “*Method Tetrahedrons*”. Then it is added a “*Face Sizing*” with a dimension of 0.088 mm to increase the number of nodes and elements in the contact area in order to obtain more satisfactory results and to decrease the computational effort. For this purpose, it is drawn on the *XY* plane with the “*Sketch*” command a circumference of radius 4 mm and it is used the “*Face Split*” tool where the upper surface of the disk is selected as “*Target Face*” and the “*Sketch*”, previously drawn, as “*Tool Geometry*”. To obtain the projection of the “*Face Split*” on the pin it is used the “*Projection*” tool where the “*Sketch*” previously drawn is selected as “*Edges*” and the half sphere as “*Target*”. The total number of nodes and elements in the model is, respectively, 7257 and 27345. The complete mesh and that of the individual bodies are shown in the following figure.

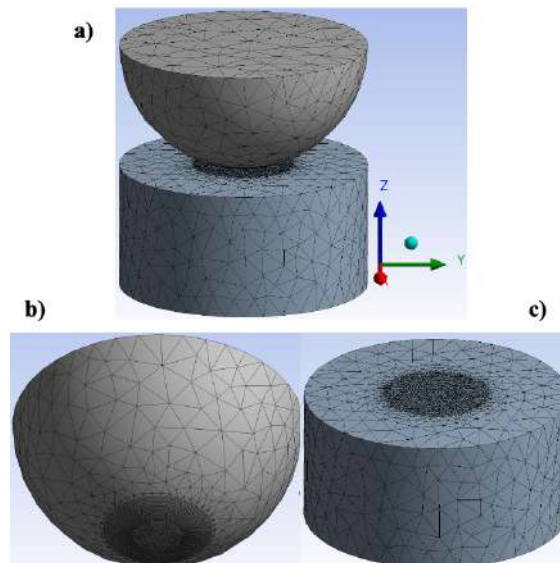


Fig 3. 3 a) Mesh of pin on disc; b) mesh of pin; c) mesh of disc

Another important aspect concerns the definition of the contact area between pin and disc. Contact settings (Fig 3.4) are defined in the Connections folder. The pin surface is modelled as “*Contact Body*” and the disc surface as “*Target Body*”. Specifically, 3D linear eight-node elements (*CONTA174*) are used for contact elements and 3D linear eight-node elements (*CONTA170*) are used for target elements. In addition, *CONTA174* elements, which do not support the remeshing routine which is the reason why the remeshing routine would not seem to work in Workbench, can also be used with first-order solid elements since the mid-side nodes are automatically eliminated. The

“Type”, the “Behaviour”, the “Trim Contact” of the “Definition” item are set, respectively, to “Frictionless”, “Asymmetric” and “Off”. The “Formulation” of the “Advanced” item is set to “Augmented Lagrange” with an automatic stiffness calculation and an updating at each iteration by setting “Update Stiffness” to “Each Iteration”. Other settings of them make the system labile. The “Advanced” of “Detection Method” item is set to “Nodal-Normal To Target” because, in order to activate the wear routine in the Ansys® software, it is necessary that the integration points are “Nodal Points” and not “Gauss Point”. “Pinball Region” is set to “Radius” and its size is 2 mm. Finally, the “Interface Treatment” of the “Geometric Modification” item is set to “Adjust To Touch”, other settings make the system labile.

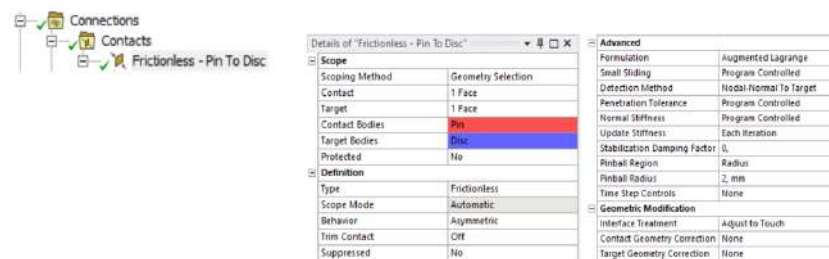


Fig 3. 4 Settings for contact options of unilateral hard-on-hard pin on disc

Moreover, an APDL Command Snippets is added to simulate the phenomenon of wear (Fig 3.5). Specifically, the kinematics is modelled by multiplying the wear coefficient by the sliding velocity. Therefore, the sliding velocity is uniform throughout the contact zone and equal to the multiplicative coefficient inserted at the end of the wear coefficient. In other words, the relative sliding movement is translatory and not rotational, indeed, in the last case the linear velocity varies depending on the radius while the angular velocity remains constant. Consequently, the implicit kinematics, which reduces the computational cost compared to the explicit one, is subject to a simplification that involves an error.

```

Commands
.....
1  ! Commands inserted into this file will be executed just after the contact region definition.
2  ! The type and mat number for the contact type is equal to the parameter "cid".
3  ! The type and mat number for the target type is equal to the parameter "tid".
4  ! The real number for an asymmetric contact pair is equal to the parameter "cid".
5  ! The real numbers for symmetric contact pairs are equal to the parameters "cid" and "tid".
6
7  ! Active UNIT system in Workbench when this object was created: Metric (mm, kg, N, s, mV, mR)
8  ! NOTE: Any data that requires units (such as mass) is assumed to be in the consistent solver unit system.
9  ! See Solving Units in the help system for more information.
10
11
12  PINCID=CID
13
14  !Wear Material Details
15
16  K1=(1.2E-07)*25      !(C1) Wear coefficient that include the effect of velocity
17  H1=1                !(C2) Hardness coefficient
18  m1=1                !(C3) Pressure coefficient
19  n1=0                !(C4) Velocity coefficient (=0, because it is included in K1)
20  CS=0                !(C5) Use contact pressure in the wear calculations
21
22  TB,WEAR,EINCID,,,ARCD  !ACTIVATE WEAR MODEL
23  TBFIELD,TIME,0         !WEAR PROPERTIES WILL BE DEFINED FOR TIME = 0
24  TBDATA,1,0,1,1,0,0    !NO WEAR FOR CONTACT ELEMENTS
25  TBFIELD,TIME,1        !WEAR PROPERTIES WILL BE DEFINED FOR TIME = 1
26  TBDATA,1,0,1,1,0,0    !NO WEAR FOR CONTACT ELEMENTS
27  TBFIELD,TIME,1.0001   !WEAR PROPERTIES WILL BE DEFINED FOR TIME = 1.0001
28  TBDATA,1,K1,H1,m1,n1,CS !ASSIGN WEAR PROPERTIES TO CONTACT ELEMENTS
29  TBFIELD,TIME,200      !WEAR PROPERTIES WILL BE DEFINED FOR TIME = 200
30  TBDATA,1,K1,H1,m1,n1,CS !ASSIGN WEAR PROPERTIES TO CONTACT ELEMENTS
31

```

Fig 3. 5 Command Snippets for wear routine of unilateral hard-on-hard pin on disc

Boundary conditions (Fig 3.6) are defined within the section “Static Structural”. Precisely, a “Fixed Support” is added on the upper face of the pin while a “Force” with intensity of 21 N is applied on the lower face of the disc and a free “Displacement” along Z axis is applied on the side face of the disc.

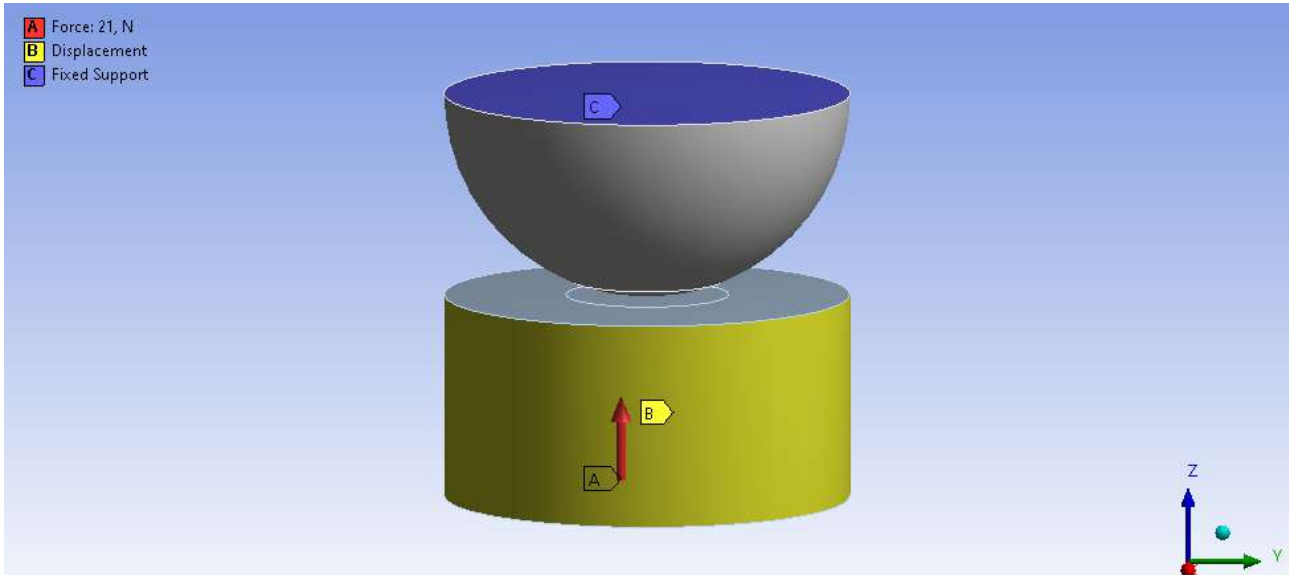


Fig 3. 6 Boundary conditions of unilateral hard-on-hard pin on disc

In the same section of the boundary conditions an APDL Command Snippets (Fig 3.7) is inserted to allow the updating of the mesh. The *NLAD* command is used to smooth out the distorted elements during the wear simulation, defining a “Critical Ratio” equal to 0.8. Specifically, when the ratio between the wear volume and the initial volume of the underlying contact elements exceeds 0.8, the software restarts the analysis with an improved mesh.

```

Commands
1  ! Commands inserted into this file will be executed just prior to the ANSYS SOLVE command.
2  ! These commands may supersede command settings set by Workbench.
3
4  ! Active UNIT system in Workbench when this object was created: Metric (mm, kg, N, s, mV, mA)
5  ! NOTE: Any data that requires units (such as mass) is assumed to be in the consistent solver unit system.
6  ! See Solving Units in the help system for more information.
7
8
9  /SOLU
10
11 !Define component for NLAD
12 allsel,all,all
13 esel,s,type,,PINCID
14 cm,CONWEARELEM,elem
15 allsel,all,all
16
17 !Define non linear adaptivity criterion
18 NLAD,CONWEARELEM,ADD,CONTACT,WEAR,0.80 !MORPH AFTER 80% IS LOST IN WEAR
19 NLAD,CONWEARELEM,ON,ALL,ALL,1,,200
20 NLAD,CONWEARELEM,LIST,ALL,ALL
21

```

Fig 3. 7 Command Snippets for remeshing of unilateral hard-on-hard pin on disc

As for the analysis settings (Fig 3.8), they include two steps with a duration of one second and 120 seconds respectively. The first one is characterised by a force applied gradually, through a ramp, up to the value of 21 N that are necessary to calculate the maximum contact pressure and to ensure the convergence of the solution. In other words, this is useful to ensure the contact during the entire simulation. The second one, where the wear routine is simulated, is characterised by a free displacement along the Z component and equal to zero along the other two to ensure the convergence. In addition, “Auto Time Step” is set to “On”, “Define By” is set to “Time” and “Initial Time Step and Minimum Time Step” to 0.01 second and “Maximum Time Step” to 0.1 second to ensure convergence. Finally, “Large Deflection” is set to “On” because the analysis is nonlinear.

Details of "Analysis Settings"	
Step Controls	
Number Of Steps	2,
Current Step Number	2,
Step End Time	121, s
Auto Time Stepping	On
Define By	Time
Carry Over Time Step	Off
Initial Time Step	1,e-002 s
Minimum Time Step	1,e-002 s
Maximum Time Step	0,1 s
Solver Controls	
Solver Type	Program Controlled
Weak Springs	Off
Solver Pivot Checking	Program Controlled
Large Deflection	On
Inertia Relief	Off
Rotordynamics Controls	
Restart Controls	
Nonlinear Controls	
Advanced	
Output Controls	
Analysis Data Management	
Visibility	

Fig 3. 8 Analysis Settings options of unilateral hard-on-hard pin on disc

A mesh convergence and a sensitivity analysis are then performed, in which the trend of wear volume and the maximum contact pressure is studied as function of some contact setting parameters. Precisely, regarding the mesh, it is possible to observe the trend of the maximum contact pressure by changing the order of the elements: linear or quadratic. Moreover, it is possible to observe the trend of the maximum contact pressure, wear volume and wear depth by changing the type of elements: tetrahedral or hexahedral. As for the contact settings, it is possible to observe how the maximum contact pressure varies according to the choice of "Formulation", "Detection Method" and "Type". It is also possible to observe how the maximum contact pressure varies according to the value of "Normal Stiffness".

3.1.3 Results

The following sections, as mentioned before, compares the results in terms of maximum contact pressure, wear volume and wear depth obtained from an implicit pin on disc model with Hertz's theory, Archard's law and the experimental results of *Podra et al.* In addition, the conclusions obtained following a sensitivity analysis of the mesh and contact settings are reported.

As for the maximum contact pressure, the analytical value calculated using Hertz's theory is:

$$P_{max} = 1294.5 \text{ MPa} \quad \text{Eq. 3.5}$$

The maximum contact pressure value determined by the pin on disc model in the unworn conditions is:

$$P_{max} = 1297.1 \text{ MPa} \quad \text{Eq. 3.6}$$

Therefore, the finite element model predicts the maximum contact pressure with a high level of accuracy, the error is less than 3 %. The maximum contact pressure trend as function of time is shown in the figure below. It can be seen that the maximum contact pressure decreases rapidly during the first wear cycles as the contact area increases, resulting in a more compliant contact, as affirmed in literature [4], [52], and converges to a value of approximately 30 MPa.

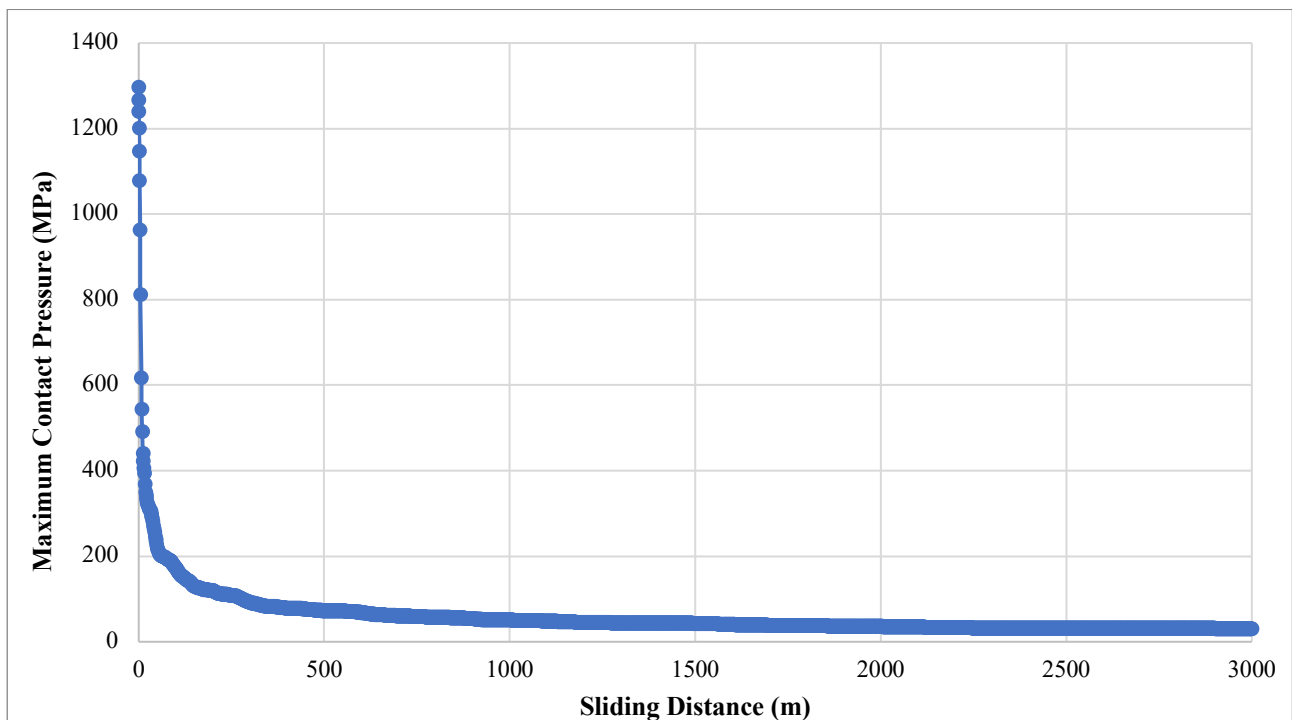


Fig 3. 9 Trends of maximum contact pressure of unilateral hard-on-hard pin on disc

As for the wear volume, the analytical value calculated using Archard's law is:

$$V_{wear} = 7.875 \times 10^{-3} \text{ mm}^3 \quad \text{Eq. 3.7}$$

The wear volume determined by the pin on disc model after 3000 metres is:

$$V_{wear} = 7.880 \times 10^{-3} \text{ mm}^3 \quad \text{Eq. 3.8}$$

Therefore, the finite element model predicts the wear volume with a high level of accuracy, the error is less than 1 %. The wear volume trend is shown in figure below as a function of the sliding distance. It can be seen that the wear volume trend is linear, confirming the correct implementation of Archard's law in the wear routine in the Ansys ® software.

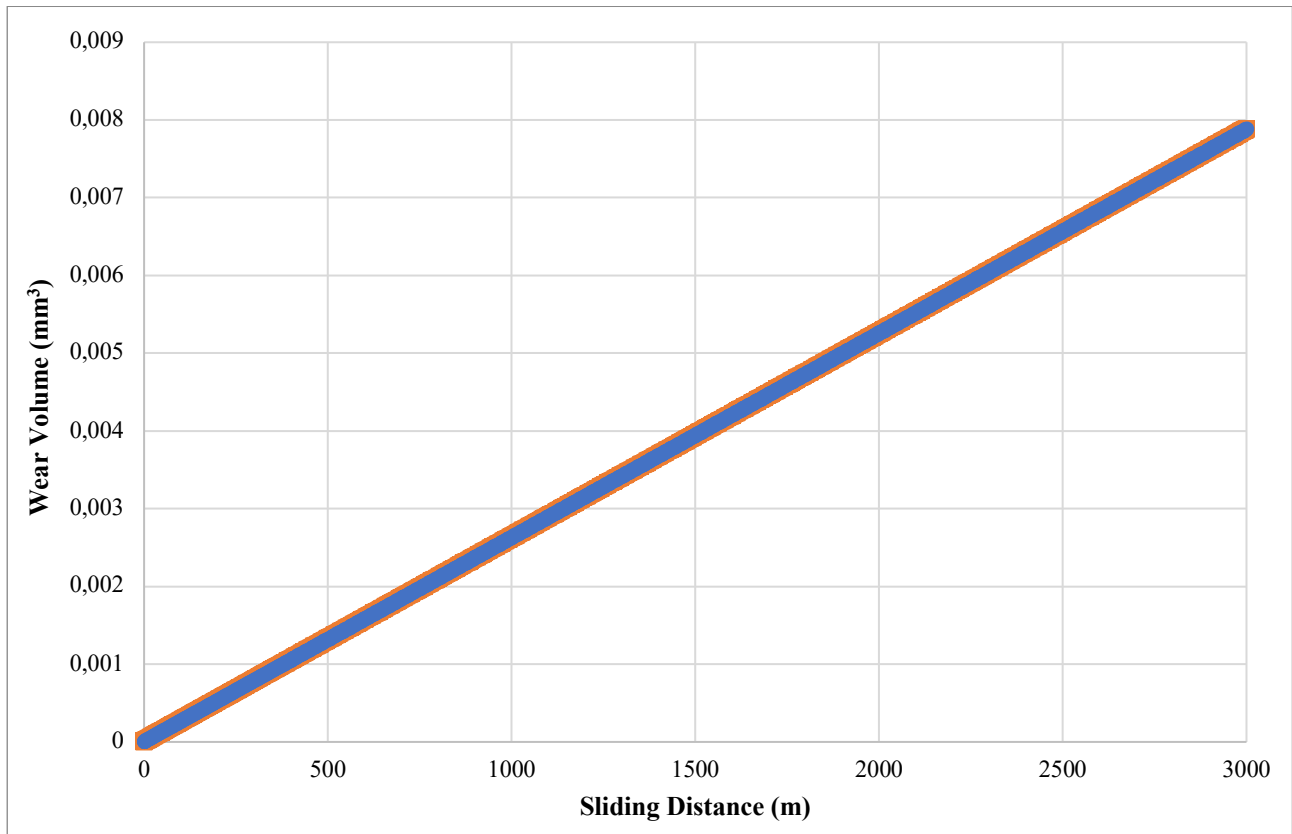


Fig 3. 10 Trends of wear volume of unilateral hard-on-hard pin on disc

As for the wear depth, the experimental value obtained by Podra et al [52] is:

$$h_{wear} = 23.16 \mu\text{m} \quad \text{Eq. 3.9}$$

The wear volume determined by the pin on disc model after 3000 metres is:

$$h_{wear} = 21.6 \mu m \quad Eq. 3.10$$

Therefore, the finite element model predicts the wear depth with a high level of accuracy, the error is less than 7 %. The wear depth trend as a function of the sliding distance is shown in figure below. It can be seen that the wear depth trend is not linear, as expected.

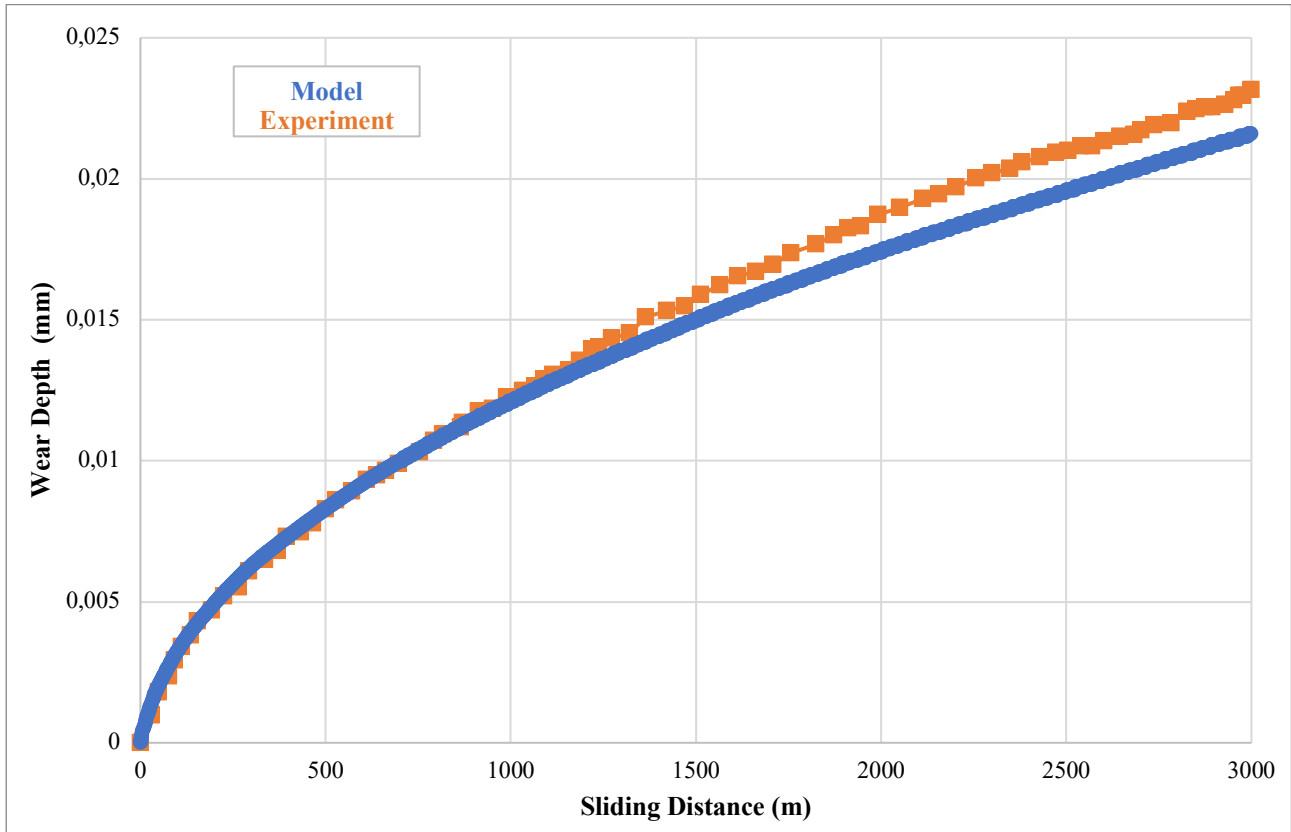


Fig 3. 11 Trends of wear depth of unilateral hard-on-hard pin on disc

Regarding the sensitivity analysis, specifically for the type of element, the trends of the maximum contact pressure as a function of time, considering linear and quadratic elements, are observed keeping the other contact parameters unchanged. It is possible to affirm, observing the figure below, that it is necessary to use the linear elements (*SOLID185*) because the trend of the maximum contact pressure is convergent as opposed to that obtained using the quadratic elements (*SOLID187*) which is oscillating. Therefore, even if, in general, it is preferred to use the quadratic elements, the linear elements, to date, are preferred to simulate the phenomenon of wear.

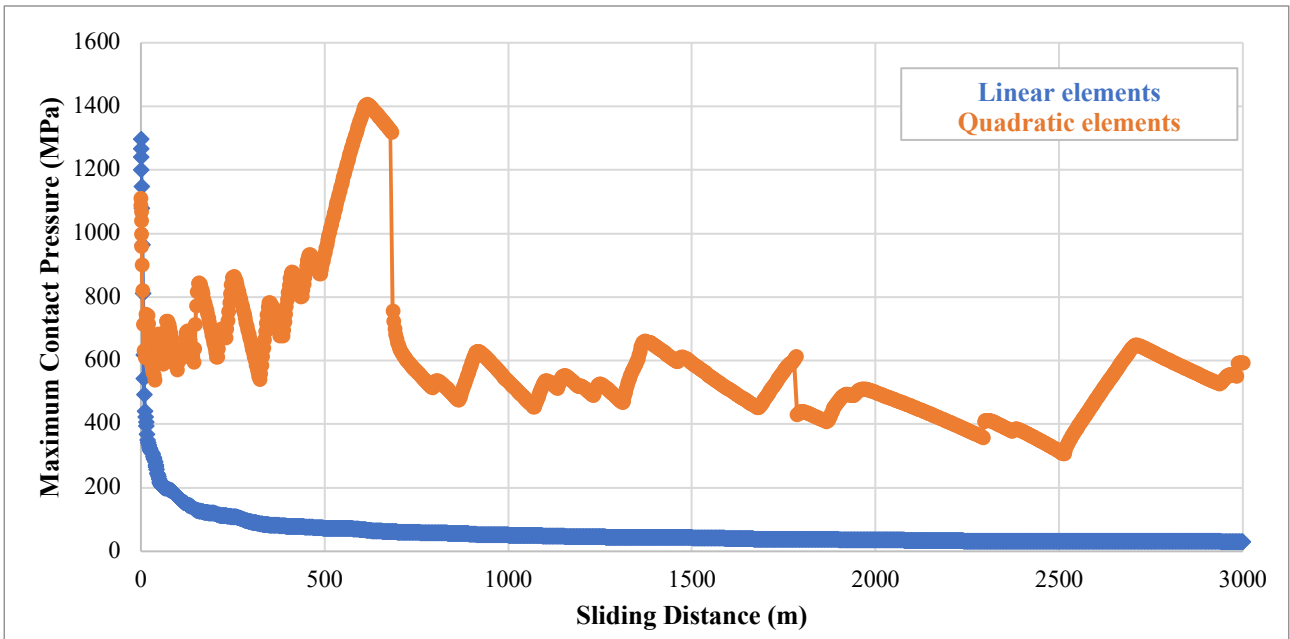


Fig 3. 12 Trends of maximum contact pressure of unilateral hard-on-hard pin on disc with linear and quadric elements

As for the element's types, it is possible to affirm, comparing the trends of maximum contact pressure shown in the figure below, that they decrease rapidly as a result of the increasing contact area and they converge to a value of 30 MPa. However, the maximum contact pressure at one second calculated with hexahedral elements is 1282.5 MPa with an error of 0.93 % compared to the value obtained by Hertz's theory, while the error obtained with tetrahedral elements is 0.2 %, as previously reported.

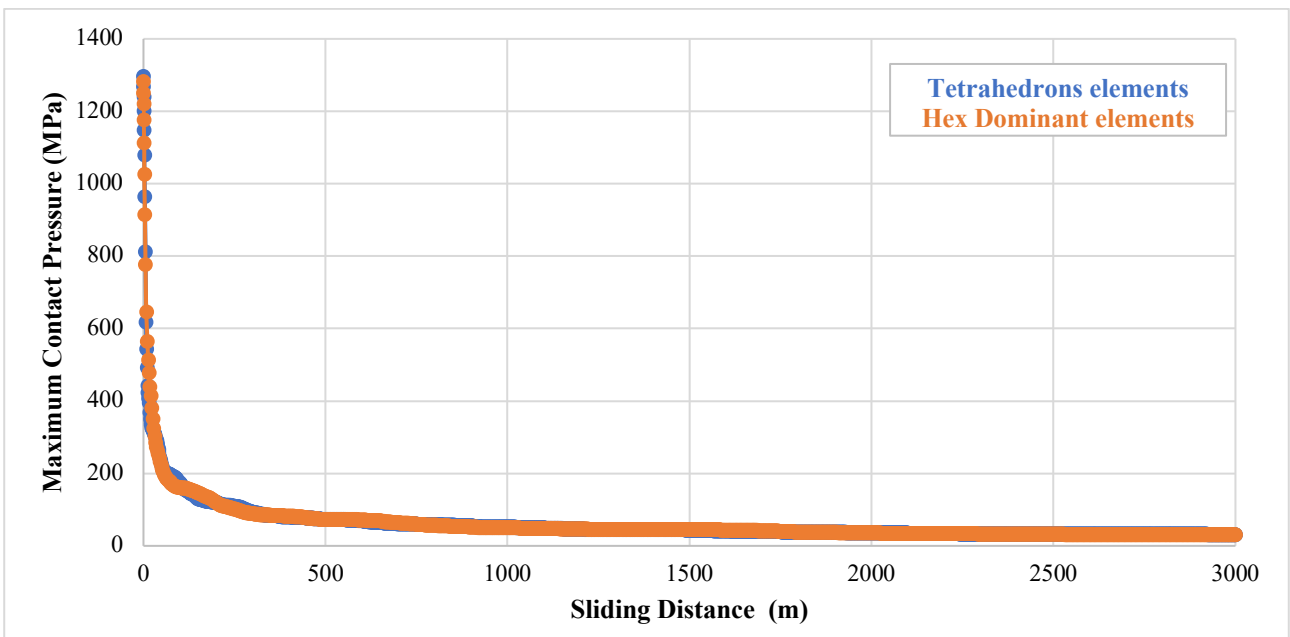


Fig 3. 13 Trends of maximum contact pressure of unilateral hard-on-hard pin on disc with tetrahedrons and hexahedrons elements

Comparing the trends of the wear volume as a function of the sliding distance, shown in the figure below, it is possible to observe that they are perfectly overlaid. Specifically, both trends are linear, confirming the correct implementation of Archard's law. Moreover, the final value obtained with hexahedral elements is equal to that obtained with tetrahedral ones.

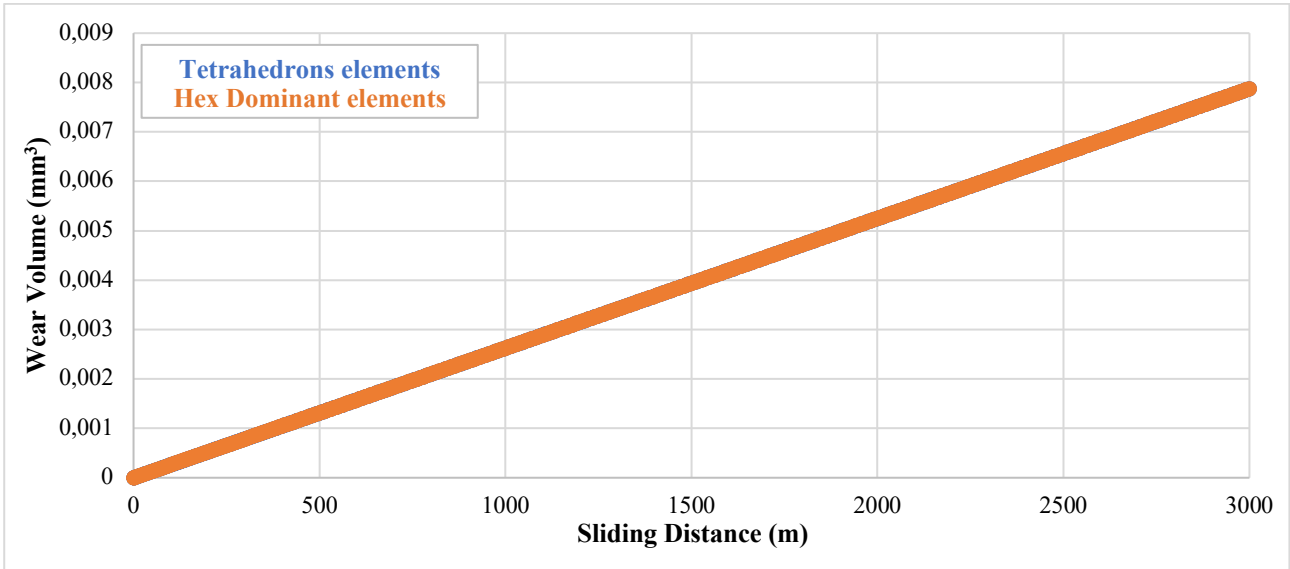


Fig 3. 14 Trends of wear volume of unilateral hard-on-hard pin on disc with tetrahedrons and hexahedrons elements

Comparing the trends of the wear depth, shown in the figure below, it is possible to observe that the wear depth trends are not linear. Moreover, the final value obtained with hexahedral elements is better than that obtained with the tetrahedral ones. Specifically, the error obtained with tetrahedral elements is 6.7 % while that obtained with hexahedral ones is 5 %.

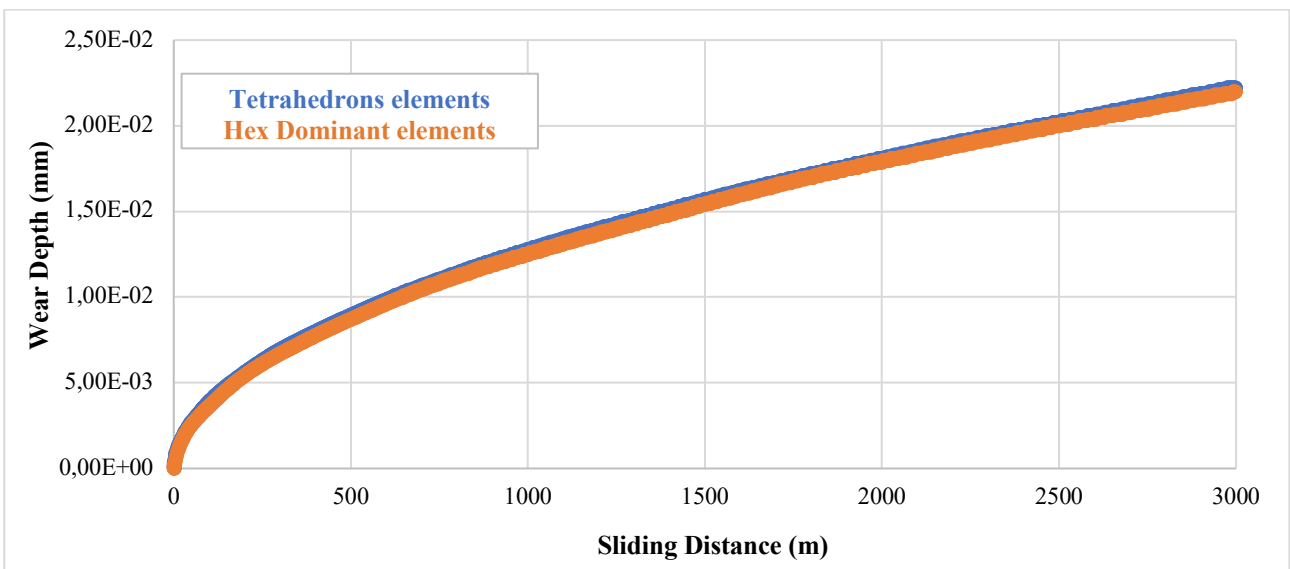


Fig 3. 15 Trends of wear depth of unilateral hard-on-hard pin on disc with tetrahedrons and hexahedrons elements

In conclusion, it is possible to state that it is convenient in this specific case to use tetrahedral elements because, although the use of hexahedral elements improves the prediction in terms of wear depth, the computational cost is almost double. This can be justified by the fact that in the model where hexahedrons are used, 739993 nodes and 94721 elements must be used to obtain results in line with the experiment of *Podra et al.* The model with hexahedral elements realized considering the one with tetrahedral elements but changing the type of elements without making changes (which is the one described above) estimates wear volume and wear depth in a manner consistent with the previous two models. However, the maximum contact pressure at one second predicted by the following model is 1000 N presenting therefore a clear difference. While it settles at around 30 MPa after 121 seconds, as in the two previous cases.

Regarding the “*Formulation*”, the trends of the maximum contact pressure, as a function of the degrees of freedom, can be observed by changing the algorithm of calculation and keeping the other parameters of contact fixed. It is possible to conclude, observing the figures below, that the “*Augmented Lagrange*” and “*Pure Penalty*” formulations provide similar results. Precisely, it is possible to observe a convergent trend with both formulations as the number of degrees of freedom increases, in both cases “*No Wear*” (unworn condition which correspond to a simulation time of 1 s) and “*Wear*” (after simulating wear for a total sliding distance of 50 mm). However, it is recommended to use the first one because it is less sensitive to the stiffness of the material even though it requires more iterations to bring the solution to convergence. “*Normal Lagrange*” formulation is not recommended because the trend of maximum contact pressure is increasing instead of decreasing and converging. Indeed, the maximum contact pressure, as the material begins to wear, must decrease because the contact area increases, as previously stated. Furthermore, from *Fig 3.17* it is possible to state that the maximum contact pressure begins to converge just before 100000 degrees of freedom which correspond to 76410 nodes and 172308 elements (size of each element of 0.044 mm), respectively. Furthermore, from *Fig 3.16* it is possible to state that the maximum contact pressure begins to converge just before 100000 degrees of freedom which correspond to 76410 nodes and 172308 elements (size of each element of 0.044 mm) respectively. Although the convergence analysis in the non-worn condition leads to the result just stated, performing the same analysis in a worn condition (*Fig 3.17*) we obtain a faster convergence with an element size of 0.088 mm. As a result, although the solution is not accurate in the first moments, at the end of the test even with a not very fine mesh (element size of 0.088) an accurate solution is obtained in terms of volume and wear depth, saving in terms of computational time. The latter varies between 30 seconds to several hours in the proposed sensitivity analysis.

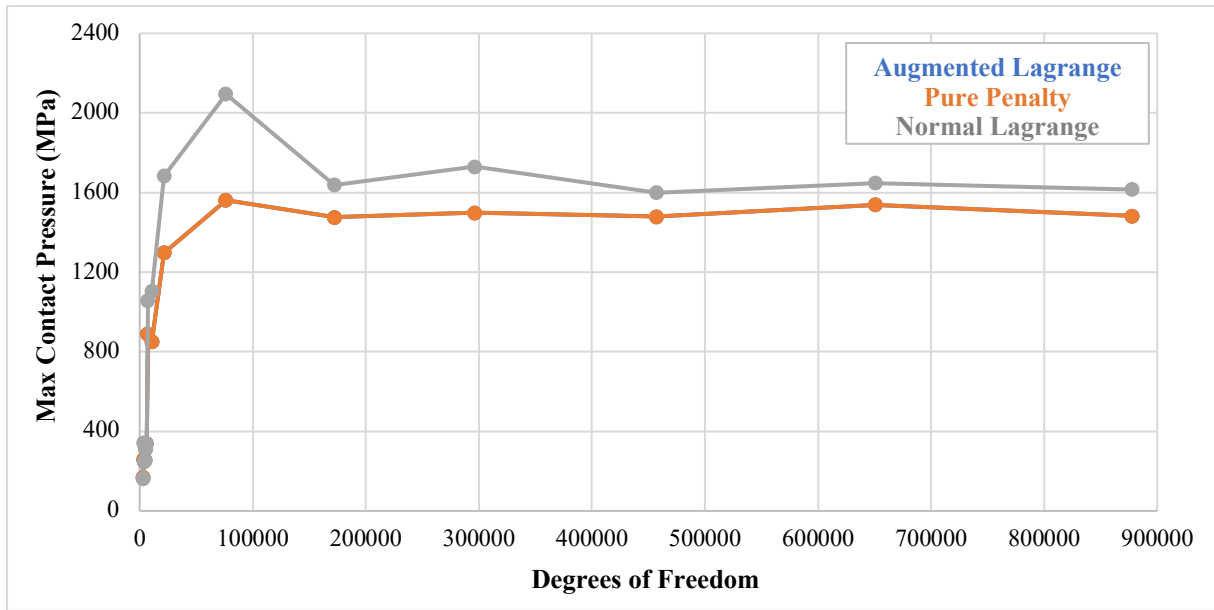


Fig 3. 16 Trends of maximum contact pressure of unilateral hard-on-hard pin on disc before wear with different formulations

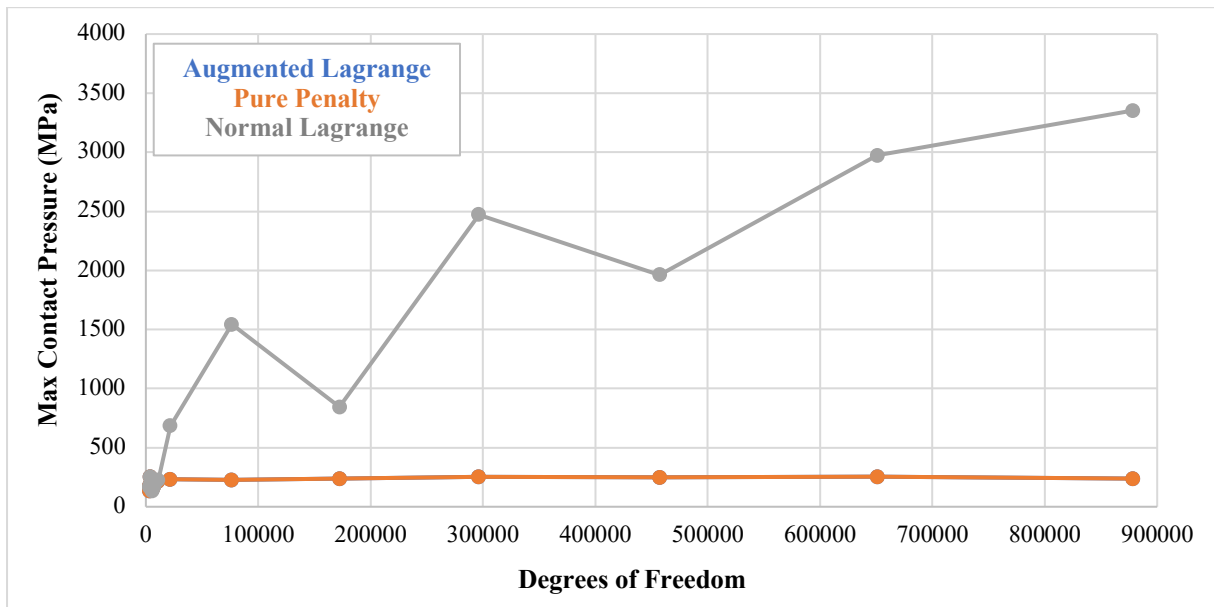


Fig 3. 17 Trends of maximum contact pressure of unilateral hard-on-hard pin on disc after wear with different formulations

As for the “Detection Method”, the trends of the maximum contact pressure can be observed by changing the “Detection Method” and keeping the other parameters of contact fixed. It is possible to state, observing the figures below, that the “Nodal-Normal To Target” and “Nodal-Normal From Contact” provide similar results. Specifically, the maximum contact pressures after one second, with elements of size 0.088 mm are, respectively, 1297.1 MPa and 1297.7 MPa and both trends converge

to a value as the number of degrees of freedom increases, in both cases “No Wear” and “Wear”. As for “Nodal-Projected Normal From Contact”, the trend of maximum contact pressure converges like two previously in both cases although in the worn condition it converges to a higher value. Moreover, the value after one second is equal to 1683.7, which is higher than those obtained in the two previous cases and for this reason this detection method is discarded. In conclusion, “Nodal-Normal To Target” is preferred to simulate wear phenomenon because gives slightly better results.

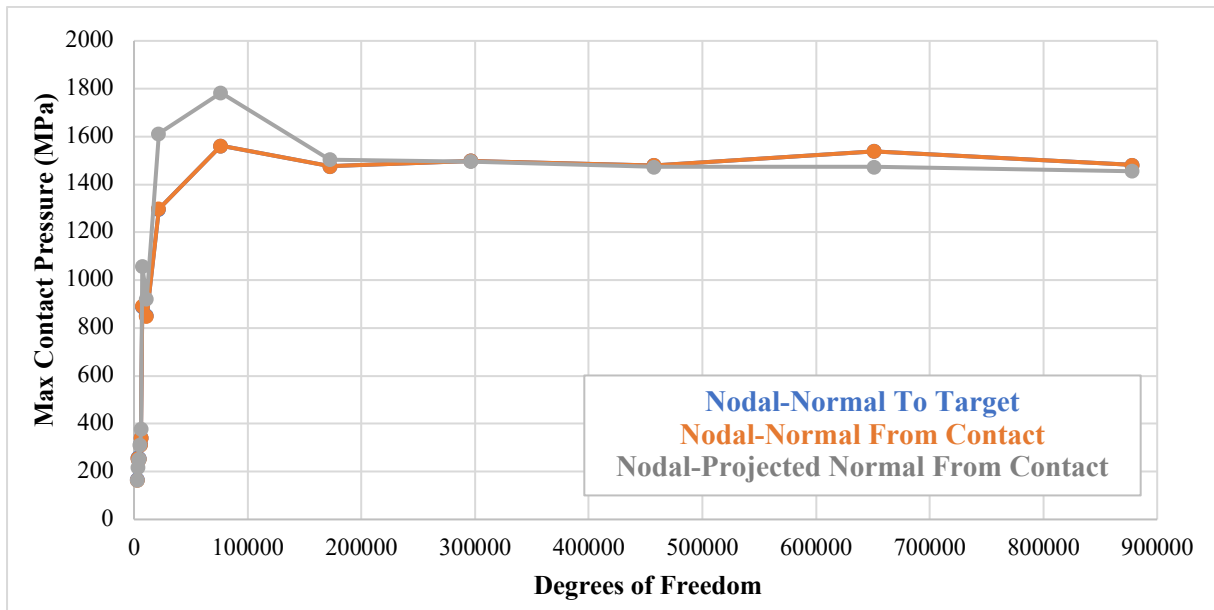


Fig 3. 18 Trends of maximum contact pressure of unilateral hard-on-hard pin on disc before wear with different detection methods

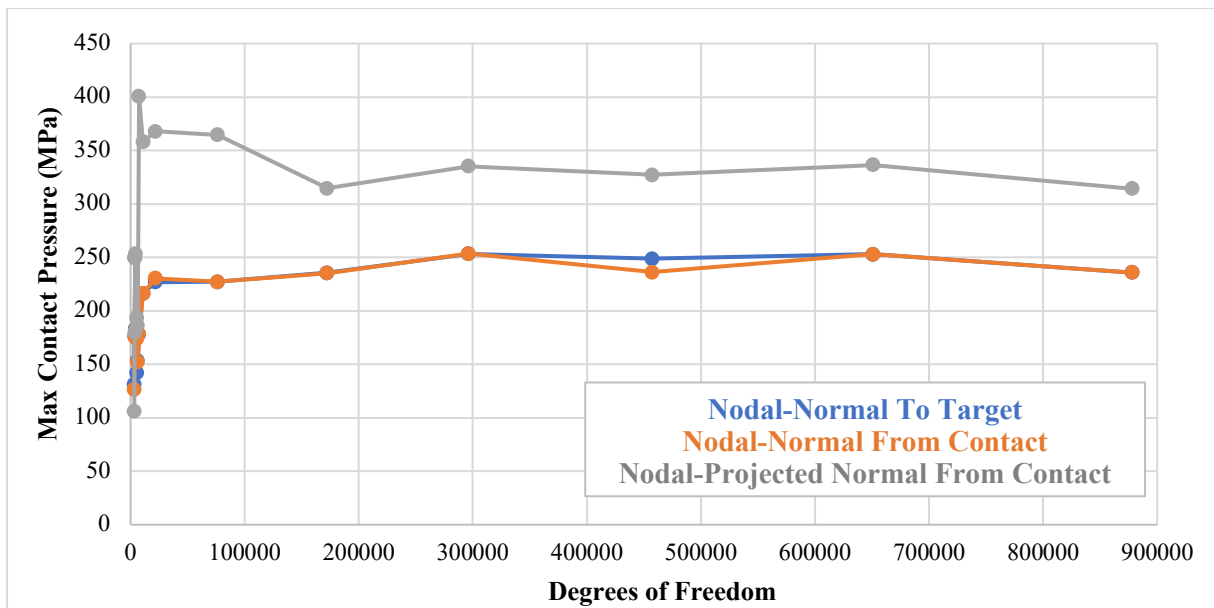


Fig 3. 19 Trends of maximum contact pressure of unilateral hard-on-hard pin on disc after wear with different detection methods

Finally, it is evaluated how the trend of the maximum contact pressure at one second of the simulation varies by changing the “Normal Stiffness” with the “Frictionless” type of contact. Observing the figure below, it is possible to state that the maximum contact pressure at one second, by increasing the “Normal Stiffness”, converges to a value.

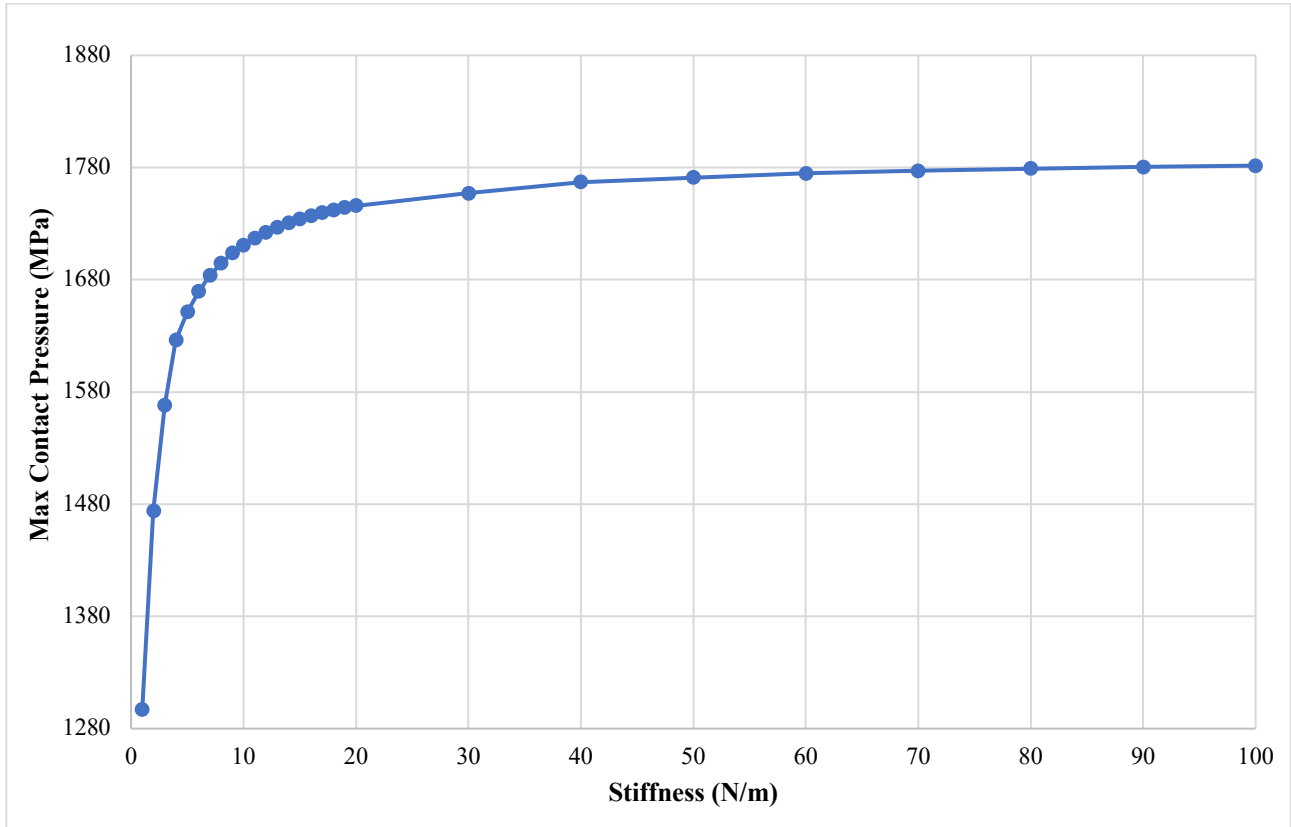


Fig 3. 20 Trends of maximum contact pressure of unilateral hard-on-hard pin on disc as a function of Normal Stiffness

3.2 Soft-on-hard bearings

The following two sections explain the test case description and the finite element model of pin on plate. The third one compares the results of the experimental test with those obtained from the model.

3.2.1 Wear test description

The finite element wear model of pin on plate is validated by comparing the results obtained in terms of wear volume with those determined by *Cornwall et al* [53] in their work. The following paper describes a pin on plate test, where the pin is made of UHMWPE and the plate of CoCr. In this work,

the wear rate ($\text{mm}^3/10^6$ cycles) and the wear coefficient (Pa^{-1}) are measured experimentally. The last one is calculated as the ratio between the wear volume (mm^3) that is equal, in turn, to the ratio between the lost mass (mg) and the density (g/cm^3), and the product between the load (N) and the sliding distance (m).

The UHMWPE pin has a spherical tip, subjected to a load of 200 N, with a diameter of 25 mm and the CoCr disk has a nominal diameter of 35 mm. The testing protocol is done according to ASTM F732-82 for a duration of 3 million cycles with a stroke length of 21 mm at a frequency of 1.02 Hz. In other words, the pin is subjected to a velocity of 21.42 mm/s. Therefore, the total distance travelled is 63 million millimetres for a total of 2.9 million seconds.

The pin is made of UHMWPE according to ASTM F648 [54], while the disk is made of CoCr according to ASTM F75 [55]. Specifically, the elastic modulus are respectively 1.3 GPa and 200 GPa and the Poisson's coefficients are respectively 0.46 (in agreement with other works in literature [56], [57]) and 0.33. In addition, the densities are, respectively, 0.93 g/cm^3 and 8.30 g/cm^3 while the tensile yield strengths are, respectively, 21 MPa and 450 MPa and tensile ultimate strengths are 34 MPa and 655 MPa, respectively.

The dimensional wear coefficient (k), derived from *Cornwall's* experiment, and used in the simulation is equal to:

$$k = 2.86 \times 10^{-12} \text{ MPa}^{-1} \quad \text{Eq. 3.11}$$

Therefore, according to Hertz's theory and Archard's law, the contact area radius, the maximum contact pressure and the wear volume are equal to:

$$a_h = 1 \text{ mm} \quad \text{Eq. 3.12}$$

$$P_{max} = 87.2 \text{ MPa} \quad \text{Eq. 3.13}$$

$$V_{wear} = 0.036 \text{ mm}^3 \quad \text{Eq. 3.14}$$

3.2.2 Model and simulation details

The characteristics of the two materials are modified in the “*Engineering Data*” block of the “*Static Structural*” of the project. Specifically, the pin and the plate have, respectively, an elastic modulus of 1.3 GPa and 200 GPa and a Poisson's coefficient of 0.46 and 0.3.

The following geometric model (*Fig 3.21*), as the previous model, is created using Design Modeler. Firstly, the pin is made as a half sphere using the “*Primitives*” command in the section “*Create*” and the “*Boolean*” tool in the same section by setting the “*Sphere*”, with a radius of 12.5 mm, as the “*Target Body*” and the “*Box*”, with dimensions and positions so that the radius of the sphere is equal to 12.5 mm, as the “*Tool Body*”. Then the disk is made like the pin but using the “*Cylinder*” with a size of 12.5 mm. As the previous model, when performing Boolean operations on two or more bodies, it is necessary to set the “*Box Operation group details*” to “*Add Freeze*” option.

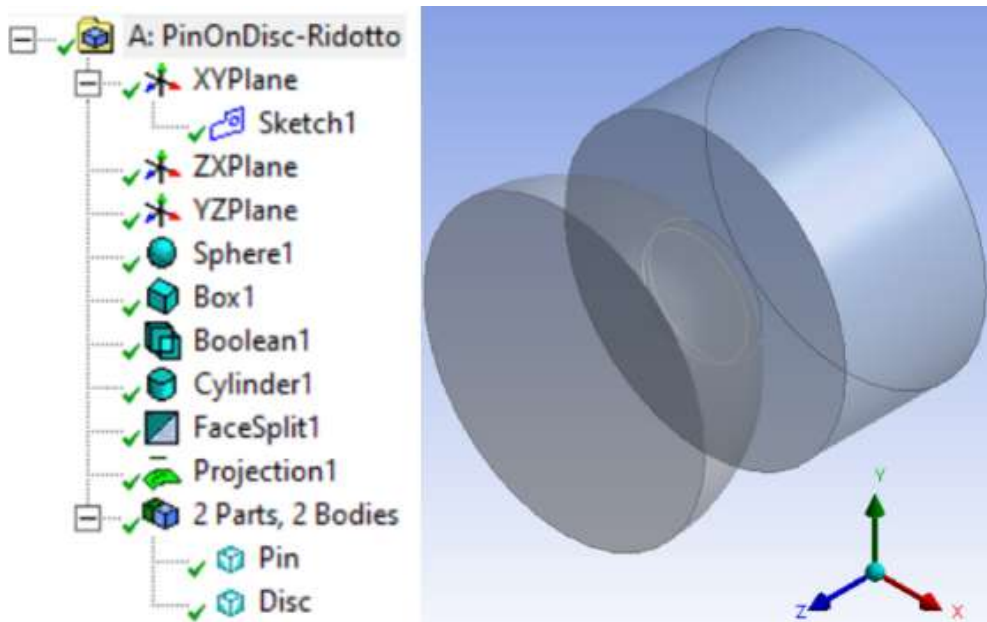


Fig 3. 21 Definition of the geometry of unilateral hard-on-soft pin on plate

As for the mesh, the “*Element Order*” in “*Defaults*” item is set to “*Linear*” (*SOLID185*) and the “*Error Limits*” in “*Quality*” item is set to “*Standard Mechanical*”. Afterwards, a “*Method*” is inserted by selecting the two bodies as “*Geometry*” and by setting them as “*Method Tetrahedrons*”. Then it is added a “*Face Sizing*” with a dimension of 0.5 mm to increase the number of nodes and elements in the contact area, in order to obtain more satisfactory results and to decrease the computational cost. In this model the circumference, drawn on the *XY* plane and with the “*Sketch*” command, has a radius of 10 mm. To obtain the projection of the “*Face Split*” on the pin, as described in the previous model, it is used the “*Projection*” tool where the “*Sketch*” previously drawn is selected as “*Edges*” and the half sphere as “*Target*”. The total number of nodes and elements is, respectively, 2010 and 7176. The complete mesh and that of the individual bodies are shown in the following figure.

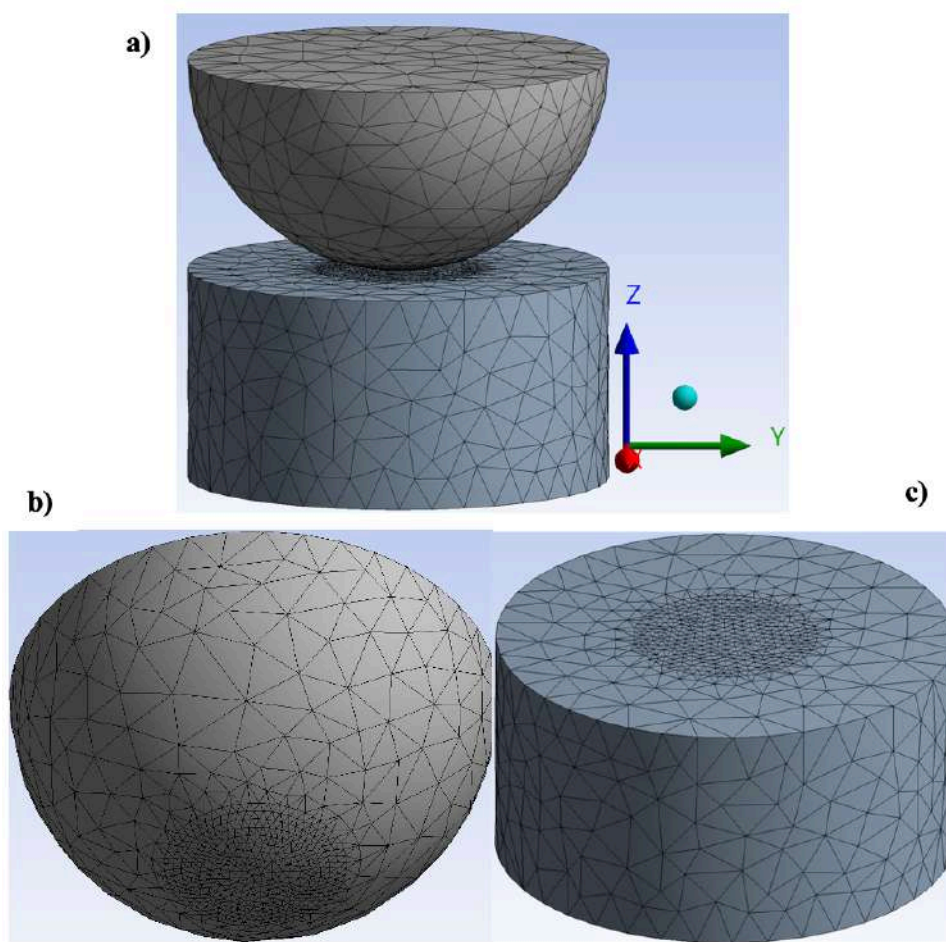


Fig 3. 22 a) Mesh of pin on plate; b) mesh of pin; c) mesh of plate

Contact settings (Fig 3.23) are defined in the Connections folder. The pin surface is modelled as “Contact Body” and the plate surface as “Target Body”. Specifically, 3D linear eight-node elements (CONTA174) are used for contact elements and 3D linear eight-node elements (CONTA170) are used for target elements. The “Type”, the “Behaviour”, the “Trim Contact” of the “Definition” item are set, respectively, to “Frictionless”, “Asymmetric” and “Off”. The “Formulation” of the “Advanced” item is set to “Augmented Lagrange” with an automatic stiffness calculation and an updating at each iteration by setting “Update Stiffness” to “Each Iteration”. Other settings of them make the system labile. The “Advanced” of “Detection Method” item is set to “Nodal-Normal To Target”, because, in order to activate the wear routine in the Ansys® software, it is needed that the integration points are “Nodal Points” and not “Gauss Point”. “Pinball Region” is set to “Radius” and its size is 2 mm. Finally, the “Interface Treatment” of the “Geometric Modification” item is set to “Adjust To Touch”, other settings make the system labile.

Details of "Frictionless - Pin To Disc"		Advanced	
Scope		Formulation	Augmented Lagrange
Scoping Method	Geometry Selection	Small Sliding	Program Controlled
Contact	1 Face	Detection Method	Nodal-Normal To Target
Target	1 Face	Penetration Tolerance	Program Controlled
Contact Bodies	Pin	Normal Stiffness	Program Controlled
Target Bodies	Disc	Update Stiffness	Each Iteration
Protected	No	Stabilization Damping Factor	0,
Definition		Pinball Region	Radius
Type	Frictionless	Pinball Radius	5, mm
Scope Mode	Automatic	Time Step Controls	None
Behavior	Asymmetric	Geometric Modification	
Trim Contact	Off	Interface Treatment	Adjust to Touch
Suppressed	No	Contact Geometry Correction	None
		Target Geometry Correction	None

Fig 3. 23 Settings for contact options of unilateral hard-on-soft pin on plate

Wear phenomenon is simulated using a very similar Command Snippets to that used in the previous model with the only difference related to the wear coefficient. Specifically, the kinematics is modelled by multiplying the wear coefficient to the sliding velocity. For this reason, it is important to note that the velocity is multiplied by a factor of 10^5 with respect to that of the experimental test to reduce the simulation time to 30.4 seconds. It is shown by running several simulations that this approach does not affect the results in terms of wear volume.

```

Commands
1  !   Commands inserted into this file will be executed just after the contact region definition.
2  !   The type and mat number for the contact type is equal to the parameter "cid".
3  !   The type and mat number for the target type is equal to the parameter "tid".
4  !   The real number for an asymmetric contact pair is equal to the parameter "cid".
5  !   The real numbers for symmetric contact pairs are equal to the parameters "cid" and "tid".
6
7  !   Active UNIT system in Workbench when this object was created:  Metric (mm, kg, N, s, mV, mA)
8  !   NOTE: Any data that requires units (such as mass) is assumed to be in the consistent solver unit system.
9  !   See Solving Units in the help system for more information.
10
11
12 PINCID=CID
13 K1=(2.86E-12)*2142657      !(C1) Wear Coefficient that includes the effect of velocity
14 H1=1                      !(C2) Hardness coefficient
15 m1=1                      !(C3) Pressure coefficient
16 n1=0                      !(C4) Velocity coefficient (=0, because it is include in K1)
17 C5=0                      !(C5) Use contact pressure in the wear coefficient
18
19 TB,WEAR,PINCID,,ARCD     ! ACTIVE WEAR MODEL
20 TBFIELD,TIME,0          ! WEAR PROPERTIES WILL BE DEFINED FOR TIME = 0
21 TBDATA,1,0,1,1,0,0     ! NO WEAR FOR CONTACT ELEMENTES
22 TBFIELD,TIME,1          ! WEAR PROPERTIES WILL BE DEFINED FOR TIME = 1
23 TBDATA,1,0,1,1,0,0     ! NO WEAR FOR CONTACT ELEMENTES
24 TBFIELD,TIME,1.0001     ! WEAR PROPERTIES WILL BE DEFINED FOR TIME = 1.0001
25 TBDATA,1,K1,H1,m1,n1,C5 ! ASSIGN WEAR PROPERTIES TO CONTACT ELEMENTES
26 TBFIELD,TIME,200        ! WEAR PROPERTIES WILL BE DEFINED FOR TIME = 200
27 TBDATA,1,K1,H1,m1,n1,C5 ! ASSIGN WEAR PROPERTIES TO CONTACT ELEMENTES

```

Fig 3. 24 Command Snippets for wear routine of unilateral hard-on-soft pin on plate

As for boundary conditions (Fig 3.25), a “Fixed Support” is added on the upper face of the pin, a “Force” with intensity of 200 N on the lower face of the plate and free “Displacement” along Z axis on the side face of the plate.

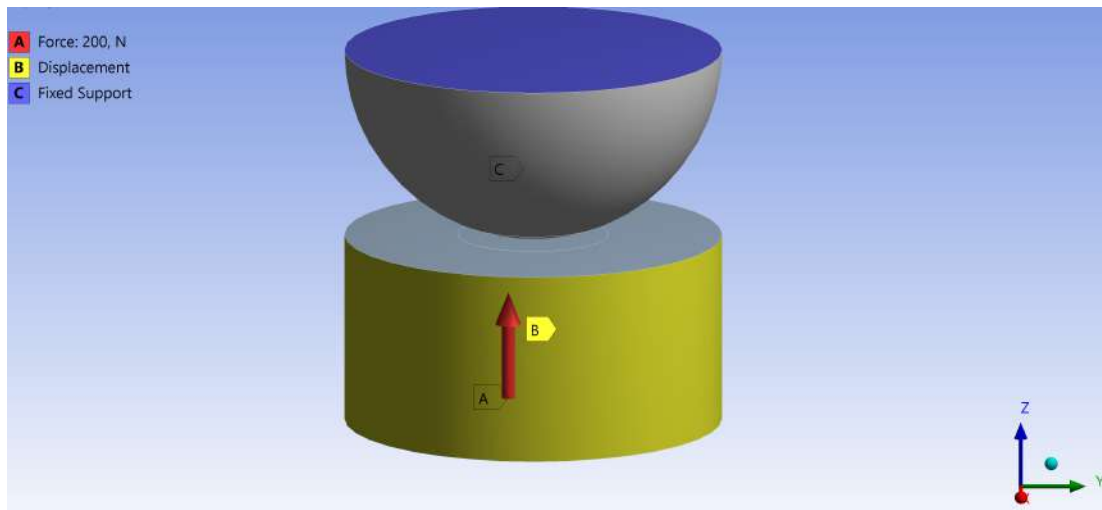


Fig 3. 25 Boundary conditions of unilateral hard-on-soft pin on plate

Moreover, as in the previous model, a very similar Command Snippets is inserted in the same section of the boundary conditions to update the mesh, as shown in the following figure.

```

Commands
1  ! Commands inserted into this file will be executed just prior to the ANSYS SOLVE command.
2  ! These commands may supersede command settings set by Workbench.
3
4  ! Active UNIT system in Workbench when this object was created: Metric (mm, kg, N, s, mV, mA)
5  ! NOTE: Any data that requires units (such as mass) is assumed to be in the consistent solver unit system.
6  ! See Solving Units in the help system for more information.
7
8
9  /SOLU
10
11 !Define component for NLAD
12 allsel,all,all
13 esel,s,type,,FINCID
14 cm,CONWEARELEM,elem
15 allsel,all,all
16
17 !Define non linear adaptivity criterion
18 NLAD,CONWEARELEM,ADD,CONTACT,WEAR,0.80 !MORPH AFTER 80% IS LOST IN WEAR
19 NLAD,CONWEARELEM,ON,ALL,ALL,1,,200
20 NLAD,CONWEARELEM,LIST,ALL,ALL
21

```

Fig 3. 26 Command Snippets for remeshing of unilateral hard-on-soft pin on plate

As for the analysis settings (Fig 3.27), they include two steps with a duration of 1 second and 29.4 seconds, respectively. The first one is characterised by a force applied gradually, through a ramp, up to the value of 200 N, that is necessary to calculate the maximum contact pressure and to ensure the convergence of the solution. The second one, where the wear routine is simulated, is characterised by a free displacement along the Z component and it is equal to zero along the other two in order to ensure the convergence. In addition, “Auto Time Step” is set to “On”, “Define By” is set to “Time” and “Initial Time Step and Minimum Time Step” is set to 0.01 seconds and “Maximum Time Step” is set to 0.1 seconds to ensure convergence. Finally, “Large Deflection” is set to “On” because the analysis is nonlinear.

Details of "Analysis Settings"	
[-] Step Controls	
Number Of Steps	2,
Current Step Number	2,
Step End Time	30,4 s
Auto Time Stepping	On
Define By	Time
Carry Over Time Step	Off
Initial Time Step	1,e-002 s
Minimum Time Step	1,e-002 s
Maximum Time Step	0,1 s
[-] Solver Controls	
Solver Type	Program Controlled
Weak Springs	Off
Solver Pivot Checking	Program Controlled
Large Deflection	On
Inertia Relief	Off
[+] Rotordynamics Controls	
[+] Restart Controls	
[+] Nonlinear Controls	
[-] Advanced	
Inverse Option	No
[+] Output Controls	
[+] Analysis Data Management	
[+] Visibility	

Fig 3. 27 Analysis Settings options of unilateral hard-on-soft pin on plate

3.2.3 Results and experimental comparison

The following section compares the results in terms of maximum contact pressure and wear volume, obtained from an implicit pin on plate model with Hertz's theory, Archard's law, and the experimental results of *Cornwall et al* [53].

As for the maximum contact pressure, the analytical value calculated using Hertz's theory is:

$$P_{max} = 87.2 \text{ MPa} \quad \text{Eq. 3.15}$$

The maximum contact pressure determined by the pin on plate model after one second is:

$$P_{max} = 86.6 \text{ MPa} \quad \text{Eq. 3.16}$$

Therefore, the finite element model predicts the maximum contact pressure at one second of the simulation with a high level of accuracy, the error is less than 1 %. The maximum contact pressure trend as a function of time is shown in figure below. It can be seen that the maximum contact pressure does not decrease as fast as in the previous case of pin on plate. This can be justified by the fact that the value of the wear coefficient obtained experimentally is much smaller compared to that obtained by *Podra et al*. Also, the contact pressure in the unworn condition is lower to one obtained in the

previous example (this is due to the fact that the contact is more conformal, and the pin is made of a soft material) and the wear rate in the initial phase of the test is this slower.

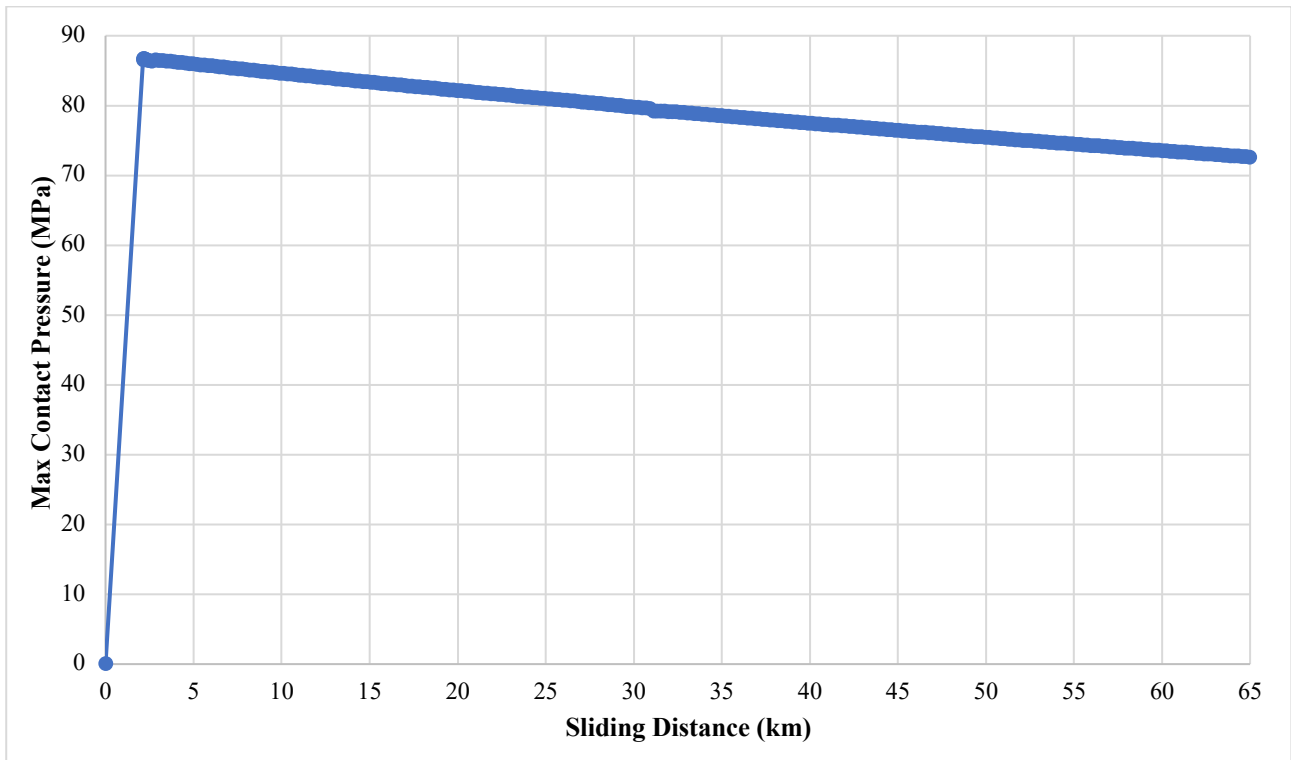


Fig 3. 28 Trends of maximum contact pressure of unilateral hard-on-soft pin on plate

As for the wear volume, the experimental value obtained by *Cornwall et al* is:

$$V_{wear} = 0.0360 \text{ mm}^3 \quad \text{Eq. 3.17}$$

The wear volume determined by the pin on plate model after 65 kilometres is:

$$V_{wear} = 0.0359 \text{ mm}^3 \quad \text{Eq. 3.18}$$

Therefore, the finite element model predicts the wear volume with a high level of accuracy, the error is less than 1 %. The wear volume trend is shown in the figure below, where it can be seen that its trend is linear, confirming the correct implementation of Archard's law in the wear routine in the Ansys® software.

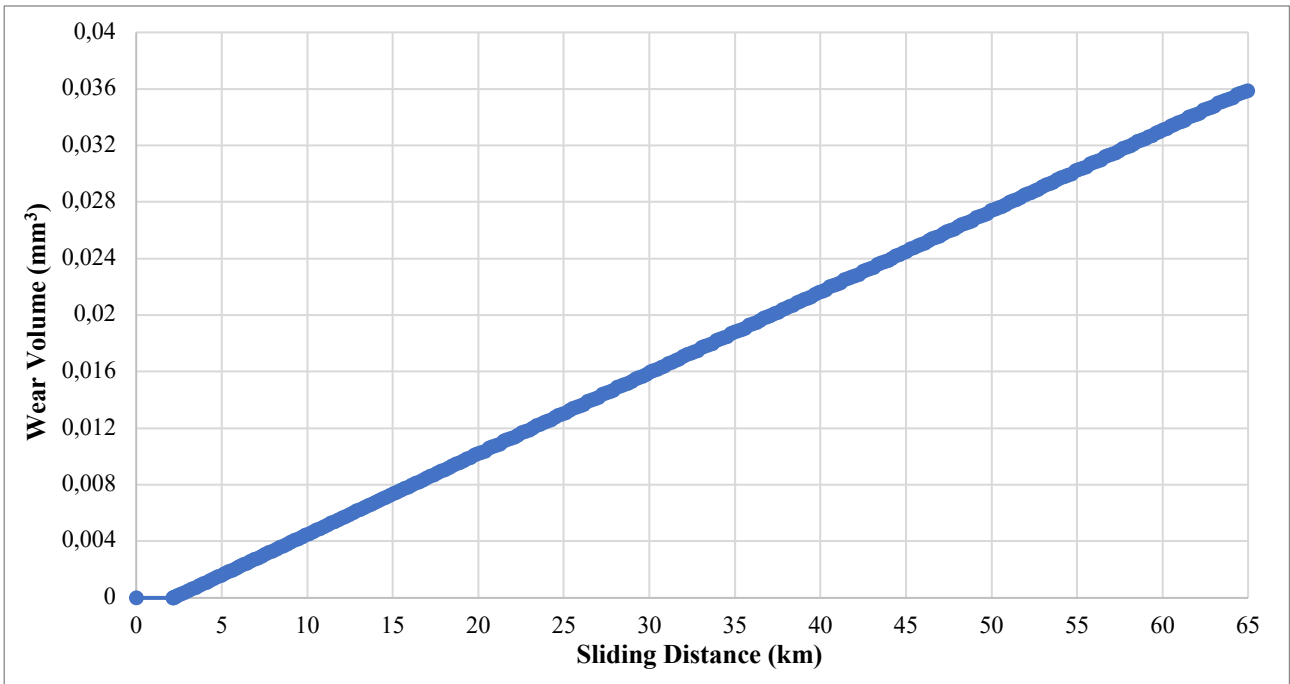


Fig 3. 29 Trends of wear volume of unilateral hard-on-soft pin on plate

In addition, the wear depth trend as a function of the sliding distance is reported in the following figure, it cannot be compared with experimental results because in the work of *Cornwall et al* only the wear volume is evaluated.

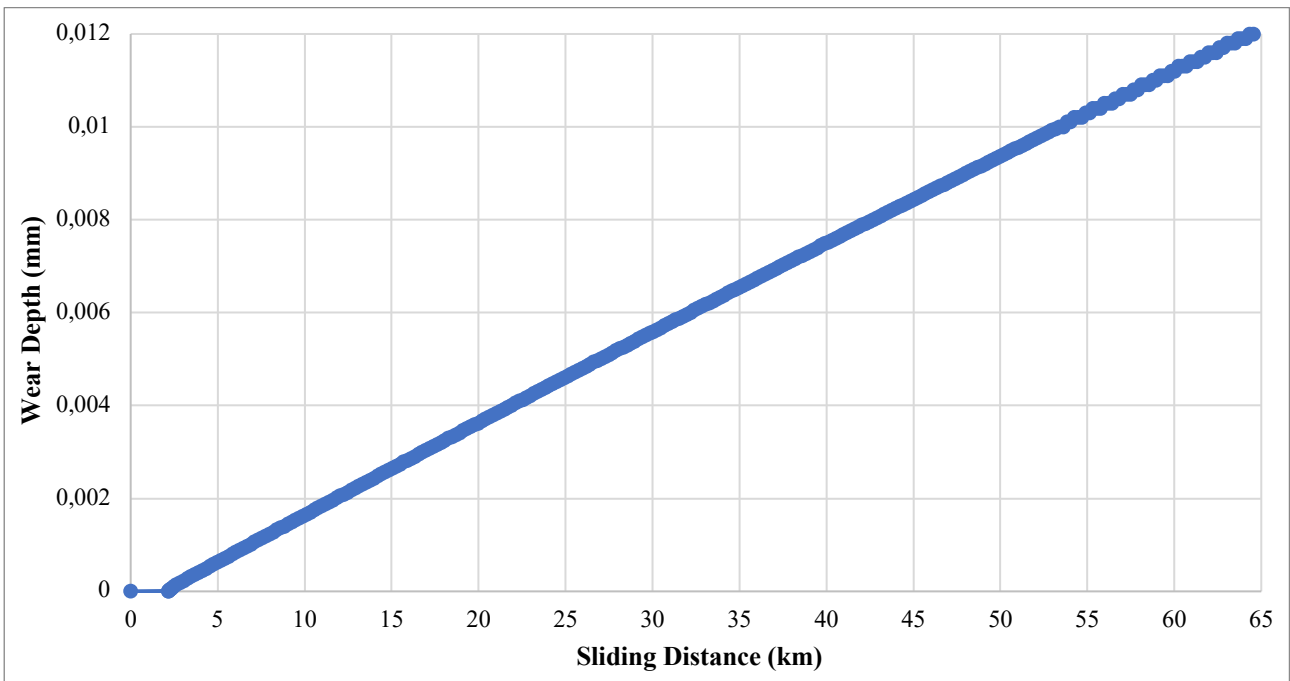


Fig 3. 30 Trends of wear depth of unilateral hard-on-soft pin on plate

It can be observed that the wear depth trend is fairly linear, and the wear test studied seems to be characterized by a steady-state phase.

3.3 Bilateral wear

The following two sections describe the experimental test and the finite element model of pin on plate. The third one compares the results of the experimental test with those obtained from the model.

3.3.1 Wear test description

The finite element wear model of pin on plate is validated by comparing the results obtained in terms of wear volume with those determined by *J. L. Tipper et al* in their experiment [58]. This article discusses the bilateral wear of a pin on plate test. Specifically, the pin has a spherical tip with a radius of 100 mm, and it is subjected to a load of 80 N and to a velocity of 30 mm/s for the entire sliding distance. Moreover, the stroke length is equal to 30 mm. Both the pin and the plate are made of steel with an elastic modulus of 210 GPa and a Poisson's coefficient equal to 0.3.

The experimental dimensional wear coefficients of the pin and of the plate are respectively:

$$k_{pin} = 1.55 \times 10^{-9} \text{ MPa}^{-1} \quad Eq. 3.19$$

$$k_{plate} = 4.50 \times 10^{-9} \text{ MPa}^{-1} \quad Eq. 3.20$$

Therefore, according to Hertz's theory and Archard's law the contact area radius and the total wear volume, given by the sum of the wear volume of the pin and the dis, are respectively equal to:

$$a_h = 0.37 \text{ mm} \quad Eq. 3.21$$

$$V_{wear} = 0.057 \text{ mm}^3 \quad Eq. 3.22$$

3.3.2 Model and simulation details

The characteristics of the two materials (i.e., elastic modulus and Poisson's coefficient) are modified in the “*Engineering Data*” block of the “*Static Structural*” of the project. Precisely, the pin and the plate have an elastic modulus of 210 GPa and a Poisson's coefficient of 0.3.

The following geometric model (*Fig 3.31*) is created using Design Modeler. Firstly, the pin is made as a half sphere with a radius of 100 mm, using the “*Primitives*” command and the “*Boolean*” tool, selecting the “*Sphere*” as the “*Target Body*” and the “*Box*” as the “*Tool Body*”. Then the plate is

made using the “Box” primitive with length, width and height of 180 mm, 100 mm and 20 mm respectively. However, to reduce the computational effort of the simulation the geometry is reduced as shown in *Fig 3. 32*. Specifically, the radius of the sphere is 100 mm while “Box1” has been positioned to remove most of the sphere. Moreover, four additional “Boxes” are used, and the relative Boolean operations to give the pin the above-mentioned shape. As for the plate, a “Box” with length, width and height of 60, 30 and 6 mm respectively is used. Therefore, the descriptions that follow refer to the reduced geometry.

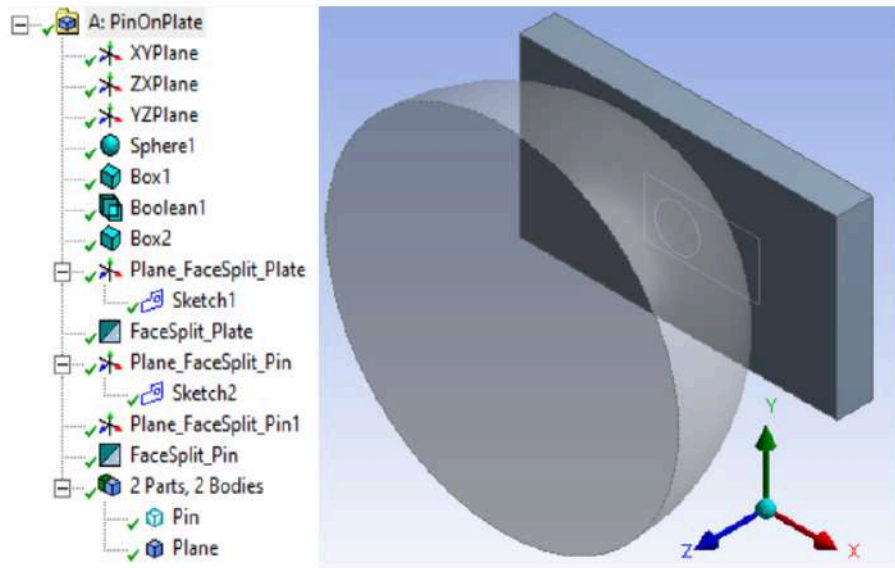


Fig 3. 31 Definition of the geometry of bilateral hard-on-hard pin on plate

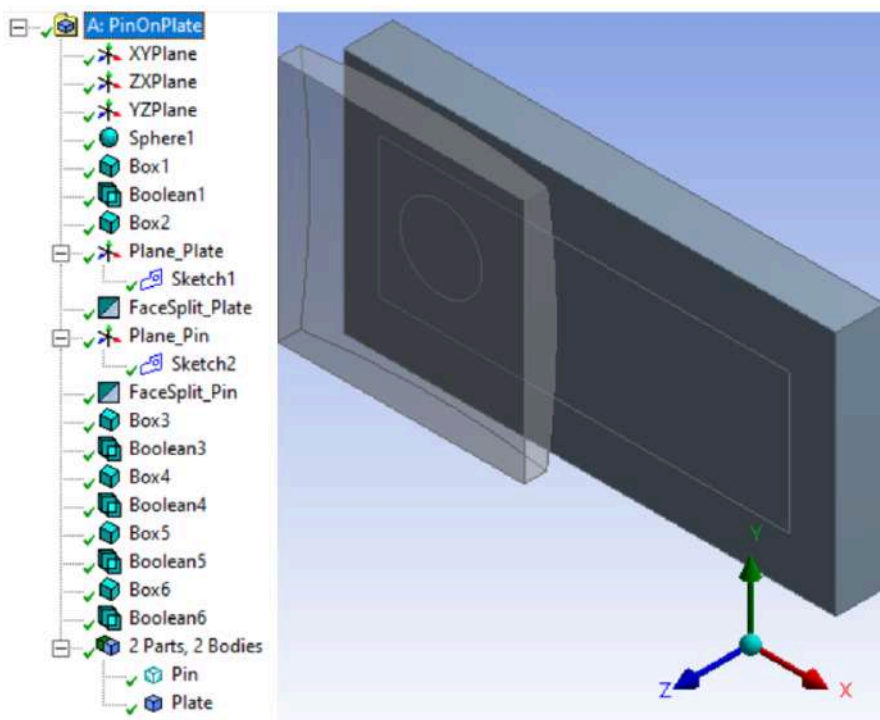


Fig 3. 32 Definition of the geometry of bilateral hard-on-hard pin on plate reduced

As for the mesh, the “*Element Order*” in “*Defaults*” item is set to “*Linear*” (*SOLID185*) and the “*Error Limits*” in “*Quality*” item is set to “*Standard Mechanical*”. Afterwards, a “*Method*” is inserted by selecting the two bodies as “*Geometry*” and by setting them as “*Method Tetrahedrons*”. Then it is added a “*Face Sizing*” with a dimension of 0.37 mm to increase the number of nodes and elements in the contact area in order to obtain more satisfactory results. For this aim, it is drawn, on the *XY* plane with the “*Sketch*” command, a rectangle with length 50 mm along the x-axis and 17.05 mm along the y-axis, and it is used the “*Face Split*” tool where the upper surface of the disk is selected as “*Target Face*” and the “*Sketch*” previously drawn as “*Tool Geometry*”. As for the pin, it is drawn, on the *XY* plane with the “*Sketch*” command, a circumference with radius 10 mm and it is used the “*Face Split*” tool where the lower surface of the pin is selected as “*Target Face*” and the “*Sketch*” previously drawn as “*Tool Geometry*”. The total number of nodes and elements in the model is, respectively, 12810 and 48861. The complete mesh and that of the individual bodies are shown in the following figure.

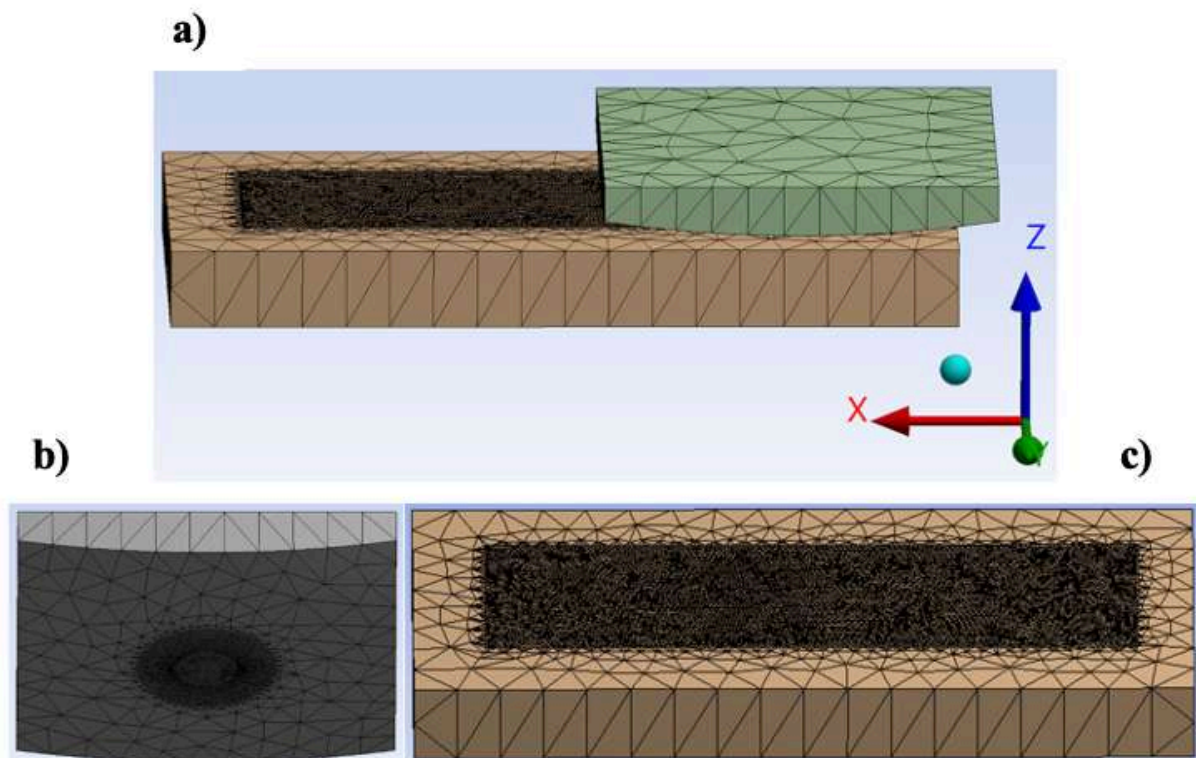


Fig 3. 33 a) Mesh of pin on plate; b) mesh of pin; c) mesh of plate

Both bodies are modelled as “*Contact Body*” and “*Target Body*” because in this case a bilateral contact is simulated as opposed to the previous ones that are unilateral. Then, only the pin is subject to wear. In addition, two contact pairs with “*Asymmetric*” behaviour are defined for the same reason. However, in this regard, it is important to underline that it is possible to model bilateral contact by

defining a single contact pair with “*Symmetric*” behaviour. The main difference is the possibility to define two different wear coefficients in case of double “*Asymmetric*” behaviour. However, this limitation can be overcome by defining both contact surface (*CID*) and target surface (*TID*) in the routine Command Snippets. The last one is generally not defined because wear occurs exclusively on the contact surface. However, when using the “*Symmetric*” behaviour, the software not only defines a contact surface and a target surface, as in the asymmetric case, but also generates a twin copy in which it exchanges the target and the contact. This is the reason why the symmetric contact has usually a lower efficiency or in other words a higher computational cost. In general, “*Symmetric*” behaviour is recommended when the distinction between the contact and target surface is not clear, when both surfaces have very coarse meshes and when one side of contact surface is closed and the other one is open. In the latter case, it is possible to set $KEYOPT(8) = 1$. With this setting the program uses the same contact pair characteristics (contact depth, length, pinball radius, contact normal stiffness, contact damping, tolerances and so on) for both pairs. However, in this specific case it could represent a forcing because the pin has a spherical surface while the plate has a flat one. Finally, as described in the first section of chapter two, in general it is recommended to set $C5 = 1$ and therefore refer the wear calculation to the nodal stress and not to the contact pressure. However, regarding the maximum contact pressure, some simulations show a less smooth trend using $C5=1$ rather than $C5=0$.

As for the other settings, the “*Type*” and the “*Trim Contact*” of the “*Definition*” item and the “*Formulation*” of the “*Advanced*” item are set, respectively, to “*Frictionless*”, “*Off*” and “*Augmented Lagrange*” for both pairs of contact. Moreover, the “*Update Stiffness*” of the “*Advanced*” item is set to “*Each Iteration*” for both pairs of contact. The “*Advanced*” of “*Detection Method*” item is set to “*Nodal-Normal To Target*”, because, in order to activate the wear routine in the Ansys ® software, it is necessary that the integration points are “*Nodal Points*” and not “*Gauss Point*”. “*Pinball Region*” is set to “*Program Controlled*” for both pairs of contact. Finally, the “*Interface Treatment*” of the “*Geometric Modification*” item is set to “*Adjust To Touch*” for both pairs of contact. These settings are shown in the figure below. In addition, as in the previous two models, 3D linear eight-node elements (*CONTA174*) are used for contact elements and 3D linear eight-node elements (*CONTA170*) are used for target elements.

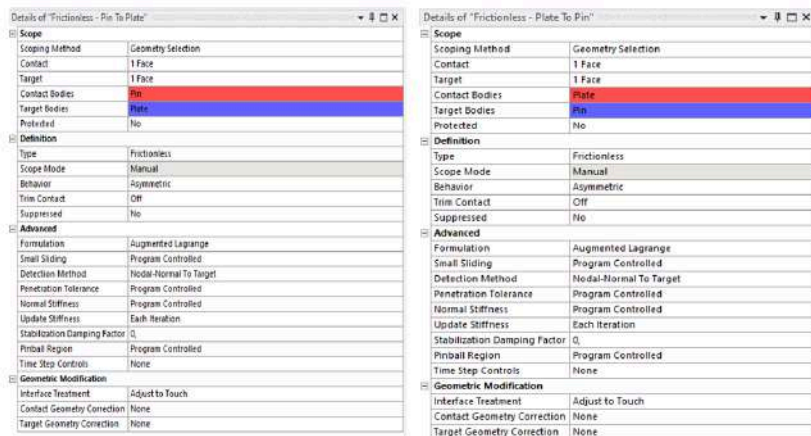


Fig 3. 34 Settings for contact options of bilateral hard-on-hard pin on plate, on the left are shown the settings in which the pin is defined as contact surface and on the right those in which the plate is defined as contact surface

Moreover, since a wear law is required for each surface of the coupling, two APDL Commands Snippets are added (Fig 3.35 and Fig 3.36). Bilateral wear requires explicit kinematics, thus the variable of the exponential coefficient of the velocity (m) is equal to 1. Using implicit kinematics, it is possible to assess the total wear volume also when both bodies get worn. However, this is a global indicator of wear and in most cases an accurate prediction of the wear depth is needed in both bodies, which is possible only if relative motion is explicitly modelled. Indeed, during the wear test, the stress field in the plate is differently than the one in the pin. Specifically, during the movement of the pin, the top surface of the plate is subjected to a varying contact pressure while those of the pin remain almost the same during a wear cycle.

```

Commands
1  ! Commands inserted into this file will be executed just after the contact region definition.
2  ! The type and mat number for the contact type is equal to the parameter "cid".
3  ! The type and mat number for the target type is equal to the parameter "tid".
4  ! The real number for an asymmetric contact pair is equal to the parameter "cid".
5  ! The real numbers for symmetric contact pairs are equal to the parameters "cid" and "tid".
6
7  ! Active UNIT system in Workbench when this object was created: Metric (mm, kg, N, s, mV, mA)
8  ! NOTE: Any data that requires units (such as mass) is assumed to be in the consistent solver unit system.
9  ! See Solving Units in the help system for more information.
10
11
12  PINCID1=CID
13  K1=(1.55E-09)  !(C1) Wear Coefficient
14  H1=1          !(C2) Hardness coefficient
15  m1=1         !(C3) Pressure coefficient
16  n1=1         !(C4) Velocity coefficient
17  C5=0         !(C5) Use contact pressure in the wear coefficient
18
19  TB,WEAR,PINCID1,,ARCD  ! ACTIVE WEAR MODEL
20  TBFIELD,TIME,0        ! WEAR PROPERTIES WILL BE DEFINED FOR TIME = 0
21  TBDATA,1,0,1,1,1,0   ! NO WEAR FOR CONTACT ELEMENTS
22  TBFIELD,TIME,1        ! WEAR PROPERTIES WILL BE DEFINED FOR TIME = 1
23  TBDATA,1,0,1,1,1,0   ! NO WEAR FOR CONTACT ELEMENTS
24  TBFIELD,TIME,1.0001  ! WEAR PROPERTIES WILL BE DEFINED FOR TIME = 1.0001
25  TBDATA,1,K1,H1,m1,n1,C5  ! ASSIGN WEAR PROPERTIES TO CONTACT ELEMENTS
26  TBFIELD,TIME,5000    ! WEAR PROPERTIES WILL BE DEFINED FOR TIME = 5000
27  TBDATA,1,K1,H1,m1,n1,C5  ! ASSIGN WEAR PROPERTIES TO CONTACT ELEMENTS

```

Fig 3. 35 Command Snippets for wear routine of bilateral hard-on-hard pin on plate where the pin is the contact and the plate is the target

```

Commands
1  !  Commands inserted into this file will be executed just after the contact region definition.
2  !  The type and mat number for the contact type is equal to the parameter "cid".
3  !  The type and mat number for the target type is equal to the parameter "tid".
4  !  The real number for an asymmetric contact pair is equal to the parameter "cid".
5  !  The real numbers for symmetric contact pairs are equal to the parameters "cid" and "tid".
6
7  !  Active UNIT system in Workbench when this object was created:  Metric (mm, kg, N, s, mV, mA)
8  !  NOTE:  Any data that requires units (such as mass) is assumed to be in the consistent solver unit system.
9  !
10         See Solving Units in the help system for more information.
11
12  PINCID2=CID
13  K1=(4.50E-09)  !(C1) Wear Coefficient
14  H1=1          !(C2) Hardness coefficient
15  m1=1         !(C3) Pressure coefficient
16  n1=1         !(C4) Velocity coefficient
17  C5=0         !(C5) Use contact pressure in the wear coefficient
18
19  TB,WEAR,PINCID2,,,ARCD      ! ACTIVE WEAR MODEL
20  TBFIELD,TIME,0              ! WEAR PROPERTIES WILL BE DEFINED FOR TIME = 0
21  TBDATA,1,0,1,1,1,0         ! NO WEAR FOR CONTACT ELEMENTS
22  TBFIELD,TIME,1              ! WEAR PROPERTIES WILL BE DEFINED FOR TIME = 1
23  TBDATA,1,0,1,1,1,0         ! NO WEAR FOR CONTACT ELEMENTS
24  TBFIELD,TIME,1.0001        ! WEAR PROPERTIES WILL BE DEFINED FOR TIME = 1.0001
25  TBDATA,1,K1,H1,m1,n1,C5     ! ASSIGN WEAR PROPERTIES TO CONTACT ELEMENTS
26  TBFIELD,TIME,5000          ! WEAR PROPERTIES WILL BE DEFINED FOR TIME = 5000
27  TBDATA,1,K1,H1,m1,n1,C5     ! ASSIGN WEAR PROPERTIES TO CONTACT ELEMENTS

```

Fig 3. 36 Command Snippets for wear routine of bilateral hard-on-hard pin on plate where the plate is the contact and the pin is the target

As for boundary conditions (Fig 3.37) a “Fixed Support” is added on lower face of the disc, a “Force” with intensity of 80 N on the upper face of the pin; the “Displacement” of the side and upper faces of the pin is allowed only along XY axis. As for the “Displacement” the pin covers a distance of 30 mm (which corresponds to the stroke length) and returns to the initial position, then repeating this movement for the entire simulation.

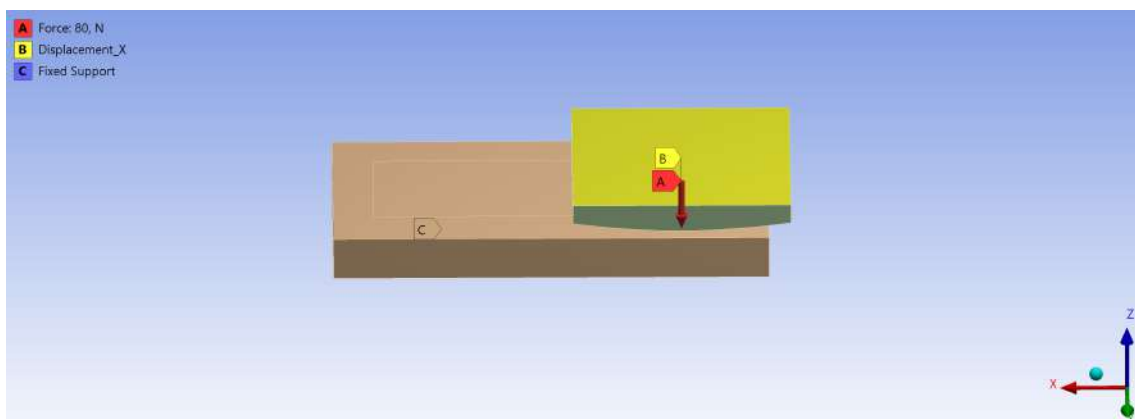


Fig 3. 37 Boundary conditions of bilateral hard-on-hard pin on plate

In the same section of the boundary conditions, two APDL Commands Snippets (Fig 3.38 and Fig 3.39) are inserted to allow the mesh updating, as in previous models.

```

Commands
1  !  Commands inserted into this file will be executed just prior to the ANSYS SOLVE command.
2  !  These commands may supersede command settings set by Workbench.
3
4  !  Active UNIT system in Workbench when this object was created: Metric (mm, kg, N, s, mV, mA)
5  !  NOTE: Any data that requires units (such as mass) is assumed to be in the consistent solver unit system.
6  !
7      See Solving Units in the help system for more information.
8
9  /SOLU
10 !define component for NLAD
11
12 allsel,all,all
13 esel,s,type,,PINCID1
14 cm,CONWEARELEM,elem
15 allsel,all,all
16
17 !Define non linear adaptivity criterion
18 NLAD,CONWEARELEM,ADD,CONTACT,WEAR,0.80
19 NLAD,CONWEARELEM,ON,ALL,ALL,1,,5000
20 NLAD,CONWEARELEM,LIST,ALL,ALL

```

Fig 3. 38 Command Snippets for remeshing of bilateral hard-on-hard pin on plate where the pin is the contact and the plate is the target

```

Commands
1  !  Commands inserted into this file will be executed just prior to the ANSYS SOLVE command.
2  !  These commands may supersede command settings set by Workbench.
3
4  !  Active UNIT system in Workbench when this object was created: Metric (mm, kg, N, s, mV, mA)
5  !  NOTE: Any data that requires units (such as mass) is assumed to be in the consistent solver unit system.
6  !
7      See Solving Units in the help system for more information.
8
9  /SOLU
10 !define component for NLAD
11
12 allsel,all,all
13 esel,s,type,,PINCID1
14 cm,CONWEARELEM,elem
15 allsel,all,all
16
17 !Define non linear adaptivity criterion
18 NLAD,CONWEARELEM,ADD,CONTACT,WEAR,0.80
19 NLAD,CONWEARELEM,ON,ALL,ALL,1,,5000
20 NLAD,CONWEARELEM,LIST,ALL,ALL

```

Fig 3. 39 Command Snippets for remeshing of bilateral hard-on-hard pin on plate where the plate is the contact and the pin is the target

As for the analysis settings (Fig 3.40), they include two steps with a duration of one 1 and 2000 seconds, respectively. The first one is characterised by a gradually applied force, through a ramp up to the value of 80 N, corresponding to the needed one to calculate the maximum contact pressure and to ensure the convergence of the solution. The second one, where the wear routine is simulated, is characterised by a displacement equal to 30 mm along the *X* component and equal to zero along the other two to ensure the convergence. In addition, “Auto Time Step” is set to “On”, “Define By” is set to “Time” and “Initial Time Step and Minimum Time Step” is set to 0.01 seconds and “Maximum Time Step” is set to 0.1 seconds to ensure convergence. Finally, “Large Deflection” is set to “On” because the analysis is nonlinear.

Details of "Analysis Settings"	
[-] Step Controls	
Number Of Steps	2,
Current Step Number	2,
Step End Time	4001, s
Auto Time Stepping	On
Define By	Time
Carry Over Time Step	Off
Initial Time Step	1,e-002 s
Minimum Time Step	1,e-002 s
Maximum Time Step	0,1 s
[-] Solver Controls	
Solver Type	Program Controlled
Weak Springs	Off
Solver Pivot Checking	Program Controlled
Large Deflection	On
Inertia Relief	Off
[+] Rotordynamics Controls	
[+] Restart Controls	
[+] Nonlinear Controls	
[-] Advanced	
Inverse Option	No
[+] Output Controls	
[+] Analysis Data Management	
[+] Visibility	

Fig 3. 40 Analysis Settings options of bilateral hard-on-hard pin on plate

3.3.3 Results and experimental comparison

The following section compares the results in terms of wear volume obtained from an explicit pin on plate model using the Archard's law with the experiment of *J. L. Tipper et al* [58]:

As for the total wear volume, the experimental value obtained by *J. L. Tipper et al* after 120 metres is:

$$V_{wear} = 0.057 \text{ mm}^3 \quad Eq. 3.23$$

The total wear volume determined by the pin on plate model after 120 metres (corresponding to 2001 seconds in the Ansys Workbench ® simulation) is:

$$V_{wear} = 0.027 \text{ mm}^3 \quad Eq. 3.24$$

The wear volume trends as function of sliding distance are shown in figure below. It can be seen how the wear volume trend is linear, confirming the correct implementation of Archard's law in the wear routine in the Ansys® software.

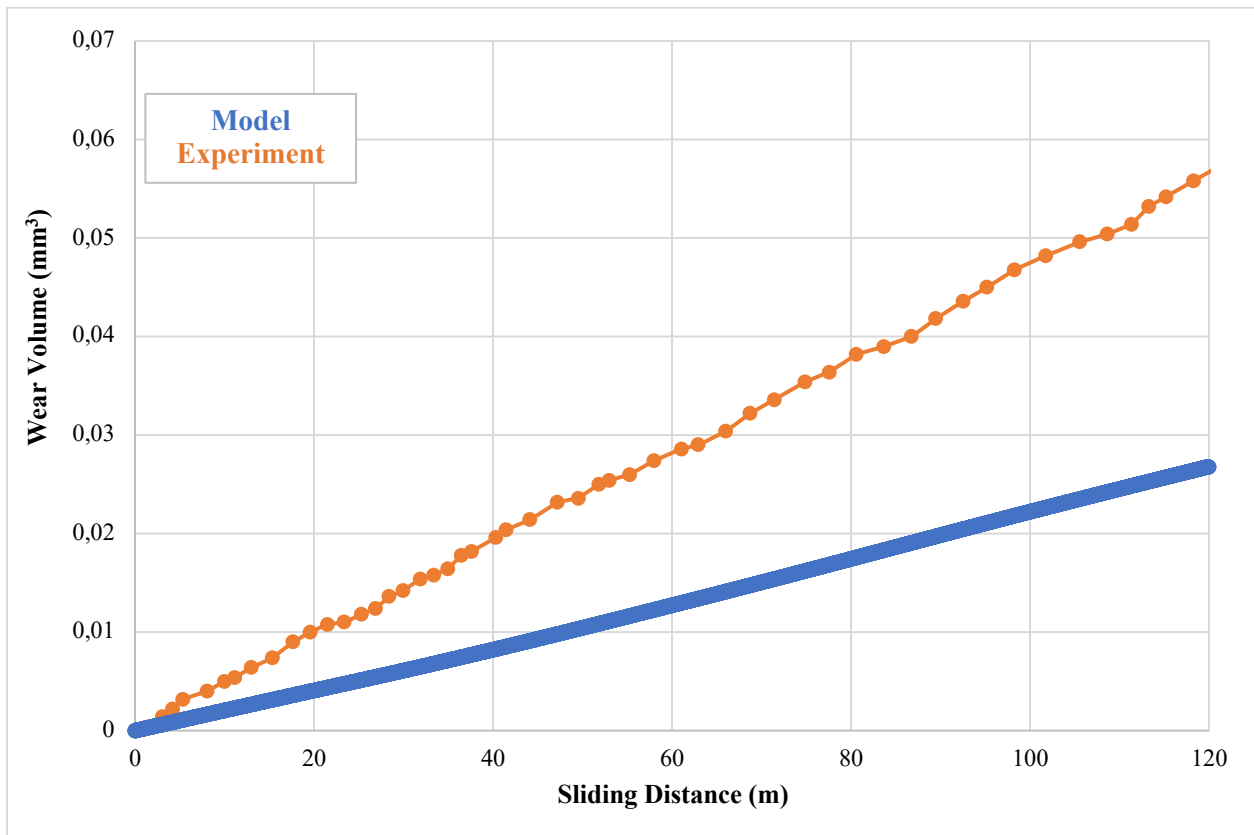


Fig 3. 41 Trends of wear volume of bilateral hard-on-hard pin on plate

The error between the total predicted wear volume and the measured one is about 52.6%. This high value is probably due to inaccuracies in predicting the stress field in both pin and plate surfaces. A coarse mesh at the contact region and contact surfaces with differently misplaced nodes at each time step during the simulation might results in a not accurate contact pressure profile and thus in a wrong wear prediction.

To demonstrate this, we simulated the first pin on disc test presented in this thesis, considering two contact pairs with “*Asymmetric*” behaviour. Specifically, we simulate bilateral wear by setting, in the wear law related to the disc surface, a coefficient of wear of the disc equal to zero. All the other model parameters were the same. We obtained different wear results volume respect to the ones previously presented considering a unilateral wear (percentage difference on the total wear volume and on the maximum wear depth respectively of around 90 % and 72 % at the end of the test), as shown in the following figure.

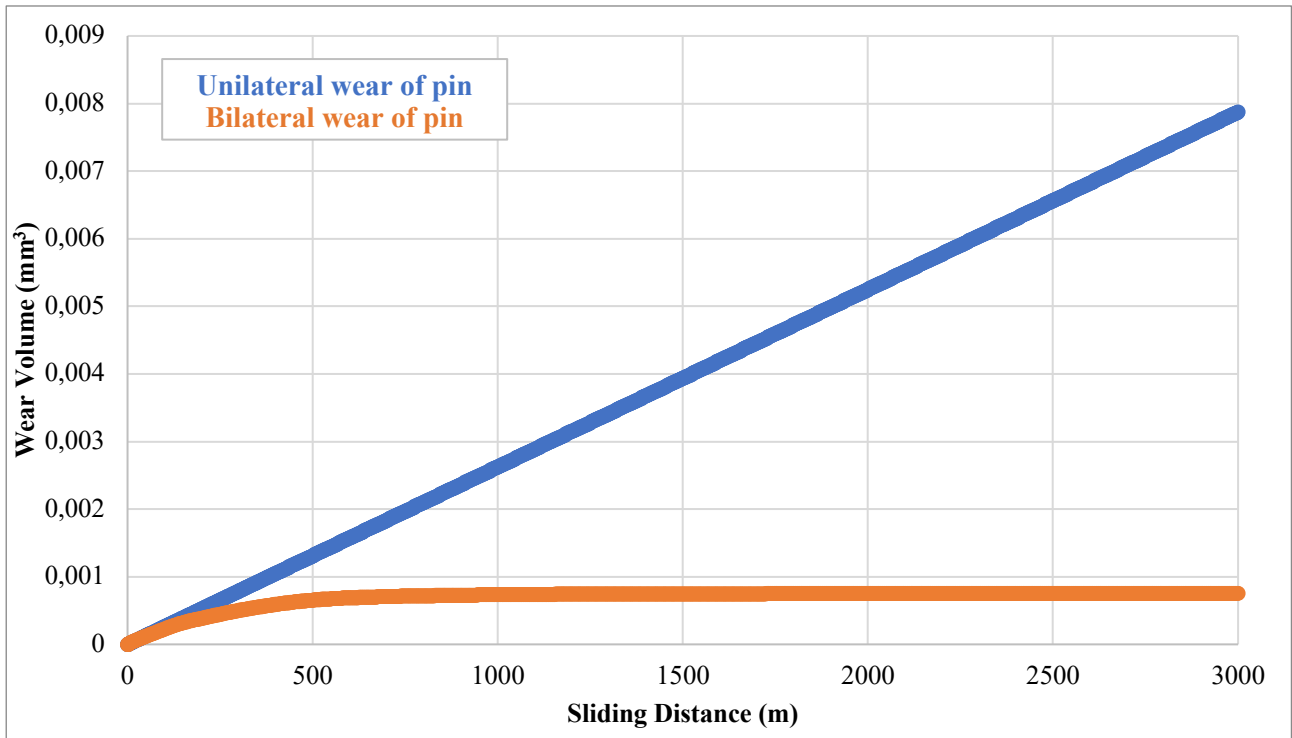


Fig 3. 42 Trends of wear volume of unilateral pin and bilateral pin

However, differences are much smaller if the mesh at the contact region is finer, as we can observe in Fig 3.43. With an element edge size of about 1µm we obtained a relative error on the total wear volume of around 9% after simulating wear for a total sliding distance of 200 mm. It is important to notice that the computational time became in this case unsustainably high.

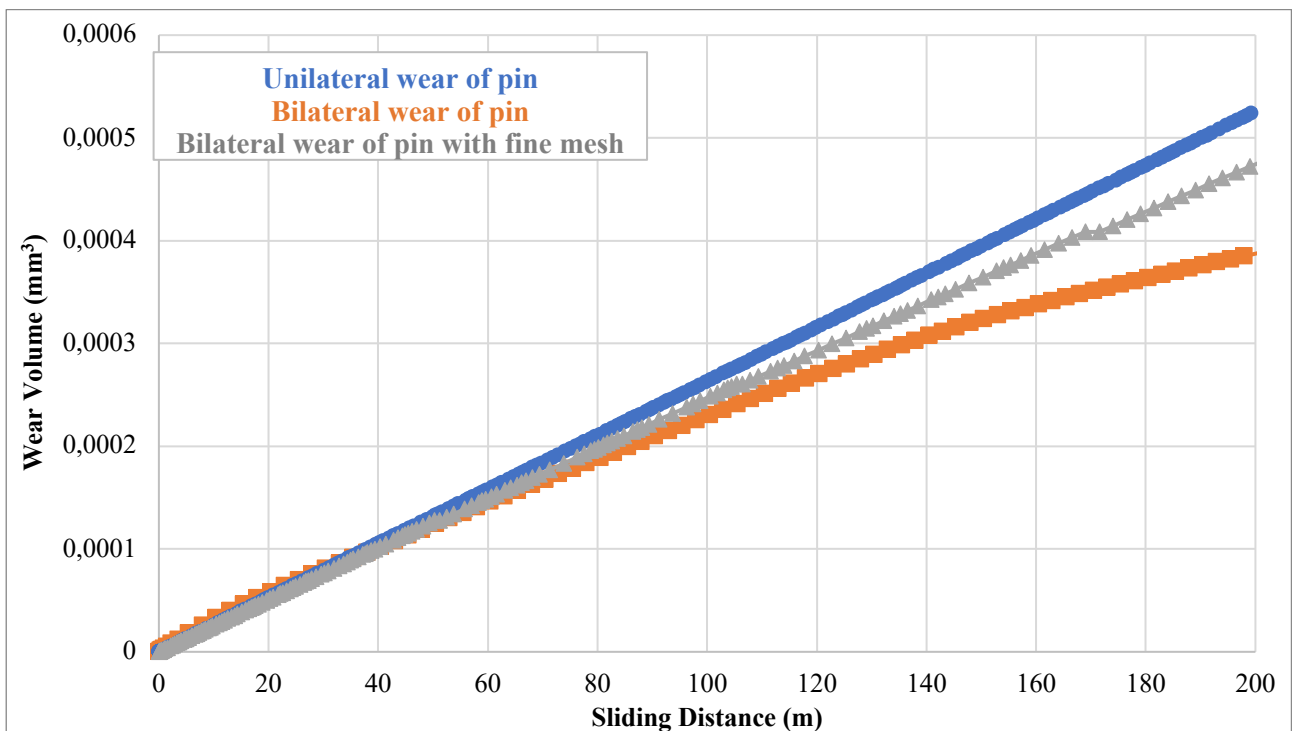


Fig 3. 43 Trends of wear volume of unilateral pin, bilateral pin and bilateral pin with fine mesh

As mentioned earlier the wear volume is not sufficient to describe the wear phenomenon involving two contacting surfaces. For this reason, it is necessary to study also the wear depth. However, the reference article [58] only examines the wear volume. For this reason, a further explicit simulation is run for a shorter time (1000 seconds, which corresponds to a sliding distance of about 60 metres) then comparing results with a second article [59] that simulates the same experimental test run by *J. L. Tipper et al* [58] with a finite element model. In the following article the maximum contact pressure, the wear volume and the wear depth are evaluated while considering the same wear coefficient equal to:

$$k_{pin} = k_{plate} = 3 \times 10^{-9} \text{ MPa}^{-1} \quad Eq. 3.25$$

Then the results in terms of wear depth are compared with those obtained from the following computational study [59]. For time reasons, the simulation is performed on 60 metres and not 240 metres. In addition, the results are obtained with the pin-on-plate model not geometrically reduced due to time constraints. It is important to notice that the model presented in [59] was developed using software ABAQUS and not the software Ansys. The following graph shows the wear depth trends of the pin and the one of the plate as predicted by the Ansys model and by the model of the reference computational study.

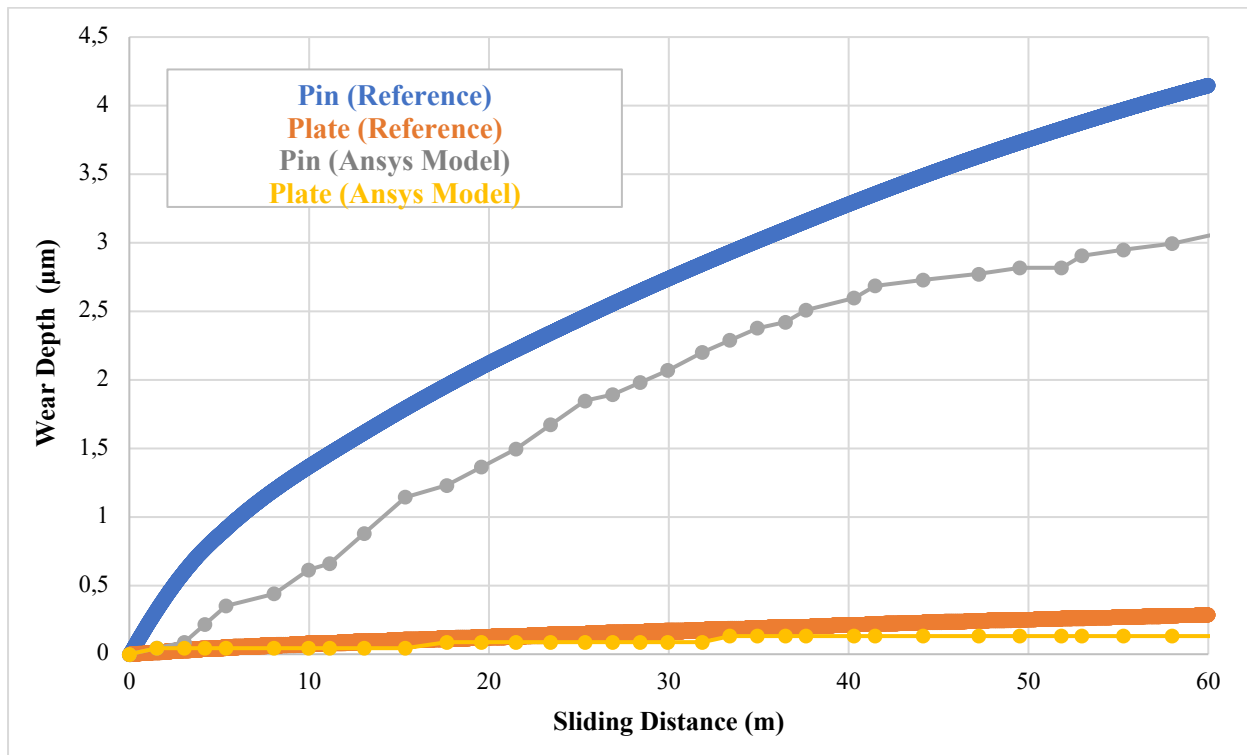


Fig 3. 44 Trends of wear depth of bilateral hard-on-hard pin on plate

4. Wear simulation on hip replacement

4.1 Materials and methods

The following four sections describe the geometry, the materials, the mesh, and the boundary conditions that characterize the CoP hip replacement model.

4.1.1 Geometry and materials definition

The CoP hip implant has a head, with a diameter of 32 mm, that is made of BioloX Delta with an elastic modulus of 350 GPa and Poisson's coefficient of 0.26 and an acetabular insert, with an internal diameter of 32.49 mm, a thickness of 8 mm and therefore an external diameter of 40 mm, that is made of UHMWPE with an elastic modulus of 0.5 GPa and Poisson's coefficient of 0.4. Moreover, the clearance between acetabular insert and femoral head is 0.245 mm [60]. However, to reduce the computational cost of the simulation, the femoral head is modeled as a rigid body by setting "Rigid" to "Stiffness Behaviour" of the "Definition" item of the above geometry. Therefore, the definition of material properties of the head component is not needed. Moreover, for the same reason the presence of the pelvic bone is neglected, and this is acceptable because its influence has a minimal effect on contact pressure, wear volume and wear depth as reported in the literature [23].

The dimensional wear coefficient (k), derived from *Maxian et al's* experiment [46], and used in the simulation is equal to:

$$k = 1.066 \times 10^{-9} \text{ MPa}^{-1} \quad \text{Eq. 4.1}$$

The acetabular insert of CoP hip model (*Fig 4.1*) is made with a sphere with radius 20.245 mm by setting the "Operation" item equal to "Add Material" and selecting as plane the XY one. Moreover, it is made with a sphere, modelled inside the previous one with radius 16.245 mm, by setting the "Operation" item equal to "Slice Material". Finally, it is used the "Slice" command selecting the external sphere as target body. In order to create the femoral head with a diameter of 32 mm, a sphere of radius 16 mm is defined by setting the "Operation" item equal to "Add Frozen".

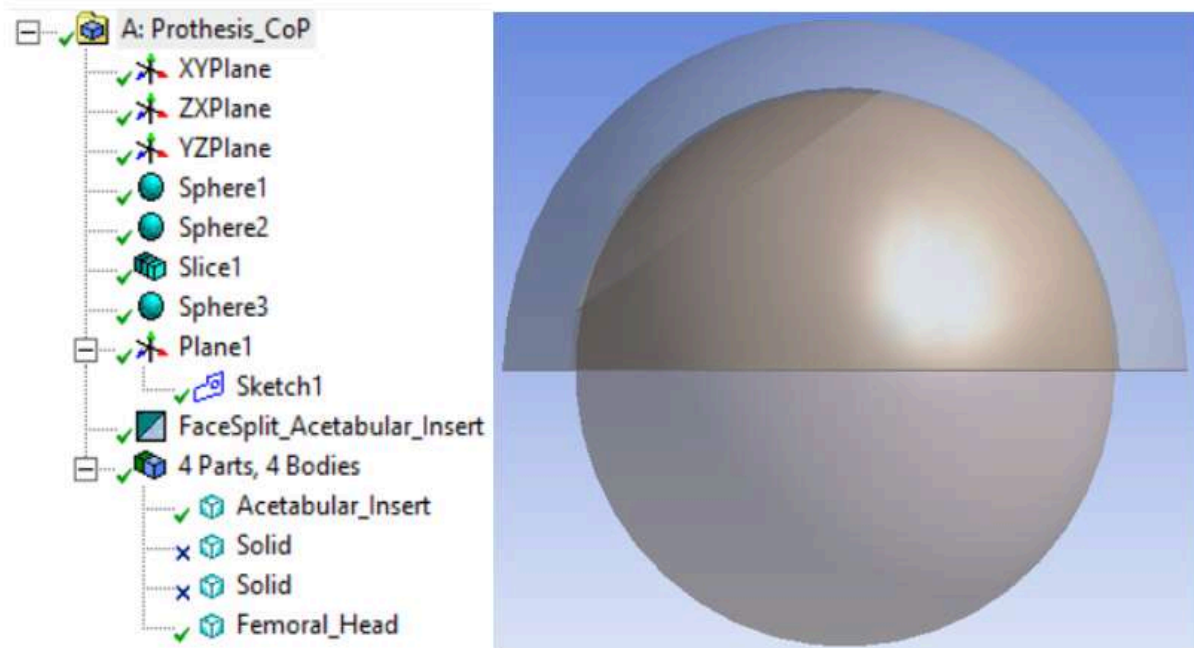


Fig 4. 1 Definition of the geometry of hip replacement

4.1.2 Mesh

The contact region between the acetabular insert and the femoral head is characterised by a finer mesh. Specifically, it is realised by defining a new plane, where a circumferential “Sketch” with radius 10 mm is drawn, and by defining a “Face Split” selecting as “Target Face” the internal surface of the acetabulum insert and as “Tool Geometry” the “Sketch” previously drawn. The “Element Order” in “Defaults” item is set to “Quadratic” (SOLID187) and the “Error Limits” in “Quality” item is set to “Standard Mechanical”. It is important to note that second-order elements were used because the applied load is of the order of kN. Indeed, the linear elements do not allow to go to convergence because of their high distortion due to the load. Afterward, a “Method” is inserted, by selecting the acetabular insert as “Geometry” and by setting them as “Method Tetrahedrons”. Then a “Face Sizing” is added by selecting “Element Size” in “Type” item with a dimension of 1 mm and another one is added by selecting “Sphere of Influence” in “Type” item with a “Sphere Centre” in a reference system integral with the global one but shifted along the z direction. In addition, the latter one is characterised by a “Sphere Radius” of 5 mm with an “Element Size” of 0.5 mm to increase the number of nodes and elements in the contact area, in order to obtain more satisfactory results. As mentioned earlier, the head does not feature mesh because it is modelled as a rigid body. The total number of nodes and elements in the model is, respectively, 11329 and 6368. In the following figure the mesh of models is shown.

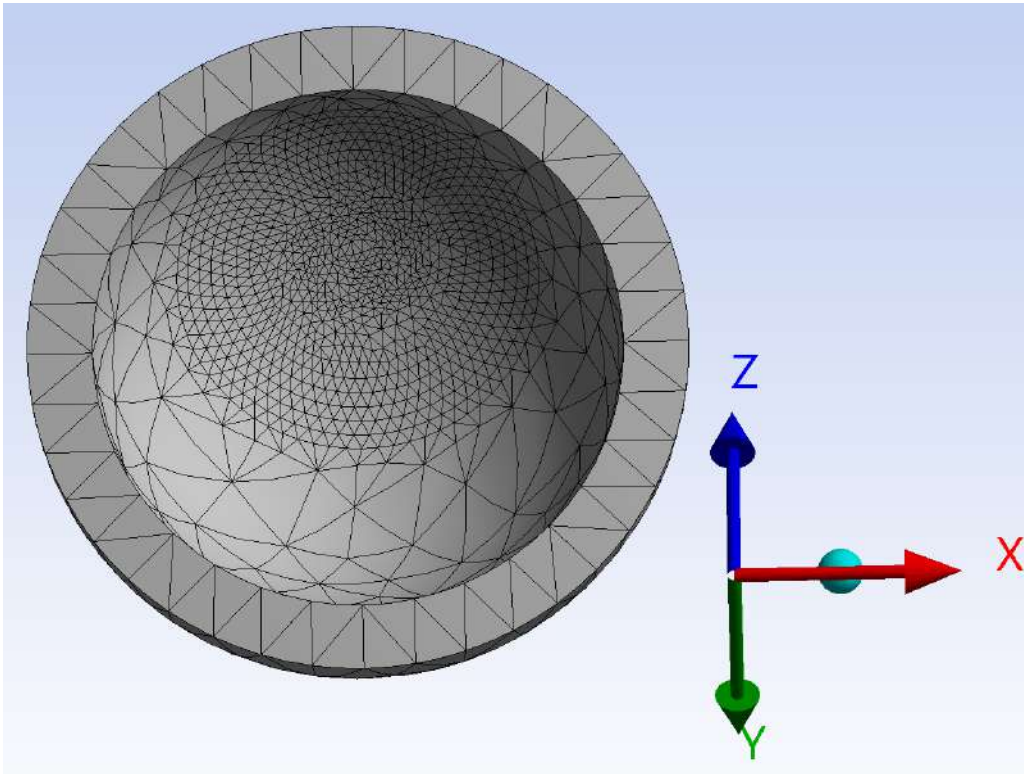


Fig 4. 2 Mesh of acetabular insert

4.1.3 Contact and wear implementation

The femoral head is modelled as “*Target Body*” because it is the most resistant material while the acetabular insert as “*Contact Body*”. Specifically, 3D linear eight-node elements (*CONTA174*) are used for contact elements and 3D linear eight-node elements (*CONTA170*) are used for target elements. The “*Type*”, the “*Behaviour*”, the “*Trim Contact*” of the “*Definition*” item are set respectively to “*Frictional*”, with a coefficient of friction equal to 0.05 because it is the value that characterizes the *hard-on-soft* couplings as stated in the literature [61], “*Asymmetric*” and “*Off*”. The “*Formulation*” of the “*Advanced*” item is set to “*Augmented Lagrange*” with an automatic stiffness calculation and an updating at each iteration by setting “*Update Stiffness*” to “*Each Iteration*”. Other settings of them make the system labile. The “*Advanced*” of “*Detection Method*” item is set to “*Nodal-Normal To Target*” because, in order to activate the wear routine in the Ansys® software, it is necessary that the integration points are “*Nodal Points*” and not “*Gauss Point*”. “*Pinball Region*” is set to “*Program Controlled*”. Finally, the “*Interface Treatment*” of the “*Geometric Modification*” item is set to “*Adjust To Touch*”, other settings make the system labile. The settings just described apply in the finite element model are reported in the following figure.

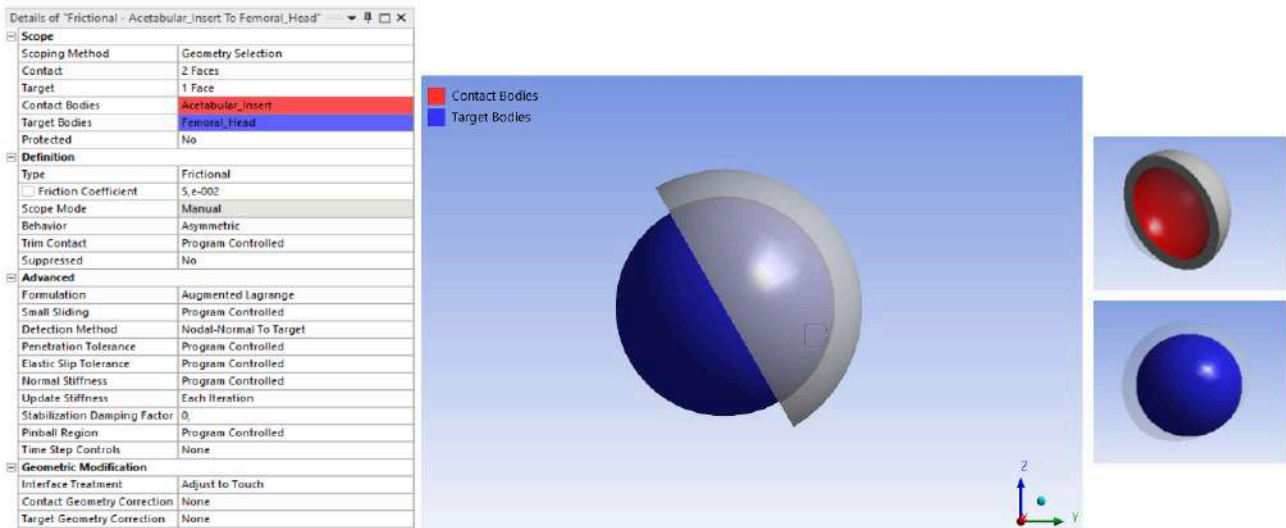


Fig 4. 3 Settings for contact options of hip replacement

Moreover, an APDL Command Snippets is added to simulate the phenomenon of wear, (Fig 4.4). Specifically, the models are characterised by an explicit kinematics so that the variable of the exponential coefficient of the velocity is equal to 1. The model is also simulated with implicit kinematics to assess whether the error committed by using implicit versus explicit kinematics is small and to verify the actual gain in computational effort.

```

Commands
1  !  Commands inserted into this file will be executed just after the contact region definition.
2  !  The type and mat number for the contact type is equal to the parameter "cid".
3  !  The type and mat number for the target type is equal to the parameter "tid".
4  !  The real number for an asymmetric contact pair is equal to the parameter "cid".
5  !  The real numbers for symmetric contact pairs are equal to the parameters "cid" and "tid".
6
7  !  Active UNIT system in Workbench when this object was created: Metric (mm, kg, N, s, mV, mA)
8  !  NOTE: Any data that requires units (such as mass) is assumed to be in the consistent solver unit system.
9  !  See Solving Units in the help system for more information.
10
11
12  !!!! WEAR Material details
13
14
15  K1=(1.066E-9)      !(C1) Wear coefficient
16  H1=1              !(C2) Hardness coefficient
17  m1=1              !(C3) Pressure coefficient
18  n1=1              !(C4) Velocity coefficient
19  C5=0              !(C5) Use contact pressure in the wear calculation.
20
21
22  TB,WEAR,cid,,ARCD      ! ACTIVE WEAR MODEL
23  TBFIELD,TIME,0         ! WEAR PROPERTIES WILL BE DEFINED FOR TIME = 0
24  TBDATA,1,0,1,1,1,0
25  TBFIELD,TIME,0.0001   ! WEAR PROPERTIES WILL BE DEFINED FOR TIME = 0.0001
26  TBDATA,1,K1,H1,m1,n1,C5 ! ASSIGN WEAR PROPERTIES TO CONTACT ELEMENTS
27  TBFIELD,TIME,200      ! WEAR PROPERTIES WILL BE DEFINED FOR TIME = 200
28  TBDATA,1,K1,H1,m1,n1,C5 ! ASSIGN WEAR PROPERTIES TO CONTACT ELEMENTS

```

Fig 4. 4 Command Snippets for wear routine of hip replacement

4.1.4 Boundary conditions

The boundary conditions, in terms of loads and rotations, refer to trends in agreement with ISO 14242-1 as stated by the reference articles [60]. The trends of the applied normal load and the three angular rotations around x, y and z axes are shown in the figure below.

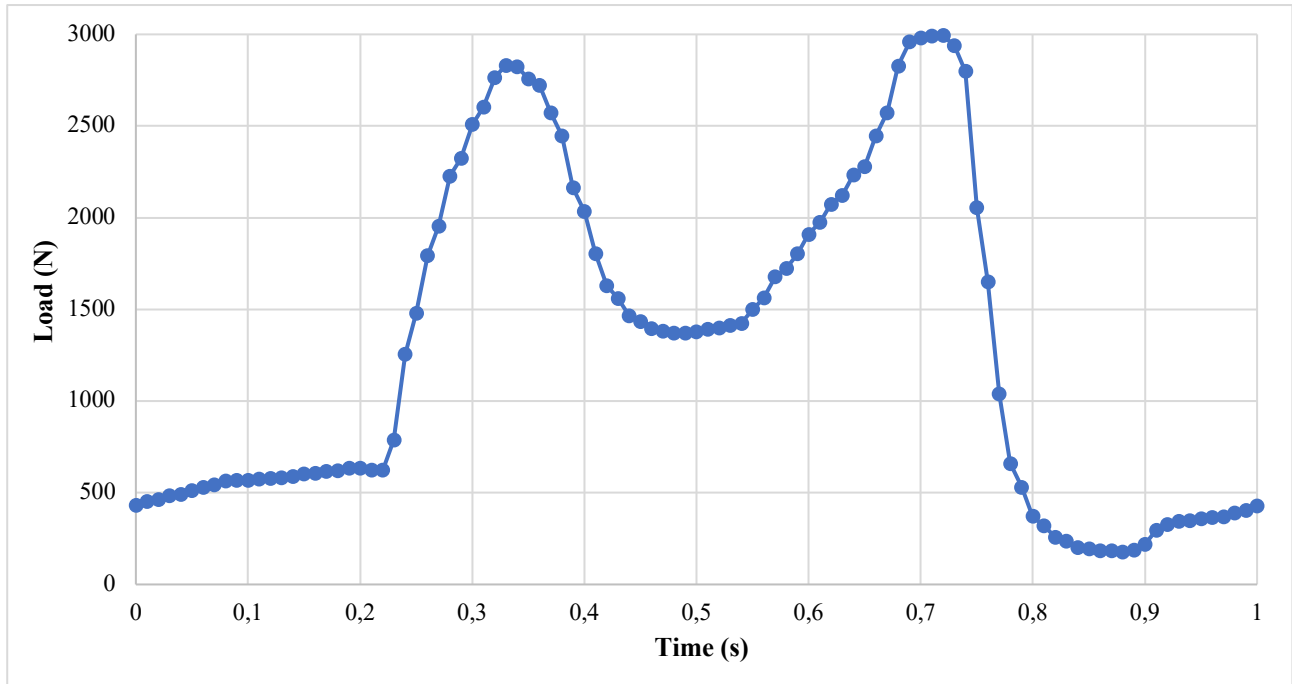


Fig 4. 5 Trends of the forces according with ISO 14242-1 [60]

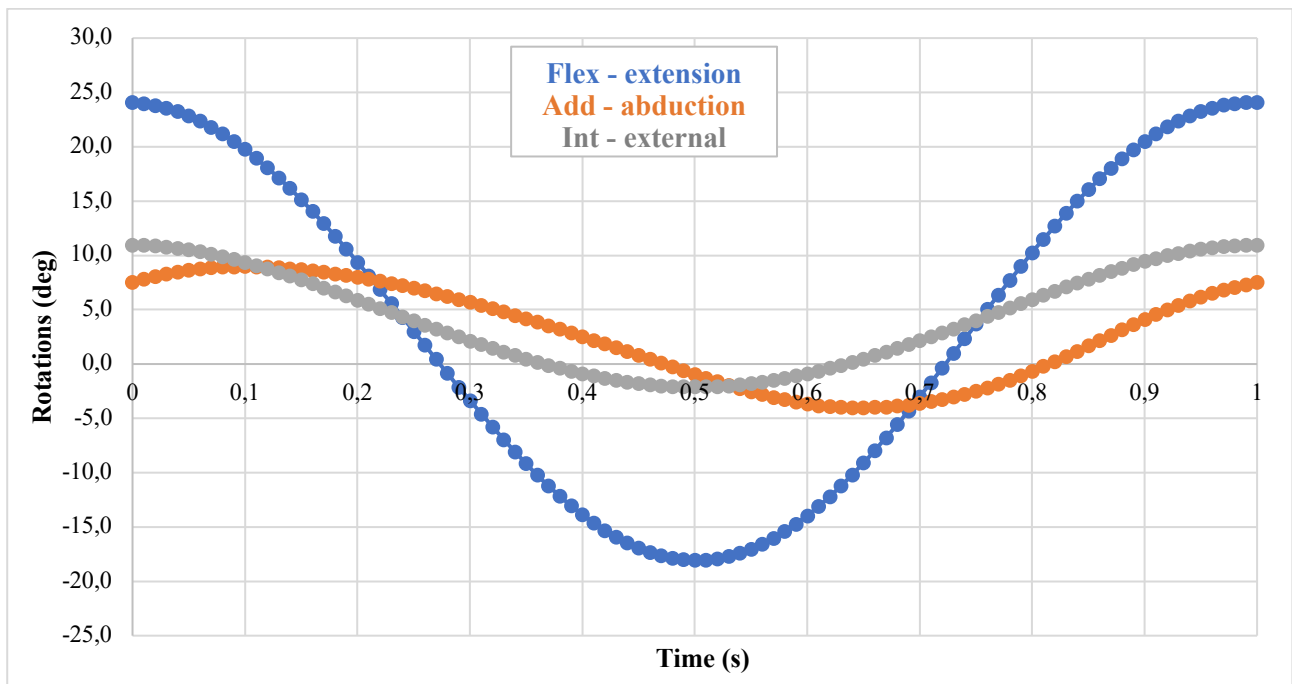


Fig 4. 6 Trends of the angular rotation, specifically flex-extension around y axis, adduction-abduction around x axis and intra extra rotation around z axis according with ISO 14242-1 [60]

The finite element model of hip replacement is characterised by a “*Remote Displacement*” that is applied to the femoral head in order to simulate flex-extension and adduction-abduction rotation around, respectively, y-axis and x-axis. In addition, it is characterised by a “*Remote Displacement*” which is applied to the external surface of the acetabular insert in order to simulate intra-extra rotation around z axis. Finally, it is characterised by a “*Remote Force*” that is applied to the external surface of acetabular insert in order to simulate the load during the cycle of a walk along z axis. The scheme summary of the boundary condition is reported in the figure below.

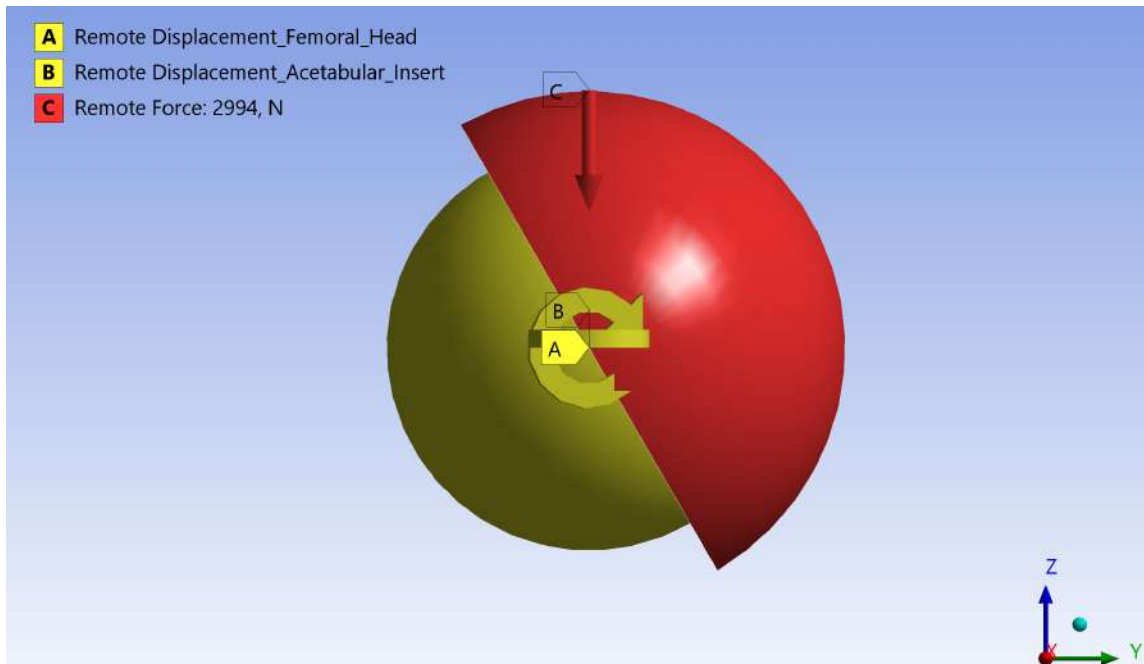


Fig 4. 7 Boundary conditions of hip replacement

Regarding the reference system (Fig. 4.10), it should be noted that a transformation is applied to rotate both bodies of 60 degrees around the x-axis with respect to the global reference system.

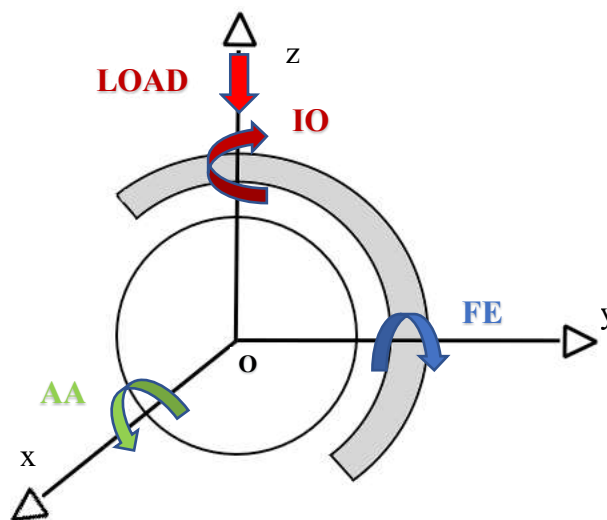


Fig 4. 8 Reference system of hip replacement

In the same section of the boundary conditions, an APDL Command Snippets (Fig 4.9) is inserted to allow the updating the mesh. The *NLAD* command is used to smooth out the distorted elements during the wear simulation by defining a "Critical Ratio" equal to 0.8.

```

Commands
1  ! Commands inserted into this file will be executed just prior to the ANSYS SOLVE command.
2  ! These commands may supersede command settings set by Workbench.
3
4  ! Active UNIT system in Workbench when this object was created: Metric (mm, kg, N, s, mV, mA)
5  ! NOTE: Any data that requires units (such as mass) is assumed to be in the consistent solver unit system.
6  ! See Solving Units in the help system for more information.
7
8
9  /SOLU
10
11 !Define component for NLAD
12 allsel,all,all
13 esel,s,type,,PINCID
14 cm,CONWEARELEM,elem
15 allsel,all,all
16
17 !Define non linear adaptivity criterion
18 NLAD,CONWEARELEM,ADD,CONTACT,WEAR,0.80 !MORPH AFTER 80% IS LOST IN WEAR
19 NLAD,CONWEARELEM,ON,ALL,ALL,1,,200
20 NLAD,CONWEARELEM,LIST,ALL,ALL
21

```

Fig 4. 9 Command Snippets for remeshing of hip replacement

As for the analysis (Fig 4.10), it includes one step with a duration of one second. Specifically, it is characterised by a force vector used to ensure the convergence of the solution. In other words, it is useful to ensure the contact during the entire simulation. In addition, it is characterised by a displacement used to make the system non-labile. Moreover, "Auto Time Step" is set to "On", "Define By" is set to "Time" and "Initial Time Step" and "Minimum Time Step" are set to 0.005 seconds and "Maximum Time Step" is set to 0.01 seconds to ensure convergence. Finally, "Large Deflection" is set to "On" because the analysis is nonlinear, and it is possible to set "Weak Springs" to "On" in order to facilitate the convergence of the simulation.

Details of "Analysis Settings"	
Step Controls	
Number Of Steps	1,
Current Step Number	1,
Step End Time	1, s
Auto Time Stepping	On
Define By	Time
Initial Time Step	5,e-003 s
Minimum Time Step	5,e-003 s
Maximum Time Step	1,e-002 s
Solver Controls	
Solver Type	Program Controlled
Weak Springs	On
Spring Stiffness	Program Controlled
Solver Pivot Checking	Program Controlled
Large Deflection	On
Inertia Relief	Off
Rotordynamics Controls	
Restart Controls	
Nonlinear Controls	
Advanced	
Inverse Option	No
Output Controls	
Analysis Data Management	
Visibility	

Fig 4. 10 Analysis Settings options of hip replacement

4.2 Results

The following section compares the results in terms of maximum contact pressure, wear volume and wear depth on the inner surface of the acetabulum obtained the explicit model with the experiment [60].

As for the trend of maximum contact pressure it follows that of the load as expected (*Fig 4.11*). It also has two maximum values of about 10 MPa, in agreement with the literature [40], [60]–[62], in correspondence of the two maximum load time instants. Therefore, the finite element model predicts the trend and the value of maximum contact pressure with a high level of accuracy.

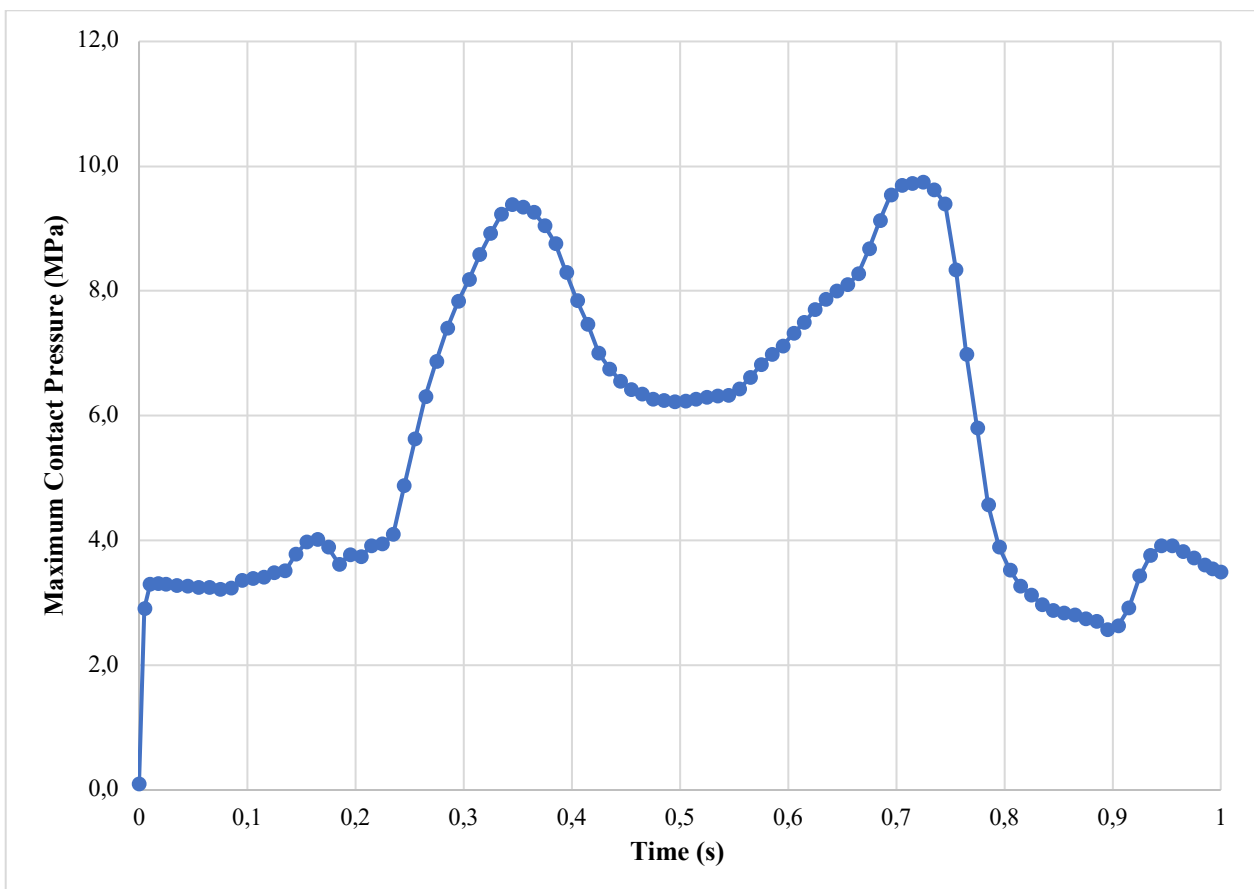


Fig 4. 11 Trends of maximum contact pressure of hip replacement

Moreover, the maximum pressure values are concentrated in the contact zone between the acetabulum and the head. Precisely, they gather at the region where the applied load passes, consistently with what is expected. The following figure shows the contact pressure maps at the initiated instant (1), at the instant of the first maximum (2), at the instant of the second maximum (3) and at one of the final instants (4), respectively.

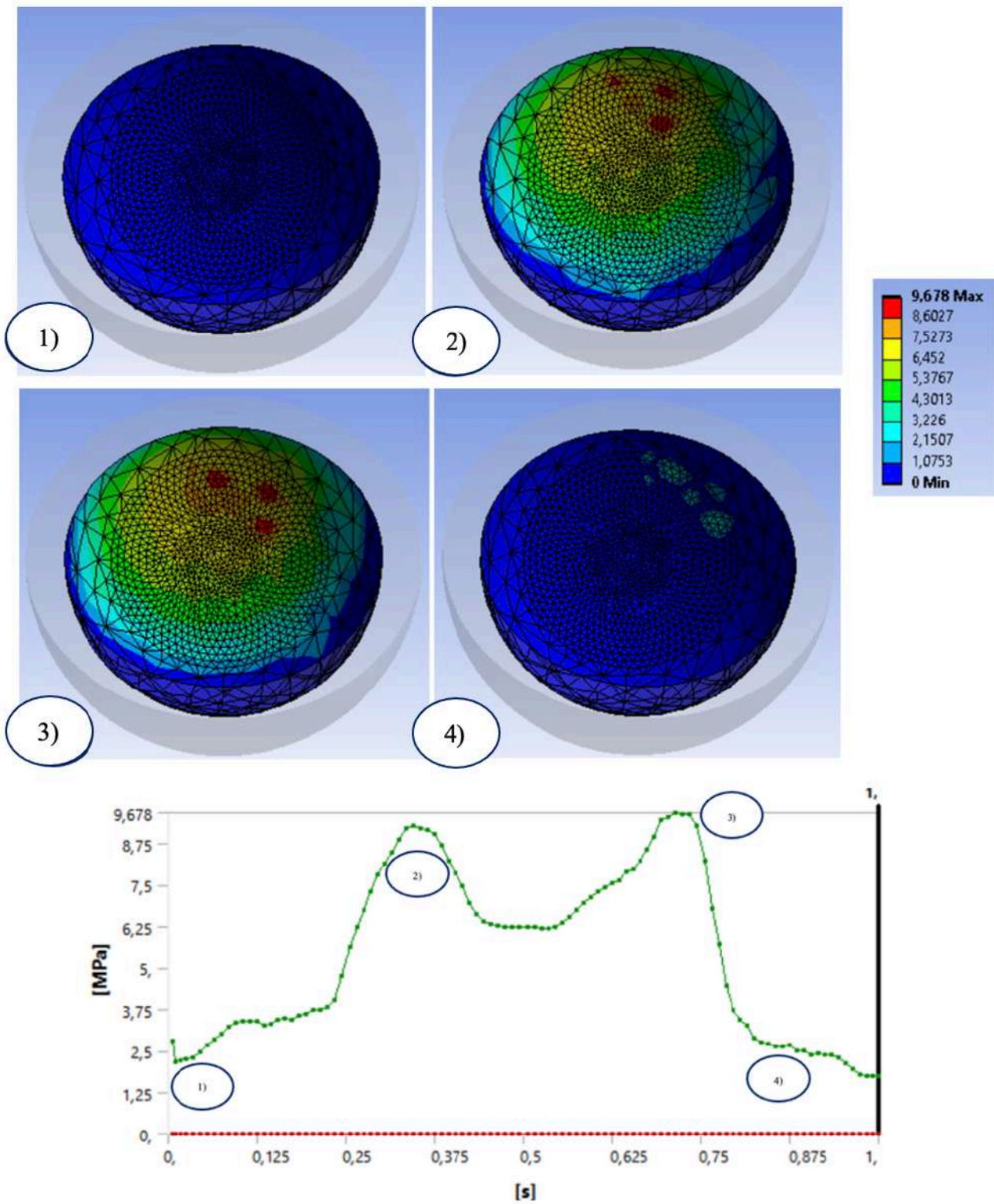


Fig 4. 12 Maps of the maximum contact pressure of hip replacement

As for the wear volume, the experimental value calculated by [60] after two million cycles is:

$$V_{tot_wear} = 110 \text{ mm}^3 \quad \text{Eq. 4.2}$$

The wear volume determined by the model after 1 gait cycle is:

$$V_{wear} = 5.07 \times 10^{-5} \text{ mm}^3 \quad \text{Eq. 4.3}$$

If we multiply this value by $2 \cdot 10^6$, corresponding to two years of hip replacement life, assuming a proportional increment of wear volume during the test, we obtain a good estimate of the final result:

$$V_{tot_wear} = 101.4 \text{ mm}^3 \quad \text{Eq. 4.4}$$

Therefore, the finite element model predicts the wear volume with a high level of accuracy, with an error less than 10 %.

As for the wear depth, the experimental value calculated by [60] after two million cycles is:

$$h_{tot_wear} = 0.24 \text{ mm} \quad \text{Eq. 4.5}$$

The wear depth determined by the model after 1 gait cycle is:

$$h_{wear} = 1.26 \times 10^{-7} \text{ mm} \quad \text{Eq. 4.6}$$

Moreover, in the following figure the wear depth map is represented.

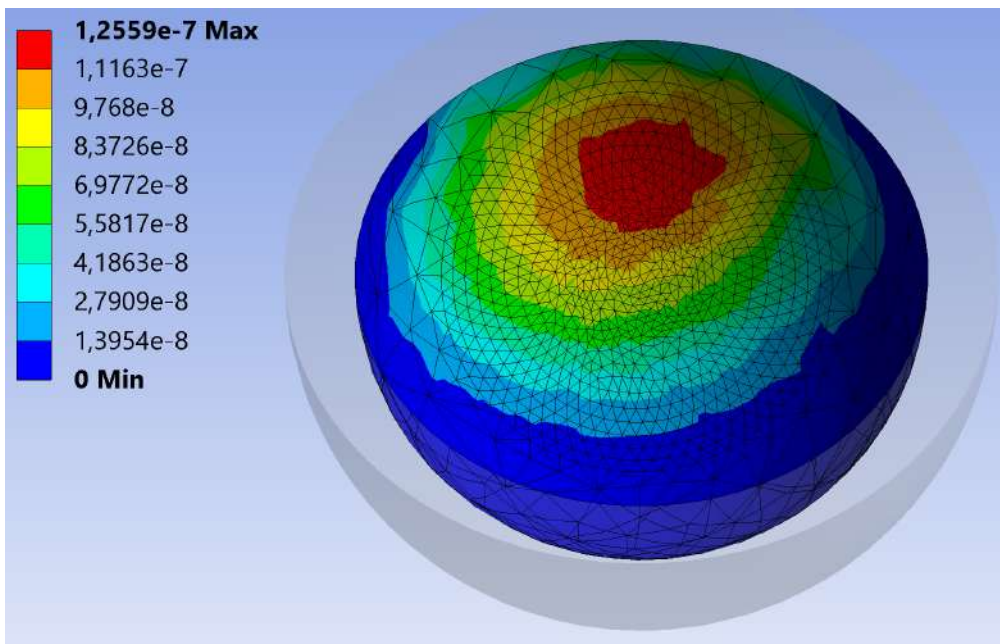


Fig 4. 13 Map of the depth wear of hip replacement

If we multiply this value by $2 \cdot 10^6$ assuming a proportional increment of wear depth during the test, we obtain a good estimate of the final result:

$$h_{tot_wear} = 0.25 \text{ mm} \quad Eq. 4.7$$

Therefore, the finite element model seems to predict the wear depth with a high level of accuracy, with an error less than 5 %.

Furthermore, the growth of the volume in a manner directly proportional to the number of cycles was verified by running a simulation with a duration of 10 gait cycles. Consequently, the effect of the change in geometry due to wear on the estimation of contact pressures can be neglected. Comparing the volume obtained from the latter simulation and that obtained from a gait cycle simulation yields a difference of about 5 %. Specifically, the value of wear volume obtained after 10 gait cycles is:

$$V_{wear} = 4.81 \times 10^{-4} \text{ mm}^3 \quad Eq. 4.8$$

The analysis that follows aims to verify if the use of implicit kinematics, and therefore the simplification of the model, allows a real gain in terms of computational costs and if the error introduced by the simplifications that characterize it is contained. Implicit kinematics, as described above, is characterised by the product of the wear coefficient and the sliding velocity resulting in a fictitious wear coefficient. The instantaneous sliding velocity (v) is calculated as the ratio between the difference between two consecutive computed values of the sliding distance and the time increment, as shown by the following equation:

$$v = \frac{S_i - S_{i-1}}{t_i - t_{i-1}} \quad Eq. 4.9$$

A first model with implicit kinematics was developed considering the same load history implemented in the explicit model and for the velocity term 28.26 mm/s. Regarding the boundary conditions, the implicit model does not present any kind of movement, consequently, the "*Remote Displacements*" are not used to implement the three rotations but only to allow the convergence of the solution. As for the solution, the trend of maximum contact pressure follows that of the load as in the explicit case. Indeed, this trend present two maximum values of about 10 MPa, in agreement with the literature [40], [60]–[62], in correspondence of the two time instants of maximum load.

The wear volume and the wear depth determined by the implicit model after 1 gait cycle are:

$$V_{wear} = 4.99 \times 10^{-5} \text{ mm}^3 \quad Eq. 4.10$$

$$h_{wear} = 1.68 \times 10^{-7} \text{ mm} \quad Eq. 4.11$$

From the previous results, it can be observed that the wear volume has a difference of less than 2 % while the wear depth more than 30 % compared to the results obtained with the explicit model. The difference in terms of wear depth between the explicit and the implicit model is due to the fact that the contact region, and therefore the wear region, is always the same because the implicit kinematics does not present a relative movement between the two bodies. In other words, the wear phenomenon affects a smaller region.

The computational time saved with this simulation was a few minutes. In order to further simplify the analyses and reduce the computational cost of the simulations, three other different models were developed with an implicit kinematic scheme. They will be called in hereinafter Model A, Model B and Model C. The first case considers the average value of the force and the average value of the sliding velocity as a constant normal load and constant/uniform velocity term; the second case considers the maximum value of the force and the mean value of the sliding velocity while the third one (the most critical) considers the value of the force (which does not correspond to the maximum load value in general), and the sliding velocity obtained at the time instant in which the product between the load and the sliding velocity is greater. The following table summarizes the three cases just described.

<i>Table 4.1</i>		
	Load (N)	Sliding velocity (mm/s)
Model A	1306	28.26
Model B	2994	28.26
Model C	2939	38.03

As for the results, the maximum contact pressure, the wear volume and the wear depth are evaluated. The maximum contact pressure reaches its maximum after 1 gait cycle in all three models, consistent with the application of a load ramp as a boundary condition. Specifically, in the first model the maximum contact pressure after one second is 5.73 MPa which is in line with what expected because the maximum pressure value (about 10 MPa) calculated with the explicit model is obtained with a force of about 3000 N. The wear volume after 1 gait cycle is about half of that estimated with the explicit model, as shown below:

$$V_{wear} = 2.40 \times 10^{-5} \text{ mm}^3 \quad Eq. 4.12$$

This value is reasonable because the applied load is less than half of the maximum load applied in the simulation with the explicit kinematics. Finally, the predicted wear depth after 1 gait cycle is:

$$h_{wear} = 1.22 \times 10^{-7} \text{ mm} \quad Eq. 4.13$$

The following value is predictable because, as mentioned earlier, the implied kinematics implies that the contact region always remains the same.

In the second model, the maximum contact pressure after 1 gait cycle is 9.42 MPa which is in line with the expectations because the maximum pressure value (about 10 MPa) calculated with the explicit model is obtained with a force of about 3000 N. The wear volume shows a difference of 12 %, as indicated below. This difference is very small compared to the previous case because the force value in this second case corresponds to the maximum force value applied in the explicit case.

$$V_{wear} = 5.65 \times 10^{-5} \text{ mm}^3 \quad Eq. 4.14$$

Finally, the depth of wear presents a fairly obvious difference from the explicit case, as shown below. This result is in line with the reasoning made in the first model.

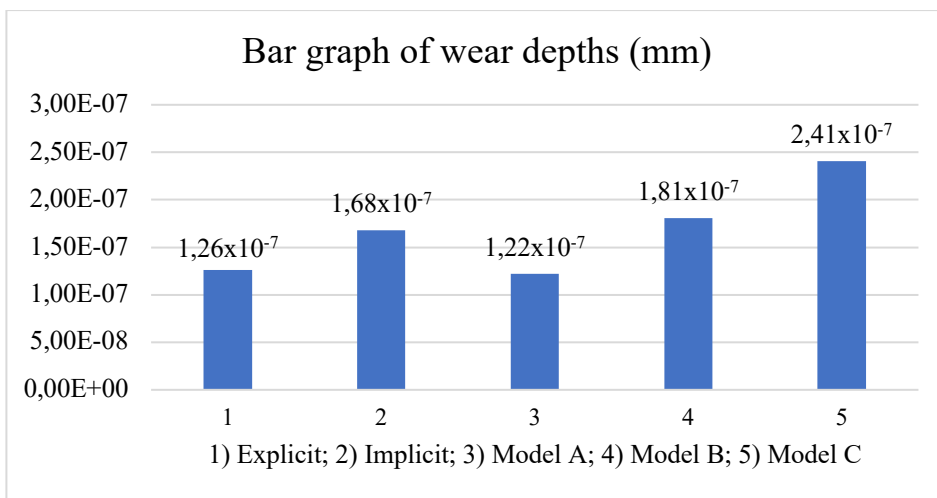
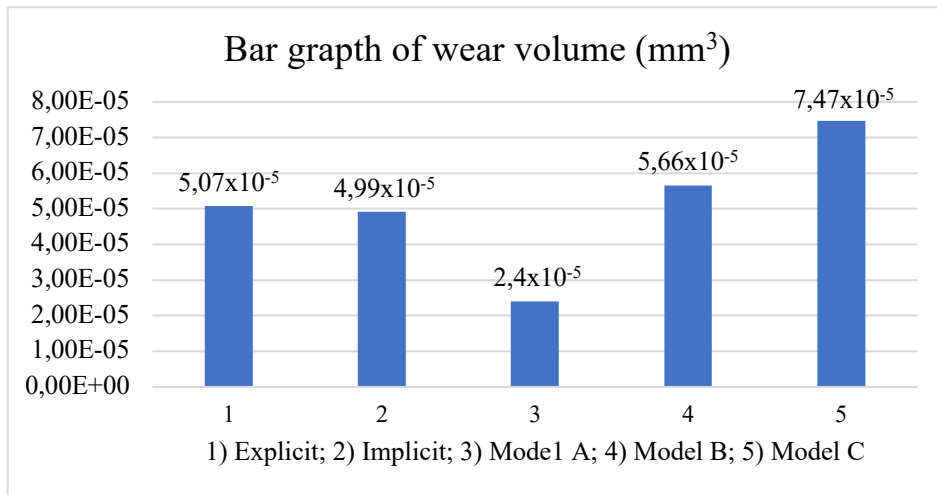
$$h_{wear} = 1.81 \times 10^{-7} \text{ mm} \quad Eq. 4.15$$

In the third model, the maximum contact pressure after 1 gait cycle is 9.30 MPa which is in line with expectations. The wear volume and wear depth present clear differences with the results obtained with the explicit model, as shown below:

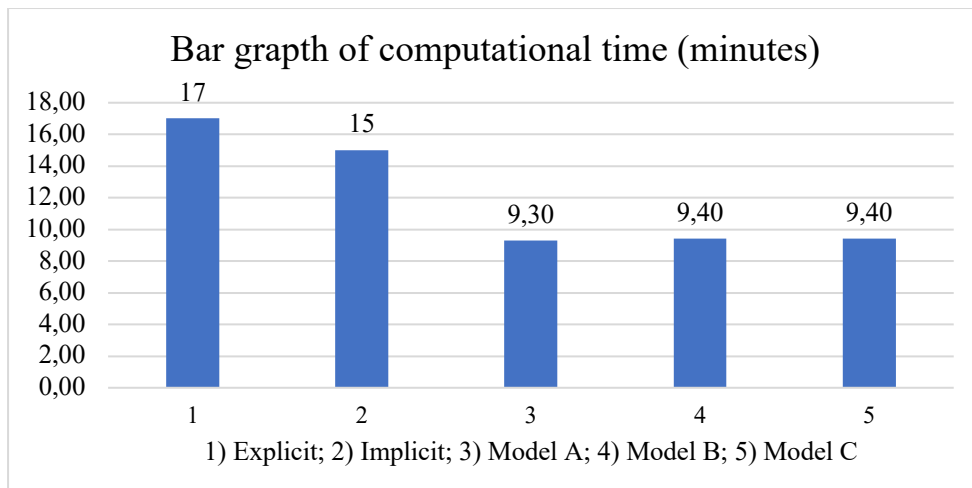
$$V_{wear} = 7.47 \times 10^{-5} \text{ mm}^3 \quad Eq. 4.16$$

$$h_{wear} = 2.41 \times 10^{-7} \text{ mm} \quad Eq. 4.17$$

In the following bar graphs re reported the results of the explicit and implicit cases described above.



In addition, the following bar graph shows the computational times of the respective simulations. It is possible to observe that the implementation of the implicit kinematics allows a small gain in this sense. Precisely, the time is almost halved in cases where the boundary conditions are further simplified. However, the results are less precise.



5. Conclusions

The objective of the following thesis was the use of the finite element method to model the wear phenomenon in hip prostheses.

In the first part of the elaboration, the wear phenomenon is studied simulating pin-on-disc and pin-on-plate tests, commonly used to evaluate the tribological properties of pairs of materials. More precisely, the first pin-on-disc test involves a *hard-on-hard* pair with unilateral wear, the second one involves a *hard-on-soft* pair with unilateral wear and the third one involves a *hard-on-hard* pair with bilateral wear. Using the first pin-on-disc test, convergence and sensitivity analyses were performed where the effect of the mesh (order and type of elements) and other contact parameters (e.g., formulation) on the wear results was evaluated. From these analyses, was possible to identify the contact and wear settings to simulate the wear phenomenon in a better way. In the first two pin-on-disc tests, an implicit kinematics was implemented. Results, in terms of maximum contact pressure, wear volume and wear depth, were found in agreement with the literature [52], [53]. Implicit kinematics reduces the computational time compared to the explicit one while ensuring high accuracy of results, as just stated. The third model is initially implemented with implicit kinematics obtaining good results in terms of maximum contact pressure and wear volume but not in terms of wear depth. Indeed, as stated before, the wear volume represents only a global index while the wear depth represents a local index. Consequently, to describe in a complete way the wear phenomenon it is necessary to simulate in an appropriate way also the wear depth. For these reasons, the third pin-on-disc case is also implemented with explicit kinematics because the contact points of the disc, unlike those of the pin, are subject to the contact pressure for a reduced time. Consequently, the wear depth of the disc should be much smaller than that of the pin. The results in terms of wear depth predicted by the explicit model are encouraging although they still differ from those predicted by the computational study [59]. The same cannot be said for the predicted wear volume which has a clear difference from the experimental case results [58]. In conclusion it is possible to state that was possible to predict with a high accuracy the unilateral wear phenomenon in a pin on disc test but the same cannot be stated in the case of bilateral wear.

In the second part of the elaboration, the wear phenomenon is studied simulating a hip replacement model with an explicit kinematics. Specifically, the model is characterised by specific materials, geometries, and boundary conditions. The latter are in accordance with ISO 14242-1. As a result, it is more realistic because it simulates loads and rotations that are applied during a gait cycle in a hip simulator. Maximum contact pressure, wear volume and wear depth are predicted with a good level

of accuracy. Moreover, the test is also simulated using an implicit kinematics scheme in order to evaluate possible combinations of input conditions that allow to obtain reasonable wear results while saving computational cost. The results show a real gain in computational cost (about half the time) however they also show in some cases an evident error due to the introduction of the implicit kinematics, in which the worn region is always the same. In conclusion, it is possible to state that the developed hip replacement model predicts wear with a good level of accuracy if the kinematic is explicitly model. Attention should be paid when using implicit kinematics, which can be considered useful in some applications (i.e., comparison studies) when an accurate wear prediction is not necessarily needed.

Considering the main limitations of this study, I suggest the following steps for future work:

- Explore the possibility to implement more complex wear laws than the simple one used in this thesis (Archard law);
- Use a wear coefficient that varies over time. Indeed, for many materials like metals, assuming a constant wear coefficient is reasonable but for others, like polyethylene, it is not because the wear resistance depends on the local re-orientation of the polymeric chains;
- Implement wear on both bodies (acetabulum and head) and work in bilateral wear;
- Implement the phenomenon of lubrication and study its effect on the wear coefficient;
- Consider geometry updating to simulate the wear phenomenon for a much higher number of cycles;
- Introduce boundary conditions from subject-specific models of musculoskeletal dynamics that are not exclusively related to tasks such as walking but also others such as stair climbing or running.

The simulations reported were performed predominantly on an HP Laptop Computer with an Intel(R) Core(TM) i7-10755H processor, with a 2.60 GHz CPU, with 16 GB RAM, and with a 64-bit Windows 10 operating system.

6. Bibliography

- [1] S. Affatato, «The history of total hip arthroplasty (THA)», in *Perspectives in Total Hip Arthroplasty*, Elsevier, 2014, pagg. 3–18.
- [2] J.-P. Courpied e J. H. Caton, «Total Hip Arthroplasty, state of the art for the 21st century», *Int. Orthop.*, vol. 35, n. 2, pagg. 149–150, feb. 2011, doi: 10.1007/s00264-011-1207-9.
- [3] S. Affatato, P. Bracco, L. Costa, T. Villa, V. Quaglini, e A. Toni, «In vitro wear performance of standard, crosslinked, and vitamin-E-blended UHMWPE», *J. Biomed. Mater. Res. A*, vol. 100A, n. 3, pagg. 554–560, mar. 2012, doi: 10.1002/jbm.a.33297.
- [4] F. D. Puccio, «Biotribology of artificial hip joints», *World J. Orthop.*, vol. 6, n. 1, pag. 77, 2015, doi: 10.5312/wjo.v6.i1.77.
- [5] L. Mattei, F. Di Puccio, B. Piccigallo, e E. Ciulli, «Lubrication and wear modelling of artificial hip joints: A review», *Tribol. Int.*, vol. 44, n. 5, pagg. 532–549, mag. 2011, doi: 10.1016/j.triboint.2010.06.010.
- [6] F. Cosmi, M. Hoglievina, G. Fancellu, e B. Martinelli, «A finite element method comparison of wear in two metal-on-metal total hip prostheses», *Proc. Inst. Mech. Eng. [H]*, vol. 220, n. 8, pagg. 871–879, ago. 2006, doi: 10.1243/09544119JEIM148.
- [7] Serope e Steven R. Kalpakjian e Schmid, *Tecnologia meccanica*. .
- [8] G. Matsoukas, R. Willing, e I. Y. Kim, «Total Hip Wear Assessment: A Comparison Between Computational and In Vitro Wear Assessment Techniques Using ISO 14242 Loading and Kinematics», *J. Biomech. Eng.*, vol. 131, n. 4, pag. 041011, apr. 2009, doi: 10.1115/1.3049477.
- [9] A. Ghosh, B. Leonard, e F. Sadeghi, «A stress based damage mechanics model to simulate fretting wear of Hertzian line contact in partial slip», *Wear*, vol. 307, n. 1–2, pagg. 87–99, set. 2013, doi: 10.1016/j.wear.2013.08.008.
- [10] «ContactHertz». .
- [11] E. Ciulli, *Elementi di Meccanica*. .
- [12] «What are the wear mechanism and what controlos them?»
- [13] Masiello Francesco e Politi Marcantonio, *Tribologia e applicazioni tribologiche*. .
- [14] Boniardi D'Erico e Micari, *Il problema dell'usura negli organi meccanici*. .
- [15] Bertin Antonio, Poli Mario e Vitale Antonio, *Fondamenti di Meccanica*. .
- [16] Corticelli Mauro A, *Elementi di Fisica Tecnica*. .
- [17] X. Li, «A pin-on-disc study of the tribology characteristics of sintered versus standard steel gear materials», pag. 11.

- [18] S. Affatato, «Tribological interactions of ceramic bearings in total hip arthroplasty (THA)», in *Perspectives in Total Hip Arthroplasty*, Elsevier, 2014, pagg. 138–146.
- [19] S. Affatato, «Tribological interactions of hybrid hard bearings in total hip arthroplasty (THA)», in *Perspectives in Total Hip Arthroplasty*, Elsevier, 2014, pagg. 147–156.
- [20] S. A. Basha e D. Sarkar, «COMPETITIVE LIFE TIME ASSESSMENT OF SrO-ZTA/SrO-ZTA AND CoCrMo/UHMWPE HIP PROSTHESIS BEARINGS», *J. Mech. Med. Biol.*, vol. 20, n. 03, pag. 2050009, apr. 2020, doi: 10.1142/S0219519420500098.
- [21] European Commission. Joint Research Centre. Institute for Health and Consumer Protection., *Total hip arthroplasty: state of the art, challenges and prospects*. LU: Publications Office, 2012.
- [22] S. Affatato, «Contemporary designs in total hip arthroplasty (THA)», in *Perspectives in Total Hip Arthroplasty*, Elsevier, 2014, pagg. 46–64.
- [23] L. Wang, G. Isaac, R. Wilcox, A. Jones, e J. Thompson, «Finite element analysis of polyethylene wear in total hip replacement: A literature review», *Proc. Inst. Mech. Eng. [H]*, vol. 233, n. 11, pagg. 1067–1088, nov. 2019, doi: 10.1177/0954411919872630.
- [24] S. Affatato, E. Castiello, L. Amendola, S. Comitini, J. L. Prudhon, e D. Tigani, «Revision of a Monoblock Metal-on-Metal Cup Using a Dual Mobility Component: Is It a Reasonable Option?», *Materials*, vol. 13, n. 9, pag. 2040, apr. 2020, doi: 10.3390/ma13092040.
- [25] S. Williams, M. Al-Hajjar, G. H. Isaac, e J. Fisher, «Comparison of ceramic-on-metal and metal-on-metal hip prostheses under adverse conditions», *J. Biomed. Mater. Res. B Appl. Biomater.*, vol. 101B, n. 5, pagg. 770–775, lug. 2013, doi: 10.1002/jbm.b.32880.
- [26] K. N. Chethan, B. Satish Shenoy, e N. Shyamasunder Bhat, «Role of different orthopedic biomaterials on wear of hip joint prosthesis: A review», *Mater. Today Proc.*, vol. 5, n. 10, pagg. 20827–20836, 2018, doi: 10.1016/j.matpr.2018.06.468.
- [27] J. S. De Mattia, E. Castiello, e S. Affatato, «Clinical issues of ceramic devices used in total hip arthroplasty», in *Advances in Ceramic Biomaterials*, Elsevier, 2017, pagg. 313–328.
- [28] P. Bracco, A. Bellare, A. Bistolfi, e S. Affatato, «Ultra-High Molecular Weight Polyethylene: Influence of the Chemical, Physical and Mechanical Properties on the Wear Behavior. A Review», *Materials*, vol. 10, n. 7, pag. 791, lug. 2017, doi: 10.3390/ma10070791.
- [29] M. Yorifuji et al., «Wear Simulation of Ceramic-on-Crosslinked Polyethylene Hip Prostheses: A New Non-Oxide Silicon Nitride versus the Gold Standard Composite Oxide Ceramic Femoral Heads», *Materials*, vol. 13, n. 13, pag. 2917, giu. 2020, doi: 10.3390/ma13132917.
- [30] F. Liu, J. Fisher, e Z. Jin, «Computational modelling of polyethylene wear and creep in total hip joint replacements: Effect of the bearing clearance and diameter», *Proc. Inst. Mech. Eng. Part J*

- J. Eng. Tribol.*, vol. 226, n. 6, pagg. 552–563, giu. 2012, doi: 10.1177/1350650112441908.
- [31] S. M. Kurtz, «The Origins of UHMWPE in Total Hip Arthroplasty», *UHMWPE Biomater. Handb.*, pag. 11.
- [32] M. Merola e S. Affatato, «Materials for Hip Prostheses: A Review of Wear and Loading Considerations», *Materials*, vol. 12, n. 3, pag. 495, feb. 2019, doi: 10.3390/ma12030495.
- [33] P. Sahoo, S. K. Das, e J. Paulo Davim, «Tribology of materials for biomedical applications», in *Mechanical Behaviour of Biomaterials*, Elsevier, 2019, pagg. 1–45.
- [34] F. W. Chan, J. D. Bobyn, J. B. Medley, J. J. Krygier, e M. Tanzer, «Wear and Lubrication of Metal-on-Metal Hip Implants», *Clin. Orthop.*, vol. 369, pagg. 10–24, dic. 1999, doi: 10.1097/00003086-199912000-00003.
- [35] V. O. Saikko, P. O. Paavolainen, e P. Slätis, «Wear of the polyethylene acetabular cup: Metallic and ceramic heads compared in a hip simulator», *Acta Orthop. Scand.*, vol. 64, n. 4, pagg. 391–402, gen. 1993, doi: 10.3109/17453679308993653.
- [36] R. M. Trommer e M. M. Maru, «Importance of preclinical evaluation of wear in hip implant designs using simulator machines», *Rev. Bras. Ortop. Engl. Ed.*, vol. 52, n. 3, pagg. 251–259, mag. 2017, doi: 10.1016/j.rboe.2016.07.004.
- [37] T. A. Maxian, T. D. Brown, D. R. Pedersen, e J. J. Callaghan, «Adaptiive finite element modeling of long-term polyethylene wear in total hip arthroplasty», *J. Orthop. Res.*, vol. 14, n. 4, pagg. 668–675, lug. 1996, doi: 10.1002/jor.1100140424.
- [38] S. M. Kurtz, «The Clinical Performance of UHMWPE in Hip Replacements», *UHMWPE Biomater. Handb.*, pag. 11.
- [39] M. S. Uddin e L. C. Zhang, «Predicting the wear of hard-on-hard hip joint prostheses», *Wear*, vol. 301, n. 1–2, pagg. 192–200, apr. 2013, doi: 10.1016/j.wear.2013.01.009.
- [40] L. Mattei, F. Di Puccio, e E. Ciulli, «A comparative study of wear laws for soft-on-hard hip implants using a mathematical wear model», *Tribol. Int.*, vol. 63, pagg. 66–77, lug. 2013, doi: 10.1016/j.triboint.2012.03.002.
- [41] Y. Peng, P. Arauz, S. An, e Y.-M. Kwon, «Computational modeling of polyethylene wear in total hip arthroplasty using patient-specific kinematics-coupled finite element analysis», *Tribol. Int.*, vol. 129, pagg. 162–166, gen. 2019, doi: 10.1016/j.triboint.2018.08.009.
- [42] S. L. Bevill, G. R. Bevill, J. R. Penmetsa, A. J. Petrella, e P. J. Rullkoetter, «Finite element simulation of early creep and wear in total hip arthroplasty», *J. Biomech.*, vol. 38, n. 12, pagg. 2365–2374, dic. 2005, doi: 10.1016/j.jbiomech.2004.10.022.
- [43] F. Liu, I. Leslie, S. Williams, J. Fisher, e Z. Jin, «Development of computational wear simulation of metal-on-metal hip resurfacing replacements», *J. Biomech.*, vol. 41, n. 3, pagg. 686–

694, 2008, doi: 10.1016/j.jbiomech.2007.09.020.

[44] L. Kang, A. L. Galvin, J. Fisher, e Z. Jin, «Enhanced computational prediction of polyethylene wear in hip joints by incorporating cross-shear and contact pressure in addition to load and sliding distance: Effect of head diameter», *J. Biomech.*, vol. 42, n. 7, pagg. 912–918, mag. 2009, doi: 10.1016/j.jbiomech.2009.01.005.

[45] A. Ruggiero, R. D'Amato, e S. Affatato, «Comparison of Meshing Strategies in THR Finite Element Modelling», *Materials*, vol. 12, n. 14, pag. 2332, lug. 2019, doi: 10.3390/ma12142332.

[46] T. A. Maxian, T. D. Brown, D. R. Pedersen, e J. J. Callaghan, «WEAR IN TOTAL HIP ARTHROPLASTY», pag. 6.

[47] S. Affatato, F. Zanini, e S. Carmignato, «Quantification of Wear and Deformation in Different Configurations of Polyethylene Acetabular Cups Using Micro X-ray Computed Tomography», *Materials*, vol. 10, n. 3, pag. 259, mar. 2017, doi: 10.3390/ma10030259.

[48] J. S.-S. Wu, J.-P. Hung, C.-S. Shu, e J.-H. Chen, «The computer simulation of wear behavior appearing in total hip prosthesis», *Comput. Methods Programs Biomed.*, vol. 70, n. 1, pagg. 81–91, gen. 2003, doi: 10.1016/S0169-2607(01)00199-7.

[49] «Workbench User's Guide», pag. 394, 2019.

[50] «Mechanical APDL Contact Technology Guide», pag. 266.

[51] Ansys, «Contact Defaults in Workbench and ANSYS».

[52] P. Pödra e S. Andersson, «Simulating sliding wear with finite element method», *Tribol. Int.*, vol. 32, n. 2, pagg. 71–81, feb. 1999, doi: 10.1016/S0301-679X(99)00012-2.

[53] G. B. Cornwall, J. T. Bryant, e C. M. Hansson, «The effect of kinematic conditions on the wear of ultra-high molecular weight polyethylene (UHMWPE) in orthopaedic bearing applications», *Proc. Inst. Mech. Eng. [H]*, vol. 215, n. 1, pagg. 95–106, gen. 2001, doi: 10.1243/0954411011533454.

[54] F04 Committee, «Specification for Ultra-High-Molecular-Weight Polyethylene Powder and Fabricated Form for Surgical Implants», *ASTM International*. doi: 10.1520/F0648-14.

[55] F04 Committee, «Specification for Cobalt-28 Chromium-6 Molybdenum Alloy Castings and Casting Alloy for Surgical Implants (UNS R30075)», *ASTM International*. doi: 10.1520/F0075-18.

[56] M. Hussain et al., «Ultra-High-Molecular-Weight-Polyethylene (UHMWPE) as a Promising Polymer Material for Biomedical Applications: A Concise Review», *Polymers*, vol. 12, n. 2, pag. 323, feb. 2020, doi: 10.3390/polym12020323.

[57] T. A. Sherazi, «Ultrahigh Molecular Weight Polyethylene», in *Encyclopedia of Membranes*, E. Drioli e L. Giorno, A c. di Berlin, Heidelberg: Springer Berlin Heidelberg, 2014, pagg. 1–2.

[58] J. L. Tipper, P. J. Firkins, E. Ingham, J. Fisher, M. H. Stone, e R. Farrar, «Quantitative

analysis of the wear and wear debris from low and high carbon content cobalt chrome alloys used in metal on metal total hip replacements», pag. 10.

[59] Z. M. Jin, P. Firkins, R. Farrar, e J. Fisher, «*Analysis and modelling of wear of cobalt-chrome alloys in a pin-on-plate test for a metal-on-metal total hip replacement*», *Proc. Inst. Mech. Eng. [H]*, vol. 214, n. 6, pagg. 559–568, giu. 2000, doi: 10.1243/0954411001535589.

[60] L. Mattei, F. Di Puccio, E. Ciulli, e A. Pauschitz, «*Experimental investigation on wear map evolution of ceramic-on-UHMWPE hip prosthesis*», *Tribol. Int.*, vol. 143, pag. 106068, mar. 2020, doi: 10.1016/j.triboint.2019.106068.

[61] Enab T.A. Nadia E. Bondok, «*Effect of Femoral Head Size on Contact Pressure and Wear in Total Hip Arthroplasty*», *Eff. Femoral Head Size Contact Press. Wear Total Hip Arthroplasty*, vol. Vol. 3, Issue 7, July 2014.

[62] M. Nagentrau, A. L. M. Tobi, S. Jamian, e Y. Otsuka, «*HAp Coated Hip Prosthesis Contact Pressure Prediction Using FEM Analysis*», *Mater. Sci. Forum*, vol. 991, pagg. 53–61, mag. 2020, doi: 10.4028/www.scientific.net/MSF.991.53.

Ringraziamenti

Desidero ringraziare il professore Viceconti Marco per l'opportunità di concludere il mio percorso magistrale con il tirocinio per tesi presso l'Istituto Ortopedico Rizzoli di Bologna. Questa esperienza seppur limitata dal periodo storico in cui stiamo vivendo mi ha permesso di conoscere persone straordinaria sia dal punto di vista professionale sia da quello umano. Ringrazio tutto lo staff del Laboratorio di Tecnologia medica del Rizzoli, in particolare l'ing. Cristina Curreli per avermi accompagnato, aiutato e supportato durante tutti questi mesi. Inoltre, desidero ringraziare Antonio La Mattina per il suo immancabile aiuto informatico e tecnico.